University of Pisa

Department Of Information Engineering

Master's Thesis

GOODPUT BASED ADAPTIVE MODULATION AND CODING ALGORITHM FOR BIC-OFDM SYSTEMS

Supervisors:

Ing.Lottici Vincenzo
Prof. Giannetti Filippo
Ing. Ivan Stupia

Author:

Domenico Montemagni

April 27, 2009

Contents

List of Figures

List of Tables

Chapter 1

Introduction

1.1 Wireless Communication

Wireless communication has brought a revolution in the world. There has been tremendous technological advancement in wireless networks in the past two or three decades. In the beginning of this new millennium we are having a new world which is the world of telecommunication. Telecommunication includes all the communication of computer networks, public telephone networks, radio networks, television networks and internet. Most of the communication networks used today are wireless in nature. Wireless means transferring the signals without wires using radio waves, infra red etc. In wireless networks there is unlimited mobility; we can access the network services from almost anywhere. In wired networks we have the restriction of using the services in fixed area. The demand of

wireless is increasing very fast as everybody wants to use the broadband services anywhere and anytime. The standardization of these wireless networks is also very important.

Wireless systems have evolved from simple network designs with low data rate and reliability to much intricate designs supporting very high data rate and reliability. This transition has been possible because of technological advancements in the hardware and the desire for high data rate wireless applications.

One of the most popular types of wireless networks is cellular networks. In cellular networks we divide the whole network into smaller cells and by this we can have more users in the network with better mobility and Quality of Service (QoS). Cellar networks are divided into different generations. First generation (1G) cellular networks were introduced around 1980s. The first system was introduced in Japan. The first cellular network in Europe was built in Scandinavia in 1981 and it was known as Nordic Mobile Telephone (NMT). It uses the 450 MHz frequency band. This NMT system was also used in other parts of Europe as well. In America, Advance Mobile Phone System (AMPS) was used. The similarity between these two systems was that they were both analog.

Second generation (2G) for cellular networks started in early 1990s. The first system was introduced in Europe as Global System for Mobile Communication (GSM). It was a digital system and nowadays it is used in more than two hundred countries with around 2.5 billion users. The purpose of this system was to have same system all over the world. GSM

uses a frequency band of 900 MHz and 1800 MHz. GSM has many services like Short Messaging Services (SMS), Caller Identification, roaming etc. Enchantments were made in GSM when General Packet radio Service (GPRS) and Enhanced Data rates for GSM Evolution (EDGE) were introduced. These two systems increased the data rate in GSM. In America, CDMAone was used as a 2G technology.

Although 2G networks focused on delivering speech services, the explosion of internet connections in the home, along with increasing availability of broadband connections has created a considerable demand for wireless data services. Moreover, bandwidth intensive or high-speed applications, such as media streaming offered by YouTube and other media sharing sites, are expected to drive huge demands on wireless networks resources, as they become available in mobile devices. Once the growth in social networks, such as Facebook and MySpace, is extended to wireless networks, the multimedia sharing experience enters the next level of anytime and anywhere access to ones community.

In the third generation (3G) cellular networks, Universal Mobile Telecommunication System (UMTS) was introduced. UMTS has higher data rates as compared to GSM while it enables more services like video conferencing, wireless television and wireless broadband as well. It has been designed to achieve the goal of global coverage. In America, CDMA 2000 was used as a 3G cellular technology. CDMA operators are upgrading their networks to 1x EV-DO (1x evolution data optimized).

In last months the demand of broadband services is growing exponentially in the last years.

Many mobile operators using GSM (global system for mobile communication) are deploying UMTS (Universal Mobile Telephone System) and HSDPA (High Speed Download Packet Access). HSDPA is the downlink interface defined in the Third-generation Partnership Project (3GPP) and is capable of providing a peak user data rate of 14.4 Mbps in a 5MHz channel. The uplink interface defined by 3GPP is HSUPA (high-speed upload packet access) that supports peak data rates up to 5.8Mbps. HSDPA and HSUPA are defined together as HSPA.

1.2 Fourth Generation Cellular Networks

In parallel, other development groups within the 802 family of the Institute of Electrical and Electronics Engineers (IEEE) standards promote nomadic broadband wireless data access that have led to the the popular Wireless Local Area Networks (WLANs), 802.11b/g, and the fixed Worldwide Interoperability for Microwave Access (WiMAX) in [1] [1].

Along the path to Fourth Generation (4G) systems, even higher spectral efficiency is sought to achieve a data rate within the order of 100 Mbit/s in mobile outdoor scenarios, and 1 Gbit/s in nomadic scenarios.

The new requirements for high-speed data and seamless connectivity and smooth handoff across heterogeneous networks are the driving force

behind research into wireless networks. Thus, several techniques that enhance the spectral efficiency of systems and allow for an increased throughput with the same spectrum have received considerable attention from the research community. A fundamental feature of wireless fading channels is the dynamic random variation of the channels strengths.
In fact, multipath and mobile environments introduce fading and uncertainty in the channel, which complicates any efforts to deliver high-speed data connections. The effect of simply increasing the transmit power or of using an additional bandwidth may not be the solution to achieve a robust broadband system . Figure 2.7 represents the evolution of standards in terms of data rate and user mobility.

The fourth generation (4G) of cellular networks is currently under development and hopefully it will be available in 2012. It will be having more efficient spectral resources and other services as well.

WiMAX or Wireless Man is a 4G technology but some organizations refer it as a 3G technology. WiMAX is in implementation phase and it is the hottest wireless technology nowadays. WiMAX will be providing wireless internet anywhere and anytime.

The Institute of Electrical and Electronic Engineers (IEEE) formed a group in 1998 called 802.16. The aim of this group was develop a standard for the Wireless Metropolitan Area Network . From the first standard approved in December 2001 until now, several standards and amend-

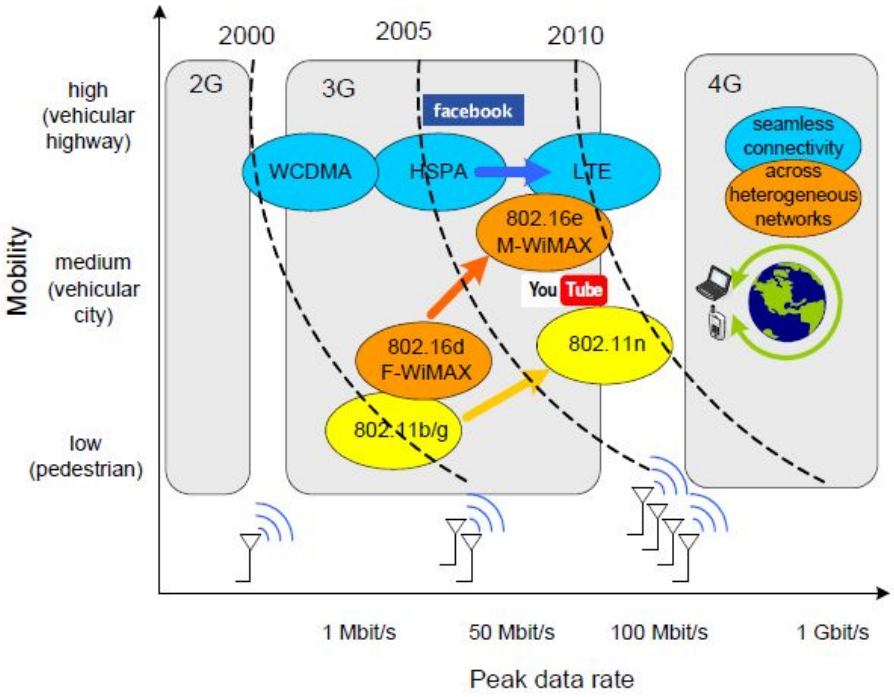

Figure 1.1. Evolution of global standard

ments has been developed. It is important to know that 802.16 is only a collection of standards that includes a wide range of variations.

The definition of the 4G systems has not yet been agreed upon and still awaits standardization and the release of spectrum, whereas evolutions of 3G systems are expected to be competitive for several years to come.

Therefore, advanced physical layer techniques are required to reduce the effect of fading in both the transmitter and receiver, without excessively increasing the systems complexity and cost.

In recent years, several spectral efficient techniques have received con-

siderable interest and support from both the research community and industry.

1.3 Mobile Broadband WIMAX

There are several wired technologies that provide us a high-speed broadband access such as Digital Subscriber Line (DSL) over twisted-pair telephone or cable over fiber optics. The main problem of these wired access technologies is the difficulty and high cost of installation and maintenance, especially in remote and rural areas.

In the last years, Internet has developed from being only an academic tool to having hundreds of millions of users around the world. Besides, the demand of a high-speed connection has caused a huge development of the broadband technologies.

As Broadband Access, wireless mobile services have grown considerably in the last years, from 11 millions of subscribers worldwide in 1990 to more than 2 billion in 2005.

This increase is due to the use of laptops, mobiles and PDAs. The main reason for the development of WiMAX (World Interoperability Microwave Access) is the demand of higher data rates not only for faster

downloading but also for the use of new applications like voice over Internet Protocol (VoIP), video streaming, multimedia conferencing, and interactive gaming.

Two very different families of WiMAX systems exist and should be treated separately: Fixed and Mobile WiMAX.

There are two different network topologies in fixed broadband wireless. The first is point-to-point applications, including interbuilding communications within a campus and microwave backhaul. The other is point-to-multipoint, usually based in a base station mounted in a tower or in a building that communicates with the subscriber.

For consumers and small business broadband, the main usage of WiMAX in the near future is broadband services like high-speed Internet access, telephony over IP (VoIP) and a host of other Internet applications.
WiMAX presents some advantages over wired technologies like lower deployment costs, lower operational costs for the maintenance, faster realization and independence of the incumbents carriers.
There are two types of deployment models, one of them requires the installation of an outdoor antenna at the costumers building and the other one requires a all-in-one radio modem installed indoors.
Using outdoor antenna improves the coverage and performance of the system; however it requires a truck-roll with a trained professional so it

implies a higher cost in developed countries but in developing countries turns to be cheaper.

The other use of Fixed WiMAX is a solution for competitive T1, fractional T1 and higher-speed services for the business market. It will be successful due to the fact that not all the buildings have access to fiber and in business exists a demand of symmetrical T1 services that cable and DSL cannot reach.

Let's consider then the usage as backhaul for Wi-Fi hotspots. They are widely deployed in public areas in developed countries. The traditional solution is using wired broadband connections to connect the hotspots back to a network point. In this case, WiMAX can be a cheaper and faster alternative for WiFi backhaul and it can also be used for 3G backhaul. WiMAX could be very successful in developing countries where a wired network is not installed. WiMAX will be a cheaper alternative to extend broadband access over the country.

In a context where the users get familiarized with the use of high-speed broadband services, they will demand same services in nomadic or mobile situations.

The first step is adding nomadic capabilities to fixed broadband connection, thus users can get connection moving within the service area with pedestrian-speed. In the market, the cellular spectrum operating licenses

are limited and very expensive so WiMAX could be a good opportunity to offer mobility services for some operators of fixed lines that do not offer mobile services. For supporting various types of media traffic, WiMAX Media Access Control (MAC) is designed from the ground up to support different types of traffic such as real time, constant bit rate, and variable bit rate traffic patterns.

Other advantages are the flexible bandwidth and multiple levels of Quality of Services (QoS) that may allow the use of WiMAX for entertainment applications. Some examples of these applications could be interactive gaming, IP-TV and streaming audio services for MP3 players. The main drawback is that the IEEE 802.16 standard only specifies an air interface so the core network has to be deployed.

- Cellular Backhaul: IEEE 802.16 wireless technology can be an excellent choice for back haul for commercial enterprises such as hotspots as well as point-to-point back haul applications due to its robust bandwidth and long range.

- Residential Broadband: Practical limitations like long distance and lack off return channel prohibit many potential broadband customers reaching DSL and cable technologies. IEEE 802.16 can fill the gaps in cable and DSL coverage.

- Underserved areas: In many rural areas, especially in developing countries, there is no existence of wired infrastructure. IEEE 802.16

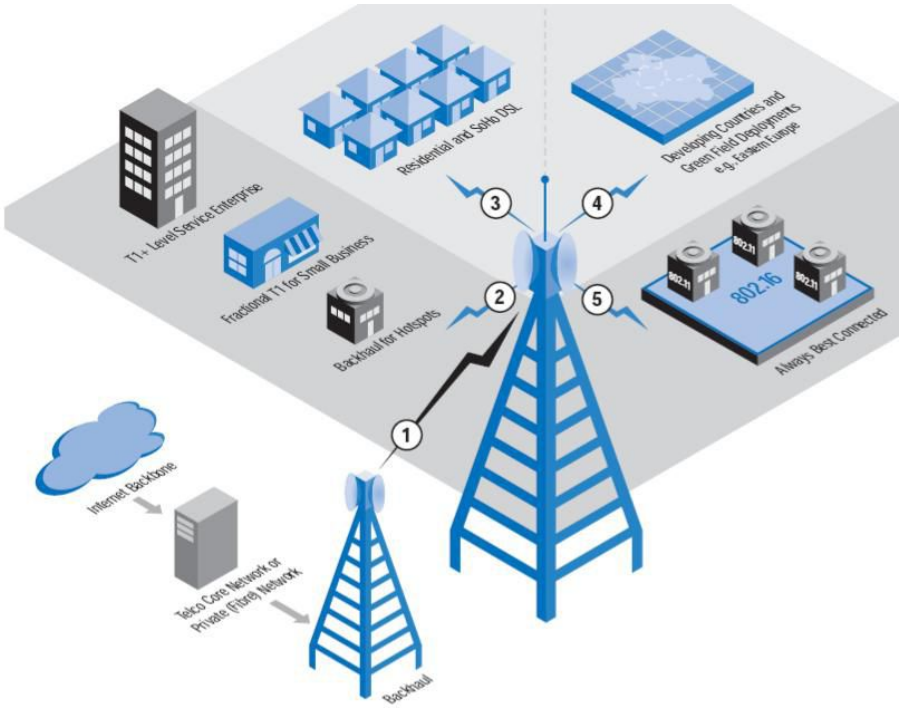

Figure 1.2. WIMAX example distribution.

can be a better solution to provide communication services to those areas using fixed CPE and high gained antenna.

- Always Best Connected: As IEEE 802.16e supports mobility , so the mobile user in the business areas can access high speed services through their IEEE 802.16/WiMAX enabled handheld devices like PDA, Pocket PC and smart phone.

1.4 Thesis Contribution

Motivated by the need to provide a greater level of adaptation to variations of wireless channels, this thesis proposes to provide an advanced model for physical layer signal processing, modulation, and coding and design MAC and joint MAC/PHY protocols for substantially enhancing data rate and reliability of wireless packet networks. Finally it is proposed a novel Adaptive Modulation and Coding based Goodput optimization

Chapter 2

Bic-OFDM transmission system for 802.16m

2.1 Introduction

The recent standardization bodies of WiMAX (Worldwide Interoperability for Microwave Access) and 3GPP/LTE (Long Term Evolution) consider radio technology such as multicarrier (MC) modulation and multiple antenna based access scheme as the corner stone to support flexible and reliable high speed packet data traffic. In particular, MC modulation, in the form of Orthogonal Frequency Division Multiplexing (OFDM), efficiently uses the available spectrum and is very robust to typical mobile radio multi-path environments. Moreover, OFDM makes feasible to exploit channel state information at the transmitter side to adapt link

resources, and thus, adaptive bit-interleaved coded modulation (BICM), space-time-frequency (STF) precoding and scheduling come in the field of vision [6].

In order to further increase the system robustness against the trouble arising from the wireless propagation channels, an efficient modulation scheme has to be combined, however, with a powerful and efficient channel coding technique. This is the case of BICM, which was first proposed in 1992 by Zehavi as a pragmatic coding scheme for bandwidth-efficient communications [23] and, later, theoretically characterized by Caire, Taricco and Biglieri in [24]. BICM technique is based on the insertion of a bit-interleaver between the channel encoder and the modulator in order to increase the diversity order. In next sections,channel characterization, transmitter and receiver model are explained.

2.2 Multipath Channel characterization

One of the main topics in a wireless communications system is the channel; and there are some factors to be considered. It is required to study all these factors of the channel to decide the amount of power necessary or the suitable modulation for a successful communication.

The radio frequency spectrum is a small part of the electromagnetic spectrum, covering the range from 3 Hz to 300 GHz.
A certain type of electromagnetic waves, called the radio waves, are gen-

erated by transmitters and received by antennas. The radio spectrum is the home of communication technologies, such as mobile phone, due to its excellent ability to carry coded information (signals). Depending on the frequency range, the radio spectrum is divided into frequency bands and sub-bands assigned for different usages.
It is crucial to have a harmonized spectrum for all regions and countries to have a suitable worldwide development for the mobile systems.

In November 2007, ITU designed the ones used by the International Mobile Telecommunications [3]:

- 450-470 MHz band frequencies to be used by IMT technologies.
- 698-862 MHz band in Region 2 and nine countries of Region 3.
- 790-862 MHz band in Regions 1 and 3.
- 2.3-2.4 GHz band frequencies to be used by IMT technologies.
- 3.4-3.6 GHz band (C Band): it is no global allocation, but accepted by many countries.

Regions and its respective countries are listed in [4].

Path loss is the reduction of density or attenuation in an electromagnetic wave as it propagates through the space. It includes the propagation losses (effects caused by the expansion of the wave in the free space), absorption losses (when signal penetrates different not transparent media), diffraction losses (when the signal is obstructed by some object

in its way), connection losses and others phenomena. Path loss is also influenced by environment (urban or rural), terrain relief, propagation medium, distance between transmitter and receptor and also the height of the antennas. The free-space path loss formula or Friis formula is:

$$P_r = P_t \frac{\lambda^2 G_t G_r}{(4\pi d)^2}$$

where P_r and P_t are the received and transmitted power respectively, λ is the wavelength, G_t and G_r are the gains of the transmitter and receiver antennas and d is the distance between them. It is more usual to use this formula in decibels units:

$$PL = 32.45 + 20\log(d[Km]) + 20\log(f(MHz)) - G_r - G_t$$

However, the terrestrial propagation environment is not free space so other factors have to be considered due to the reflections that create interference.

In wireless communications path loss can be represented by the path loss exponent n, whose valor is usually between 2 (free space) and 4 (lossy environments or flat-earth model) and a constant C measured in a fixed distance.

$$PL = 10n\log(d) + C$$

There are many other factors than can degrade the signal strength, for

example trees or buildings located between the transmitter and the receiver. Modeling all the locations and objects in the environment is impossible so the method consists in introducing a random effect called shadowing or scale-fading. Although shadowing can sometimes be beneficial, usually it modifies considerably the system performance because it requires a several dB margin to be built into the system. The empirical path loss with shadowing is:

$$P_r = P_t P_0 \chi \left(\frac{d_0}{d} \right)^{\alpha}$$

where α is the path loss exponent, P_0 is the measured path loss at a reference distance of d_0 and χ is a sample of shadowing process which is modeled as a lognormal random variable $\chi = 10^{\frac{x}{10}}$ where $x \sim N(0, \sigma_s^2)$ and $N(0, \sigma_s^2)$ is a Gaussian distribution with mean 0 and variance σ_s^2.This standard deviation is formulated in dB and its usual values are in the range 6-12 dB. The other tremendous effect that degraded wireless communication quality is the so called fading. Fading is caused by the reception of multiple versions of the same signal due to reflections in the path that are referred to as multipath. In the receiver several signals with different attenuation, phase and delay arrive. The interference caused can be constructive or destructive depending on the phase difference of the arriving signals. This effect can be dramatic even if only moving a very short distance the transmitter or the receiver. Fading is a very relevant effect in urban areas with high population density and indoors.

The characterization of a radio-mobile channel can be given by some parameters. Number of paths $N(t)$ at instant t, the amplitude $\alpha_n(t)$, the delay $\tau_n(t)$ and phase $\phi_n(t)$ of n-th path (these are independent random processes). The channel is modeled as a time-variant linear system:

$$c(t,\tau) = \sum_{n=0}^{N(t)} \alpha_n(t) e^{-j\phi_n(t)} \delta(\tau - \tau_n(t))$$

where τ represents l'intervals between the applied impulse and the observation instant t An important parameter which have to take into account is delay spread:

$$T_m = \max_n |\tau_n - \bar{\tau}|$$

The delay spread T_m measures the amount of time that elapses between the first arriving path and the last arriving path. In the frequency domain the measurement unit is the coherence bandwidth ($B_c = 1/T_m$), which measures the minimum separation in frequency after which two signals will experience uncorrelated fading. Flat fading channels ($B_c < B, or T_m \ll T$), with$B$ the signal band, occur when the coherence bandwidth is larger than the original of the signals. All frequency components will have the same magnitude of fading.

Frequency-selective fading channel ($B_c > B$) is defined when the coherence bandwidth is smaller than the original of the signal, so the frequency components will experience different magnitudes of fading.

When a user or some of the reflectors in the path are moving and this user's velocity causes a shift in the frequency of the signal, is called the

Doppler effect spread. Depending on the Doppler shift there are two kinds of fading; fast and slow fading. Doppler spread f_d, gave by the following formula, depends on the carrier frequency f_c, speed of the light c and the maximum speed between the transmitter and the receiver$v$:

$$f_d = \frac{v f_c}{c}$$

This measurement unit in the frequency domain is the coherence time ($T_c = 1/f_d$) which is a measure of the minimum time required for the magnitude change of the channel to become uncorrelated from its previous value. It has to be compared with the symbol time.
The terms slow and fast fading refer to the rate at which the magnitude and phase change imposed by the channel on the signal changes.

Fast fading ($f_d \gg 1, or, T_c \leq T$) consists of fast variations of the amplitude, phase and a Doppler shift while the transmitter or receiver is moving or the environment is changing. This fading is produced every fraction of wavelength (λ) of motion.

Slow fading ($f_d \leq 1, or, T_c \gg T$) consists of the small changes in the amplitude of the signal caused by the motion of a transmitter or receiver when they are moving a distance of more than ten times the wavelength.

A generalized formulation of transmitted and received signal (without noise addiction) is given by:

$$s(t) = \Re(r(t)e^{j2\pi f})$$

$$r(t) = \mathrm{Re}\left\{ \sum_{n=1}^{N(t)} \alpha_n(t)\, u(t - \tau_n(t))\, e^{j(2\pi f_c(t-\tau_n(t)) + \phi_{D_n})} \right\}$$

$$= \mathrm{Re}\left\{ \left[\sum_{n=1}^{N(t)} \alpha_n(t)\, e^{-j\phi_n(t)} u(t - \tau_n(t)) \right] e^{-j2\pi f_c t} \right\}$$

The phase shift related to every path due to relative delay and Doppler effect is:

$$\phi_n(t) = 2\pi f_c \tau_n(t) - \phi_{D_n}$$

In all thesis work, it's considered packet transmission. Hence is proper to use slow fading frequency selective channel, described by:

$$r(t) = \mathrm{Re}\left\{ a(t) s(t)\, e^{j2\pi f_c t} \right\}$$

in which $a(t)$ is a zero mean gaussian process with independent real and imaginary parts, with spectral density dependent on v, as suggested by Clarke using central limit theorem, with high number of N different path. We assume that $a(t)$ is constant is symbol interval or during packet transmission time so:

$$r(t) = \mathrm{Re}\left\{ a s(t)\, e^{j2\pi f_c t} \right\}$$

where a is complex coefficient, constant for 1 packet:

$$a = \rho e^{j\phi} = e^{-j2\pi f_c \tau} \sum_{n=1}^{N} a_n$$

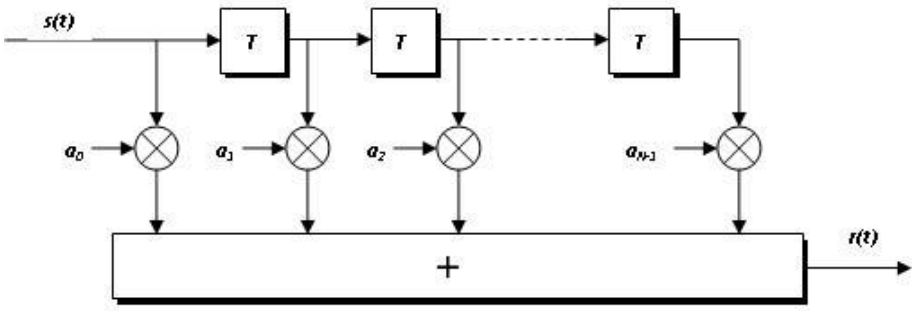

Figure 2.1. Tapped delay line channel

If $a = \rho e^{-j\phi}$ andϕ is an uniform random variable in $[0, 2\pi]$, ρ for our scenario can be studied statistically with probability functions like Rayleigh:

$$p(\rho) = \frac{\rho}{\sigma^2} \exp\left(\frac{-\rho^2}{2\sigma^2}\right)$$

In simulation environment, the channel model used is block-fading, frequency selective time-varying. The so called "tapped-delay line model" is expressed by the following formula, where is used the base band expression :

$$r\left(t\right) = \sum_{n=0}^{N-1} a_n s\left(t - nT\right)$$

Figure 2.1 represents the scheme of a Tapped delay line channel with input the transmitted signal s(t) ad output the received signal

Generally for radio-mobile scenario analysis, the variances $\sigma_n^2 \triangleq E\left\{|a_n|^2\right\}$ of distortion coefficients a_n of power-delay profiles are fixed, considering delays of N multipath channel independents. The profiles are standardized and referred to typical scenario such as Typical Urban (TU), Hilly Terrain (HT), Rural Area (RA), etc. This is sufficient in case which slow fading is represented, on the contrary would be modeling variances as random variables and not as deterministic values.

In broadband fading, frequency-selective fading causes dispersion in time or intersymbol interference (ISI), meaning that one symbol interferes with the following symbol.

Equalization is a technique for mitigate those drawbacks. The first type is linear equalization which consists of running the received signal through a filter that models the inverse of the channel. The other one is the nonlinear equalization that uses previous symbol decisions made by the receiver to cancel their subsequent interference.

The other technique,widely implemented nowadays is modulation OFDM (Orthogonal Frequency-Division Multiplexing),which is the best method to overcome ISI and it is based on the multicarrier concept. It consists of rather than sending a single signal with data rate R and bandwidth B, sending L signals with data rate R/L and bandwidth B/L. OFDM will be explained in the next section.

2.3 OFDM

Orthogonal frequency division multiplexing is a multicarrier technique [5], which splits the system bandwidth into orthogonal subchannels 2.2, each of which occupies only a narrow bandwidth and a separate subcarrier is assigned to each. Since the bandwidth of a single subchannel is generally smaller than the radio channels coherence bandwidth, it can be treated as a flat fading channel.

A unique stream with sampling rate $1/T$, is splitted in N parallel subcarriers with signaling interval $T_s = NT$. The orthogonality requires that the sub-carrier spacing is $\Delta f = k/(NT)$ Hertz, where NT seconds is the useful symbol duration (the receiver side window size), and k is a positive integer, typically equal to 1. Therefore, with N sub-carriers, the total passband bandwidth will be$B \approx N \cdot \Delta f(\text{Hz})$. In the typical modulation scheme 2.3

the output signal $x(t)$ is expressed as:

$$x\left(t\right) = \sum_{m=-\infty}^{+\infty} \sum_{k=0}^{N-1} c_k^{(m)} p\left(t - mT_s\right) e^{j2\pi f_k t}$$

with $c_k^{(m)} \in \{0, 1\}$

$$p\left(t\right) = \begin{cases} 1 \rightarrow for \ 0 \leq t \leq T_s \\ 0 \rightarrow else \end{cases}$$

$$E\left\{\left|c_k^{(m)}\right|^2\right\} = 1$$

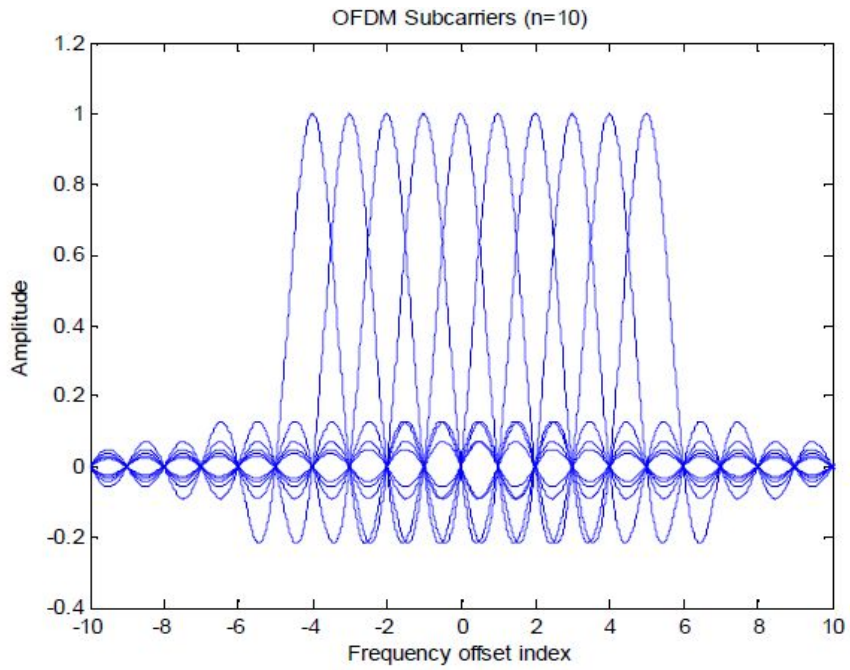

Figure 2.2. OFDM subchannels.

The optimal demodulator consists in base band conversion and matched filter for each subcarriers 2.4

$$z_k^{(0)} = \frac{1}{T_s} \int_0^{T_s} r\left(t\right) e^{-j2\pi f_k t} d$$

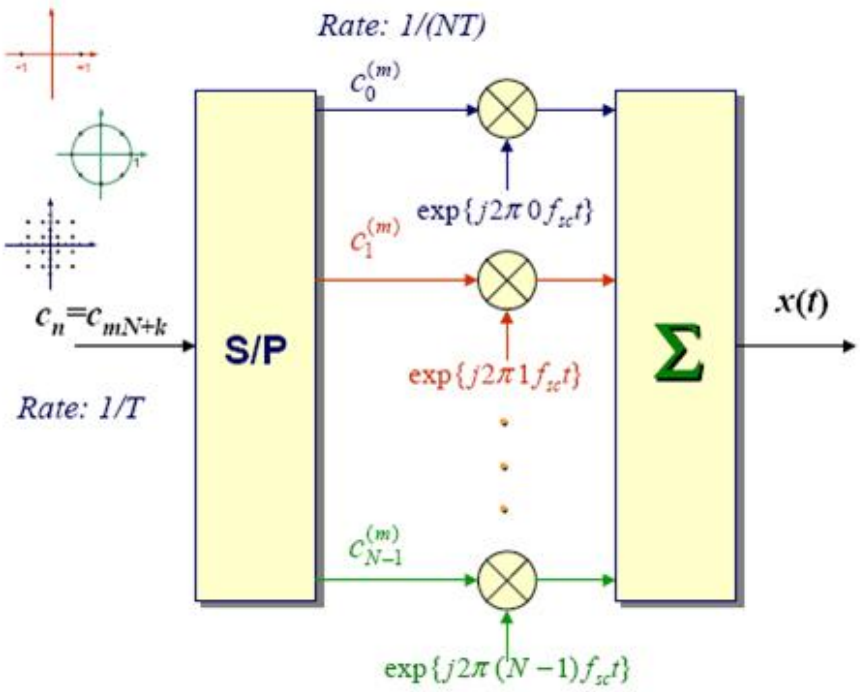

Figure 2.3. OFDM modulation scheme.

If we use the orthogonality condition $\Delta f = k/(NT)$ the OFDM signal is

$$x(t) = \sum_{m=-\infty}^{+\infty} \sum_{k=0}^{N-1} c_k^{(m)} p(t - mT_s) e^{j2\pi kt/T_s}$$

The orthogonality also allows high spectral efficiency, with a total symbol rate near the Nyquist rate. Almost the whole available frequency band can be utilized. OFDM generally has a nearly 'white' spectrum 2.5,

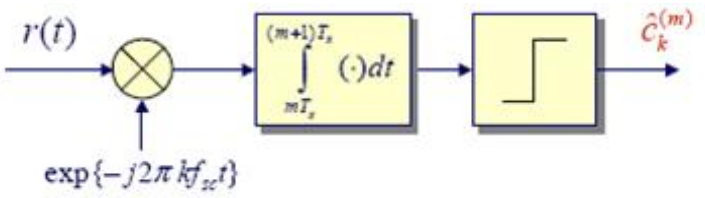

Figure 2.4. OFDM demodulation scheme.

giving it benign electromagnetic interference properties with respect to other co-channel users.

A technique to control aliasing effects is the usage of virtual subcarriers N_v, where the transmitted symbols are all 0 . The signal band now is not $1/T$, but $(N - N_v)/NT$), so the lateral lobes do not interfere with center band region of spectrum. The OFDM signal Power Spectral Density (PSD) is:

$$S_x(f) = \sum_{k=0}^{N-1-N_v} S(f - k/T_s)$$

An efficient implementation of OFDM system include IFFT and FFT blocks. It's immediate to demonstrate because the sampled version of $x(t)$ signal, $x(nT)$ or $x[n]$ with $0 \leq n \leq N-1$, considering only the first symbol, is:

$$x[n] = \frac{1}{\sqrt{N}} \sum_{k=0}^{N-1} c_k^{(0)} e^{j2\pi kn/N}$$

and the received sampled version is:

$$z_k^{(0)} = \frac{1}{\sqrt{N}} \sum_{n=0}^{N-1} r[n] e^{-j2\pi kn/N}$$

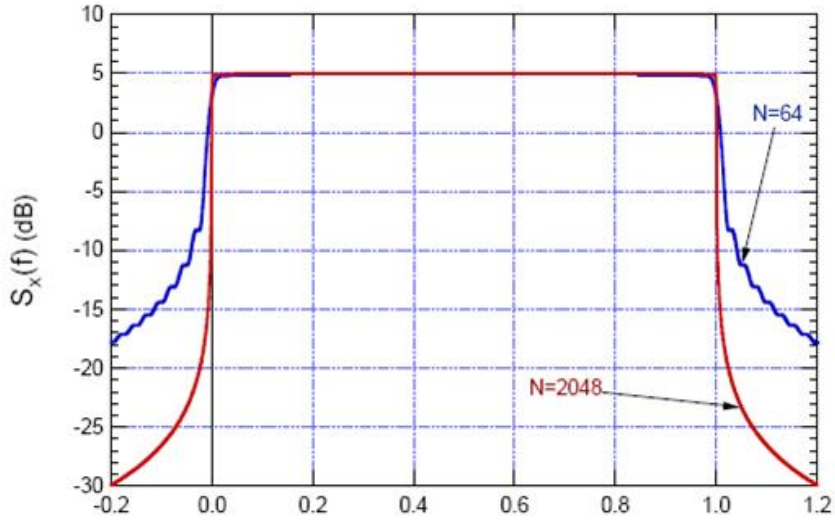

Figure 2.5. OFDM Power Spectral Density.

During the guard interval T_g, where $T_g \geq T_h$ and T_h the duration if channel impulsive response, a Cyclic Prefix (CP) is sent and usually the CP has the same length as the guard interval.

The CP consists of the end of the symbol placed in the beginning of new symbol, as can be seen in 2.6 The task of the CP is to settle the echoes form multipath propagation before the actual data ca be processed.There are also other benefits while using the CP. For example, inter-block inter-

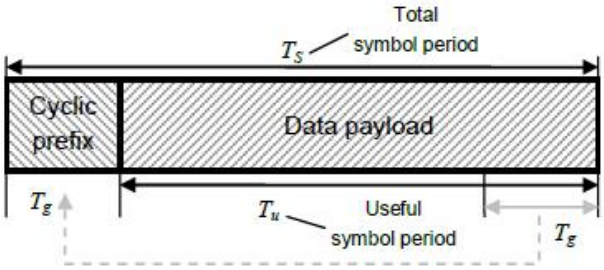

Figure 2.6. Cyclic Prefix description.

ference (hence, the interference between symbols n and $n+2$) is preventer and the channel seems circular.

In addiction, low-complexity frequency domain equalization is allowed. A negative aspect with the use of CP is the extra overhead needed and therefore the bandwith efficiency is affected. However, the channel bandwith can be used in an efficient way for data transmission since the OFDM; spectrum fades fast outside the actual window containing the carriers.

It is also important to keep the CP length defined by the Base Station (BS) during initialization, since the change of it would force all other Mobile Station (MS) to resynchronized. So, we obtain at the input of channel a pseudo-periodic signal un T_s period, of wich Fourier coefficient are , for

$$0 \leq t \leq T_s$$

,

$$x\left(t\right) = \sum_{k=0}^{N-1} c_k^{(0)} e^{j2\pi kt/T_s}$$

$$X_k = c_k^{(0)}$$

with

$$k = 0, 1, ..., N-1$$

, and also the decision varialbel out of FFT block, without termal noise

$$z_k^{(0)} = Y_k = c_k^{(0)} H\left(\frac{k}{T_s}\right) e^{j2\pi k\varepsilon/N}$$

in which εT_s is synchronism error. The max of this error is the maximum error tolerable.

2.4 SISO Bit Interleaved Coded OFDM

Bit-Interleaved Coded Modulation (BICM) has become a topic of significant research efforts in recent years. This interest has lead to the development of novel, practical, and robust transmission techniques through a number of papers on various topics and techniques related to BICM. The use of a bit-interleaver has a crucial role in this system. Zehavi (cit) has demonstrated that in a Rayleigh fading channel, there are better performances in a coded-modulation system. He preposed BICM as a pragmatic coding scheme for spectrally efficient modulations. Theoretical approach is given by Caire et al (cit). They suggested that system essentilly behaves as a memoryless binary input-output symmetric channel (BIOS) under the assumption of ideal interleaver.

2.4.1 Radio link control MAC and PHY

The BIC-OFDM system preserves mostly the originary OFDM architecture with a bit-interleaver between the coder and modulator. A frame OFDM is called packet of data. A packet defined as the fundamental piece of information to be communicated over the radio interface.

It is expected that, in the future, transport of Internet protocol (IP) packets will dominate the traffic in the wireless systems. Thus, a packet tipically corresponds to an IP packet. However, a packet could also correspond to other kinds of information to be communicated over the radio interface (e.g. Layer 3 control signaling). As proposed in [6], we assume a one-to-one mapping of packets to retransmission units of the RLC protocol (RLC-PDU). Each RLC-PDU is characterized by a sequence number, the corresponding payload and the cyclic redundancy check (CRC).

RLC-PDU of N_b "information bits" (actually including also RLC-PDU overhead) is transmitted through L consecutive OFDM symbols, denoted in the sequel as *frame*.

2.4.2 System Design

The information bits are first encoded using a convolutional code with rate R and free distance d_{free} and then randomly interleaved. The total number of coded binary symbols that are generated by encoding the RLC-PDU is thus $N_c \triangleq N_b/R$. Code diversity gain depends only on

Hamming distance. The bit-level interleaver randomly maps the generic coded binary symbol b_k into one of the label bits carried by the symbols of the OFDM subcarriers according to the notation shown below

$$b_k \rightarrow c_{\Pi(k)} \tag{2.1}$$

where $\Pi(k) \triangleq \{l_k, n_k, i_k\}$ is the interleaver operation that maps the index k of the coded binary symbol into a set of four coordinates: l_k denotes the position of the OFDM block within the frame, n_k denotes the position of the subcarrier within the OFDM spectrum, and i_k denotes the position of the binary coded symbol within the label of the modulation symbol allocated into such subchannel. The interleaver is assumed to be fully random so that the probability of mapping the generic coded binary symbol b_k (taken out of the available N_c) into the ith label bit, of the symbol transmitted on the subchannel n, into the lth OFDM block, denoted as $c_{l,n,i}$, with $l = 1, \ldots, L$, $n = 1, \ldots, N$, and $i = 1, \ldots, m^n$, is

$$\Pr\{b_k \rightarrow c_{l,n,i}\} \triangleq \frac{1}{N_c}, \tag{2.2}$$

where m^n denotes the number of bits transmitted on the subchannel n.

The interleaved bits are then Gray mapped into QAM symbols.

The $M^{(n)}$-QAM signal set used in the subcarrier n is defined as $\chi^{(n)} \triangleq \left\{\xi^{(n)}, \cdots, \xi^{(n)}_{M^{(n)}}\right\}$ with $M^{(n)} \triangleq 2^{m^{(n)}}$ Gray mapping plays a key role in BICM theory. The definition of Gray labeling begins from supposing ξ as signal set with minimum Euclidean distance d_min. A binary map

$$\mu : \{0,1\}^m \rightarrow \chi$$

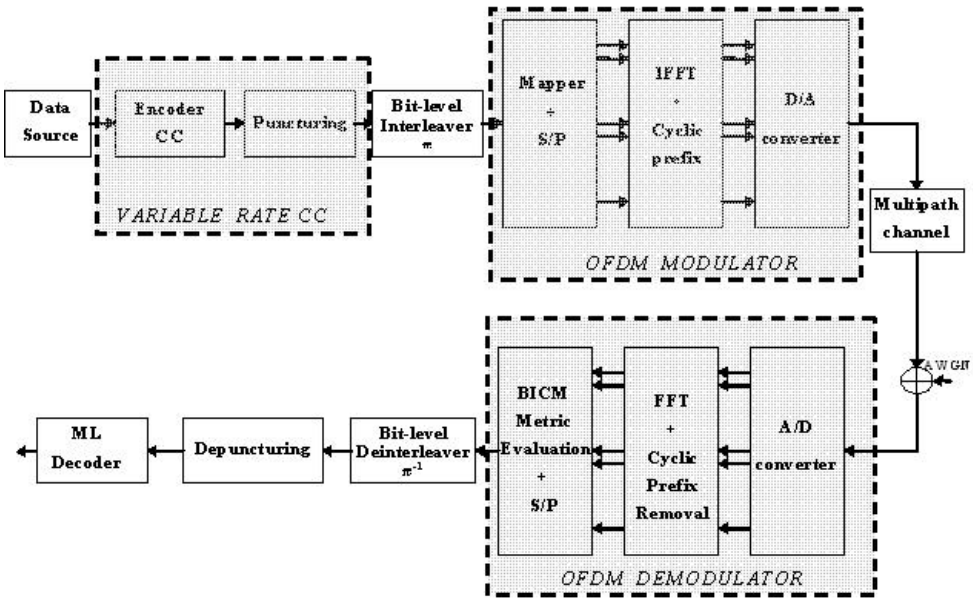

Figure 2.7. BIC-OFDM system.

is a Gray labeling for χ if, for all $i = 1, \ldots, m$, and $b \in \{0, 1\}$, each $x \in \chi_b^i$ has at most one $z \in \chi_b^i$ at distance $d_m in$ An example is 2.8:

The symbols are suitably normalized such that

$$\bar{\xi}^2 \triangleq \sum\nolimits_{\nu=1}^{M^{(n)}} \left|\xi_v^{(n)}\right|^2 / M^{(n)} = 1$$

The generic QAM data-bearing symbol $x_l^{(n)}$, belonging to the set $\chi^{(n)}$ is sent on the nth subcarrier during the lth OFDM block, and

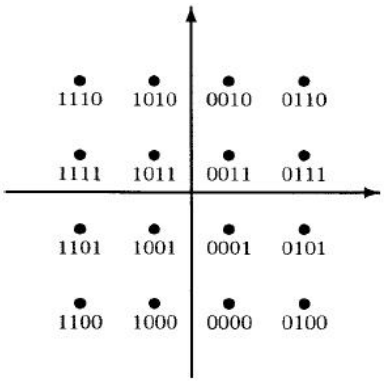

Figure 2.8. 16 QAM constellation with Gray mapping

$E_{x_l^{(n)}}\left\{\left|x_l^{(n)}\right|^2\right\} = \bar{\xi}^2 = 1$. We consider uniform bit-loading, so every subcarriers have same number of bit. The average transmit power allocated to the generic nth subcarrier is $P^{(n)} \triangleq p^{(n)}S$ where $p^{(n)}$ is a normalized power coefficient $0 \leq p^{(n)} \leq 1$ so that the constraint on the average transmit power per subcarrier is expressed by

$$\bar{P} \triangleq \frac{\sum_{n=1}^{N} P^{(n)}}{N} \leq S$$

where S is the maximum value of the average power which can be allocated to every subcarrier. By replacing the definition of P(n), we obtain also the following constraint on the normalized power

$$\sum_{n=1}^{N} p^{(n)} \leq N$$

The data-bearing QAM symbols are frequency mapped into the N available subcarriers using an Inverse Discrete Fourier Transform (IDFT) unit,

which provides one sample every T_s seconds. A conventional CP, whose length is $N_c p$ samples, is inserted at the beginning of each IDFT output block to maintain the subcarriers orthogonal with each others and avoid interference between successive symbols. The resulting OFDM signal experiences a frequency selective fading channel and channel stationarity during the whole packet duration, like said previously. At the receiver side, the samples are collected into blocks of size $N + N_c p$. After CP removal, they are transformed by a DFT unit of size N and demodulated. Let us focus now on the transmission of the coded binary symbol b_k. According to the notations outlined above, the binary coded symbol is included into the label of the QAM symbol $x_{l_k}^{(n_k)} \in \chi^{(n)}$. The expression of the sample relevant to the n_kth subcarrier in the l_kth OFDM block at the output of the DFT unit of the receiver is

$$z_{l_k}^{(n_k)} = A^{(n_k)} x_{l_k}^{(n_k)} + w_{l_k}^{(n_k)}$$

$$A^{(n_k)} = \sqrt{P^{(n_k)}} H^{(n_k)} = \sqrt{p^{(n_k)} S} H^{(n_k)}$$

while $H^{(n_k)}$ is the complex-valued channel gain experienced on the nkth subcarrier, and $w_{l_k}^{(n_k)}$ is a zero-mean unit-variance (i.e. $\sigma_n^2 \triangleq E\left\{\left|w_{l_k}^{(n_k)}\right|^2\right\}$) complex-valued Gaussian random variable (RV) representing the channel noise contribution on the n_kth subcarrier. If $A^{(n_k)}$ is perfectly known at the receiver (perfect CSI), bit per bit soft bit metrics are computed knowing $z_l^{(n)}$, and a Maximum likelihood decoding in Viterbi

decoder is done. The optimum metric is (cit)

$$\lambda^{(i,n)}\left(z_l^n, b\right) = \log \sum_{\tilde{x} \in \chi_b^{(i,b)}} p\left(z_l^n \left| x^{(n)} = \tilde{x}, A^{(n)}\right.\right)$$

where $\chi_b^{(i,b)}$ is a subset of $\chi^{(n)}$ with label $b \in \{0, 1\}$ with $i - th$ position of bit in label for $n - th$ subcarrier. An example of subsets is in 2.9:

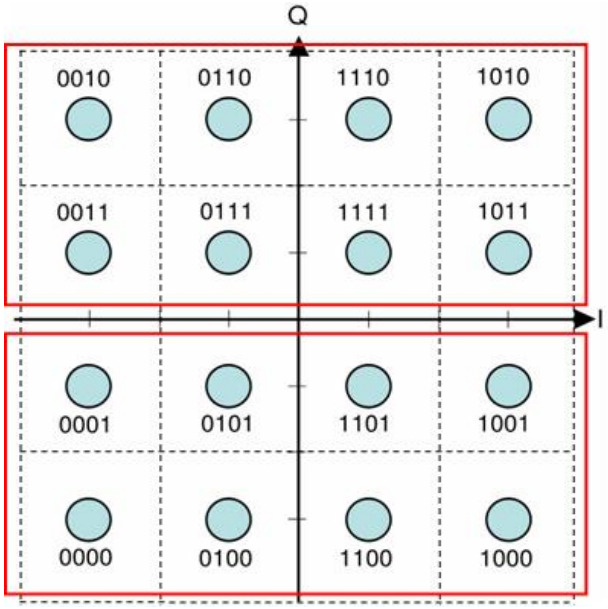

Figure 2.9. subset 16 QAM example

When there are high Signal-to-Noise Ratio (SNR), we could substitute the above expression with

$$\lambda^{(i,n)}\left(z_l^n, b\right) = \max_{\tilde{x} \in \chi_b^{(i,b)}} \log p\left(z_l^n \left| x^{(n)} = \tilde{x}, A^{(n)}\right.\right)$$

where the dominant term is sum is the nearest symbol according to Euclidean distance. The metrics come to deinterleaver, before being used by

Viterbi Decoder, which does the ML decisions, and gives the estimation of real transmitted information sequence

$$b = \arg\min_{b \in C} \sum_{k=1}^{N_C} \lambda^{(i_k, n_k)} \left(z_{l_k}^{(n_k)}, b_k \right)$$

where b is a code sequence of N_c dimension. The univocal correspondence between data and code sequence is possible if the start and final state of convolutional coder are known(i.e. zero). An example of convolutional encoder is 2.10, and is the used one for simulation made in thesis work. It's correspond a non-systematic, not feedforward,$d_free = 10$, $R = 1/2$

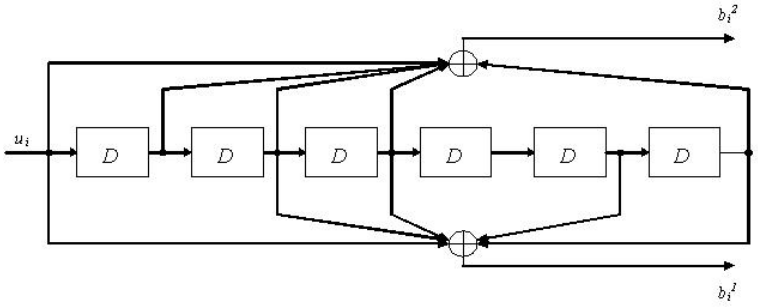

Figure 2.10. Convolutional Encoder

with 6 shift register, 64 state, and code generator

$$g_1 = 133_8 = 1011011$$

$$g_2 = 171_8 = 1111001$$

Adaptivity in modern and future systems is a corner stone. For example a flexible system adapts itself changing the coding rate since is a convenient

solution. However it's not practical having different convolutional coder parallel in a transmission system. So a smart solution is the so called puncturing. The assumption made is also very simple. After the coder, only a subset of coded bits are transmitted, therefore the code rate is increased and the decoder structure is the same as before.

If short-memory codes are used, with $R_c = 1/2$, good performances are achieved, as proved in literature [7]. According to 802.16e, punctured code is expressed by perforation matrix,

Code Rate	Puncturing Matrix	d_{free}
1/2	$\mathbf{P} == \begin{bmatrix} 1 \\ 1 \end{bmatrix}$	10
2/3	$\mathbf{P} == \begin{bmatrix} 1 & 1 \\ 1 & 0 \end{bmatrix}$	6
3/4	$\mathbf{P} == \begin{bmatrix} 1 & 1 & 0 \\ 1 & 0 & 1 \end{bmatrix}$	5
5/6	$\mathbf{P} == \begin{bmatrix} 1 & 1 & 0 & 1 & 0 \\ 1 & 0 & 1 & 0 & 1 \end{bmatrix}$	4

Table 2.1. Puncturing Matrices.

where values $0, 1$ stand for suppressed bit or not, and the raw elements are the puncturing mask applied in CC output. In decoder the punctured bits are taken into account inserting dummy bit equal to zero in received packet in position corresponding to zeros in perforation matrix. The decoding is made starting from mother code where punctured symbol code metrics are discharged instead being added to best path sum. The advantage between BIC-OFDM system and traditional OFDM is depicted in 2.11

The parameters of simulated system in 6-tap channel in TAB.

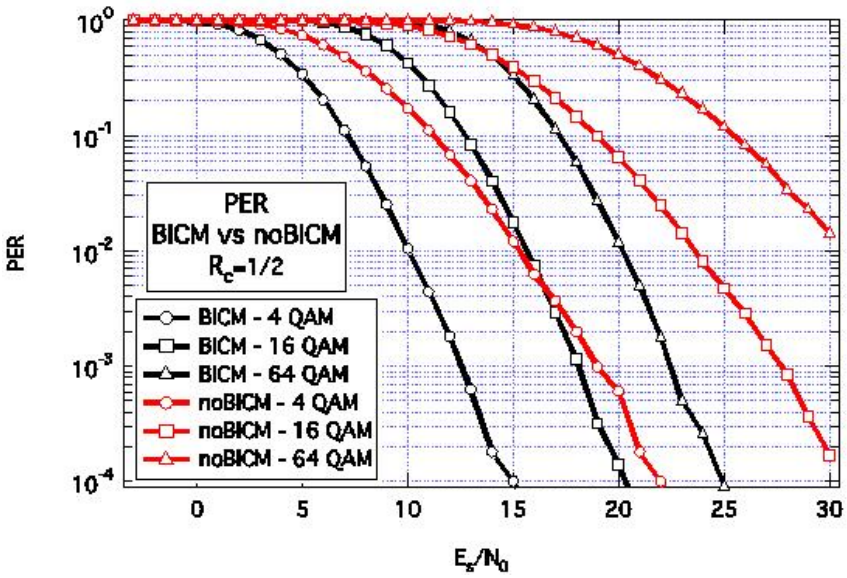

Figure 2.11. BIC-OFDM vs noBICM-OFDM comparison.

Power (dB)	-3.3	0	-1	-1.5	-3	-9.4
Delay (ns)	0	50	100	200	250	600

Table 2.2. channel profile.

The number of transmitted packet for each E_s/N_0 is 100000, therefore we could have a good accuracy of Packet Error Rate (PER) up to 10^{-3}.

Mode	Modulation	Code Rate
1	4	1/2
2	4	3/4
3	16	1/2
4	16	3/4
5	64	1/2
6	64	2/3
7	64	3/4
8	64	5/6

Table 2.3. Supported MCS.

	testcase
Number of used subcarrier	64
Convolutional mother code Rate	1/2
System Channel Bandwidth (MHz)	20
Subcarrier Spacing (KHz)	312.5
Cyclic Prefix (μs)	0.8
OFDM Symbol Duration (μs)	4
Data Packet Lenght (bit)	1024
Maximum Delay Spread (μs)	0.6
Doppler frequency (Hz)	100

Table 2.4. Main Parameters of OFDM Modulation for different testcases.

2.5 MIMO

Multiple input multiple output (MIMO) technology is a key breakthrough in wireless communication. By using multiple antennas, MIMO technology multiplies throughput without requiring additional frequency bandwidth, enhances link reliability through spatial diversity and enlarges the coverage area by increasing the transmission range. These features have

motivated extensive research on developing MIMO theory and techniques in the last decade.

In literature, first works on MIMO tecniques were [20], [18] [21]. They predicted high spectral efficiency for wireless systems by using more than 1 receiving and transmitting antennas. Those gains needs an accurate channel state information at transmitter, and also sometimes at receiver. It means more costs, occupied space and power, all included in small mobile handheld terminal. In this thesis work, the simulated MIMO technique are SM with MMSE receiver and STBC with Maximum Ratio combining receiver,which are described in next sections.

2.5.1 Parallel Gaussian Channel model. Post-processing SNR computation

MIMO-OFDM system could be represent by a set of parallel gaussian subchannels where per-channel SNRs depend on the particular STC considered. Per-channel post processing SNRs for each considered MIMO scheme are computed, so a unified helpful analysis is used in definition of a comprehensive link performance model.

Using same notations outlined above, after interleaving and modulation mapping, the binary coded symbol is included into the label of the QAM symbol $x_{l_k}^{(n_k,q_k)}$. The goal is to express the sample relevant to the subchannel (n_k, q_k) in the l_kth OFDM block at the output of the DFT unit

of the receiver as

$$z_{l_k}^{(n_k,q_k)} = A^{(n_k,q_k)} x_{l_k}^{(n_k,q_k)} + w_{l_k}^{(n_k,q_k)}, \tag{2.3}$$

where $A^{(n_k,q_k)}$ is the post-processing channel gain experienced on the subchannel (n_k, q_k) and $w_{l_k}^{(n_k,q_k)}$ is a Gaussian RV with variance ${\sigma_w^{(n_k,q_k)}}^2$,, which represents, in general, the noise plus interstream interference contribution on the (n_k, q_k) subchannel. The istantaneous post processing SNR values relevant to the generic subchannel (n, q) is then defined as

$$\gamma^{(n,q)} \triangleq \left(\frac{|A^{(n,q)}|}{\sigma_w^{(n,q)}} \right)^2 \tag{2.4}$$

Resorting to a vectorial notation, the I/O relationship relevant to the n_kth subcarrier of the l_kth MIMO-OFDM block can be expressed as

$$\mathbf{z}_{l_k}^{(n_k)} = \mathbf{A}^{(n_k)} \, \mathbf{x}_{l_k}^{(n_k)} + \mathbf{w}_{l_k}^{(n_k)} \tag{2.5}$$

where $\mathbf{A}$ is a complex diagonal matrix defined as $\mathbf{A}^{(n_k)} \triangleq \mathbf{D}(A^{(n_k,1)}, \cdots, A^{(n_k,N_s)})$, while the noise vector is $\mathbf{w}_{l_k}^{(n_k)} \triangleq [w_{l_k}^{(n_k,1)}, \cdots, w_{l_k}^{(n_k,N_s)}]^T$.

MIMO techniques are divided in 2 different categories: Open-Loop and Closed-Loop. In first case the transmitter does not know channel coefficients, differently form latter case. Open-Loop include Space-Time-Coding (STC),in particular Space-Time-Block-Coding (STBC) and Spacial Multiplexing (SM), named in WiMAX respectively Matrix A and Matrix B. Closed-loop include Eigen-Beamforming technique based on channel Single-Value-Decomposition (SVD).

Both Alamouti STBC [22] and Spatial Multiplexing with MMSE techniques, are easily implemented with simple spatial processing that does not require channel state information at the transmitter side. Therefore, in the sequel, these schemes are supposed operating with a uniform power allocation strategy.

2.5.2 Alamouti STBC, Matrix A

For the Alamouti scheme shown in figure 2.12, on each subcarrier, a single modulated symbol per OFDM symbol period is transmitted (i.e. $N_s = 1$), and maximum ratio combining is applied at the receiver. The I/O relation relevant to the n_kth subcarrier in the l_kth MIMO-OFDM block can be equivalently rewritten as[1]

$$\mathbf{z}_{l_k}^{(n_k)} = \sqrt{S}\ ||\mathbf{H}^{(n_k)}||_F^2\ \mathbf{x}_{l_k}^{(n_k)} + \mathbf{w}_{l_k}^{(n_k)}, \tag{2.6}$$

where $\mathbf{w}_{l_k}^{(n_k)}$ is a 1-dimensional Gaussian noise vector with variance $||\mathbf{H}^{(n_k)}||_F^2$. From 2.4 and 2.6 it is straightforward to derive the post processing channel gain matrix

$$\mathbf{A}^{(n)} = \sqrt{S}\ \mathbf{D}\left(\|\mathbf{H}^{(n)}\|_F^2\right) \tag{2.7}$$

[1]For the sake of notation uniformity with the SM case, the I/O scalar relationship is written as a vectorial equation

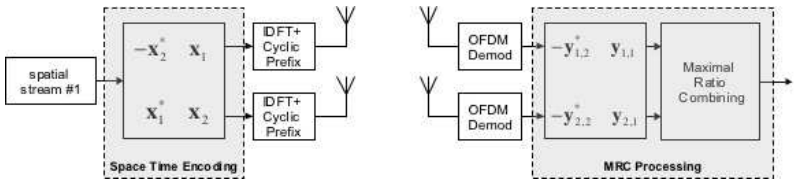

Figure 2.12. Alamouti Scheme.

2.5.3 Spatial Multiplexing with MMSE receiver, Matrix B

For SM scheme shown in figure 2.13, N_t modulated symbols are transmitted during each OFDM symbol period. Among the various linear processing techniques which can be applied to the received signal vector, we focus on the MMSE and ZF strategies, wherein [29] the received symbol vector is multiplied the following matrices

$$\mathbf{W}^{(n_k)} = \mathbf{H}^{(n_k)^H} \left(\mathbf{H}^{(n_k)} \mathbf{H}^{(n_k)^H} + \sigma_n^2 \frac{N_t}{P_t} \mathbf{I}_{N_r} \right)^{-1} \tag{2.8}$$

and

$$\mathbf{W}^{(n_k)} = \mathbf{H}^{(n_k)^H} \left(\mathbf{H}^{(n_k)} \mathbf{H}^{(n_k)^H} \right)^{-1} \tag{2.9}$$

for MMSE and ZF, respectively. In this case, the I/O relationship relevant to the n_kth subcarrier in the l_kth MIMO-OFDM block can be expressed as

$$\mathbf{z}_{l_k}^{(n_k)} = \sqrt{S}\, \mathbf{W}^{(n_k)} \mathbf{H}^{(n_k)}\, \mathbf{x}_{l_k}^{(n_k)} + \mathbf{W}^{(n_k)} \mathbf{n}_{l_k}^{(n_k)}, \tag{2.10}$$

which, for the MMSE receiver, can be rewritten as

$$\begin{aligned} \mathbf{z}_{l_k}^{(n_k)} = {} & \sqrt{S}\, \mathbf{D} \left(\mathbf{W}^{(n_k)} \mathbf{H}^{(n_k)} \right) \mathbf{x}_{l_k}^{(n_k)} \\ & + \sqrt{S} \left[\mathbf{W}^{(n_k)} \mathbf{H}^{(n_k)} - \mathbf{D} \left(\mathbf{W}^{(n_k)} \mathbf{H}^{(n_k)} \right) \right] \mathbf{x}_{l_k}^{(n_k)} + \mathbf{W}^{(n_k)} \mathbf{n}_{l_k}^{(n_k)} \end{aligned} \tag{2.11}$$

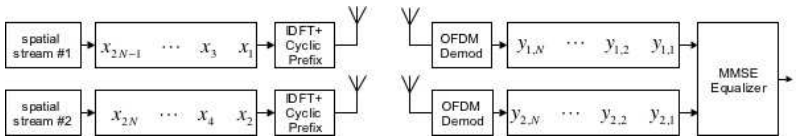

Figure 2.13. Spatial Multiplexing with Linear Receiver.

The output is then affected by a colored noise plus inter-stream interference. In order to simplify the following analysis, the interference is approximated as additive Gaussian noise as proposed in [37], so that the covariance matrix of the overall noise $\mathbf{w}_{l_k}^{(n_k)} \triangleq \mathbf{W}^{(n_k)}\mathbf{n}_{l_k}^{(n_k)}$ results

$$\mathbf{R}^{(n_k)} = S\left[\mathbf{W}^{(n_k)}\mathbf{H}^{(n_k)} - \mathbf{D}\left(\mathbf{W}^{(n_k)}\mathbf{H}^{(n_k)}\right)\right] \left[\mathbf{W}^{(n_k)}\mathbf{H}^{(n_k)} - \mathbf{D}\left(\mathbf{W}^{(n_k)}\mathbf{H}^{(n_k)}\right)\right]^H + \sigma_n^2\mathbf{W}^{(n_k)}\mathbf{W}^{(n_k)H}, \quad (2.12)$$

while the post processing channel gain matrix is given by

$$\mathbf{A}^{(n)} = \sqrt{S}\,\mathbf{D}\left(\mathbf{W}^{(n)}\mathbf{H}^{(n)}\right) \quad (2.13)$$

2.5.4 SVD based precoding, Open Loop

SVD precoding/decoding. Assuming CSI available at both the transmitter and the receiver side, it is possible to separate the MIMO channel into parallel subchannels through singular value decomposition (SVD) [26]. This techniques, which is also called multiple beamforming (MB) when combined together with BICM [35], can be easily associated with OFDM thanks to the equivalent parallel channel model. With SVD precoding/decoding, diversity and spatial multiplexing gain can be trading by exploiting only the largest N_s eigenvalues of the channel matrix.

Given the SVD of the channel matrix

$$\mathbf{H} = \mathbf{U}\Lambda^{1/2}\mathbf{V}^H = [\mathbf{u}_1\ \mathbf{u}_2 \cdots \mathbf{u}_{N_r}]\,\Lambda^{1/2}\,[\mathbf{v}_1\ \mathbf{v}_2 \cdots \mathbf{v}_{N_t}]^H\,, \tag{2.14}$$

where $\mathbf{U}$ and $\mathbf{V}$ are unitary matrices of dimensions $N_r \times N_r$ and $N_t \times N_t$, respectively, and $\Lambda^{1/2}$ is a diagonal matrix containing the r nonzero singular values of $\mathbf{H}$ in the decreasing order, the SVD-precoding can be performed exploiting the N_s largest eigenvalues of the channel matrix as shown in figure 2.14. The I/O relation relevant to the n_kth subcarrier in the l_kth OFDM block is

$$\mathbf{z}_{l_k}^{(n_k)} = \mathbf{U}_{N_s}^{(n_k)\,H}\mathbf{H}^{(n_k)}\mathbf{V}_{N_s}^{(n_k)}\mathbf{P}^{(n_k)^{1/2}}\mathbf{x}_{l_k}^{(n_k)} + \mathbf{w}_{l_k}^{(n_k)}, \tag{2.15}$$

where $\mathbf{U}_{N_s}^{(n_k)} \triangleq [\mathbf{u}_1^{(n_k)} \cdots \mathbf{u}_{N_s}^{(n_k)}]$ and $\mathbf{V}_{N_s}^{(n_k)} \triangleq [\mathbf{v}_1^{(n_k)} \cdots \mathbf{v}_{N_s}^{(n_k)}]$ are the pre- and post- MIMO processing matrices, respectively. Substituting the SVD decomposition of $\mathbf{H}^{(n_k)}$ into (2.15), we obtain the expression of the sample at the output of the subchannel (n_k, q_k), given by

$$z_{l_k}^{(n_k,q_k)} = A^{(n_k,q_k)}\sqrt{p^{(n_k,q_k)}}x_{l_k}^{(n_k,q_k)} + w_{l_k}^{(n_k,q_k)} \tag{2.16}$$

where

$$A^{(n,q)} \triangleq \sqrt{p^{(n,q)}S\ \lambda^{(n,q)}}, \tag{2.17}$$

with $\lambda^{(n,q)}$ the qth eigenvalue of $\mathbf{H}^{(n)}$, and $\mathbf{A}^{(n_k)} \triangleq \mathbf{D}(A^{(n_k,1)} \cdots A^{(n_k,N_s)})$ representing the post-processing channel gain matrix.

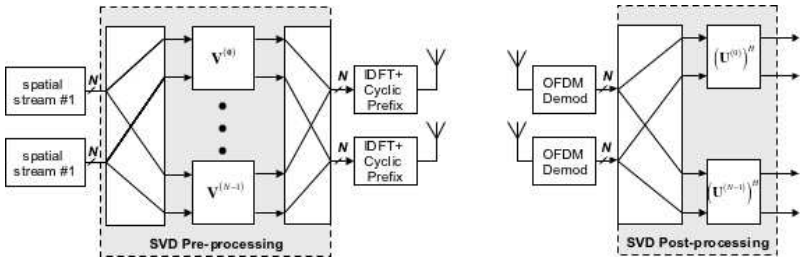

Figure 2.14. SVD precoding/decoding.

Chapter 3

Link Error Prediction methods: EESM and MIESM

3.1 Physical layer abstraction

The objective of the physical layer (PHY) abstraction is to accurately predict link layer performance in a computationally simple way [12]. In earlier systems where multi-modality was not an option, the role of performance modeling (obtained analytically or by simulation) was to simply check whether a given signal design met the pre-specified performance requirements. Once the advances in wireless systems enable multi-modal and multi-parametric design, the task of link-performance evaluation comes out in providing a compact and manageable analytic

representation of the performance results which make feasible the parametric optimization problem.

The requirement for an abstraction stems from the fact that simulating the physical layer links between multiples BSs and MSs in a network/system simulator can be computationally prohibitive. The abstraction should be accurate, computationally simple, relatively independent of channel models, and extensible to interference models and multi-antenna processing.

In the past, system level simulations characterized the average system performance, which was useful in providing guidelines for system layout, frequency planning etc. For such simulations, the average performance of a system was quantified by using the topology and macro channel characteristics to compute a geometric (or average) SNR distribution across the cell. Each subscriber's geometric SNR was then mapped to the highest modulation and coding scheme (MCS), which could be supported based on link level SINR tables that capture fast fading statistics. Current cellular systems designs are based on exploiting instantaneous channel conditions for performance enhancement. Channel dependent scheduling and adaptive coding and modulation are examples of channel-adaptive schemes employed to improve system performance.

The system level simulation must support a PHY abstraction capability to accurately predict the instantaneous performance of the PHY link layer, using statistics as Bit Error Rate (BER) or Packet Error Rate (PER).

A simple approach to estimate the packet error rate (PER) was to divide the number of erroneous packets by the total number of received packets during a given observation window.

Like said before, this estimator assumes clearly slow-varying channel but takes many packets to converge. On the contrary, predicting the future channel state information (CSI) and deriving from that a PER estimate, leads to a more accurate evaluation and faster convergence. However, obtaining the performance of all the possible transmission modes through full link-level simulations is practically unfeasible, even more so in multi-carrier systems, such as OFDM, wherein the frequency selective channel introduces large SNR variation across the subcarriers.

So it's desirable to have a simple link quality metric (LQM) with only look-up tables limited to the AWGN performance. One of the most promising link performance evaluation method to be mentioned is the effective SNR mapping(ESM) [36].

3.2 Effective SNR Mapping

In order to predict the coded performance, PER for a given received channel realization across the OFDM sub-carriers used to transmit the coded block, the post-processing SNR values at the input to the decoder are considered as input to the PHY abstraction mapping. As the link level curves are generated assuming a frequency flat channel response at

given SNR, an effective SNR, SNR_{eff} is required to accurately map the system level SNR onto the link level curves to determine the resulting PER.

The ESM PHY abstraction is thus defined as compressing the vector of received SNR values to a single effective SNR value, which can then be further mapped to a PER number as shown in 3.1.

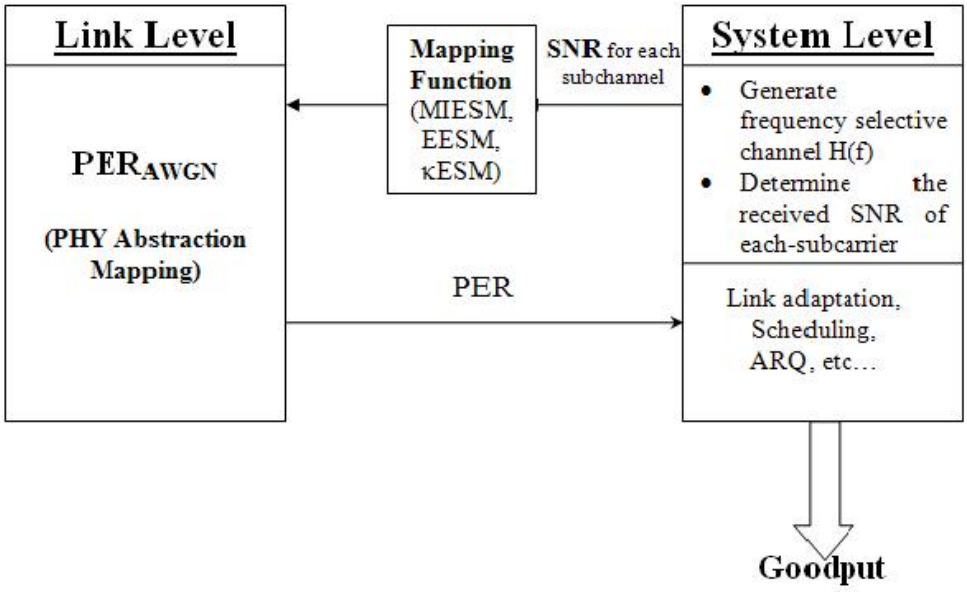

Figure 3.1. PHY link-to-system mapping procedure.

In general, the ESM PHY abstraction methods can be described [32] as

follows,

$$\gamma_{eff} = \Phi^{-1}\left\{\frac{1}{N}\sum_{n=1}^{N}\Phi\left(\boldsymbol{\gamma}_n\right)\right\}$$

In order to describe ESM models , let's start with the assumption of ideal channel state information. It's important to describe the capacity of a multiple state channel,which can be computed as

$$I(\gamma_{eff}) = \int I(\gamma) f_{SNR}(\gamma) d\gamma = \sum_i I(\gamma_i) p_i$$

where $f_{SNR}(\gamma)$ is the probability density function (pdf) for continuous-valued channel symbol SNR γ and p_i is the probability mass function (pmf) for discrete-valued SNR γ_i. The goal of effective-SNR mapping (ESM) is to find

$$\gamma_{eff} = I^{-1}\left(\int I(\gamma) f_{SNR}(\gamma) d\gamma\right) = I^{-1}\left(\sum_i I(\gamma_i) p_i\right)$$

the channel capacity is a well-defined term in information theory. In this case a loose term information measure is used to name the function $I(\gamma)$ that characterizes the channel capacity.Some commonly known information measures are in generic notation:

- Mutual Innformation

$$I_{MI}(\gamma) = E_{XY}\left\{\log_2 \frac{P(X|Y,\gamma)}{\sum_x P(X)P(Y|X,\gamma)}\right\}$$

where X is the binary input and Y is the channel output.

- I_{ACC} AWGN channel capacity

$$I_{ACC}(\gamma) = \frac{1}{2}\log_2(1+\gamma)$$

  Notice that the channel input is not constrained on a given modulation format.

- Cutoff rate I_{R0}

$$I_{R0}(\gamma) = 1 - \log_2(1+e^{-\gamma/2})$$

- Linear SNR Value,it is common used directly as an information measure, i.e.

$$I_{lin}(\gamma) = \gamma$$

- SNR value in dB $I_{\log}$

$$I_{\log}(\gamma) = \log_2(\gamma)$$

- Exponential information measure I_{EXP}

$$I_{EXP}(\gamma) = 1 - e^{-\gamma}$$

The above information measures are plotted in 3.2. Notice that, in order to compare the shape of information measure functions, these curves has been shifted such that they coincide at the (0dB,0.5) point.

Among the six curves in Fig3.2, there are mainly two characteristics: convexity and sigmoid (S-shape). The AWGN channel capacity, linear and logarithmic SNR are convex functions of γ . The mutual information and

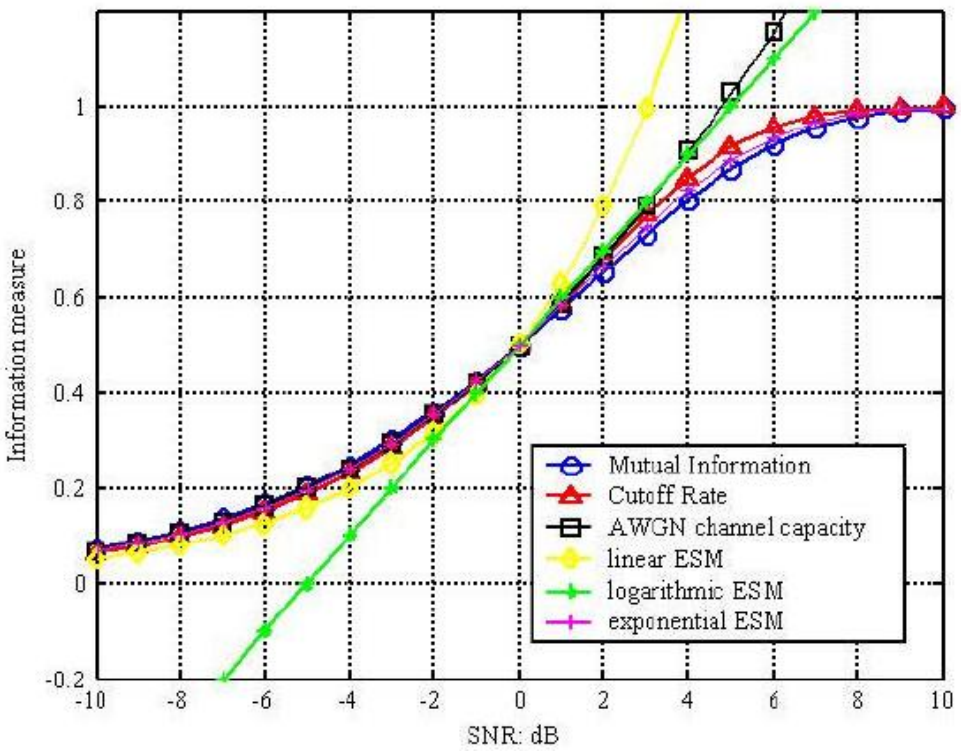

Figure 3.2. Different Information Measure vs SNR dB.

the cutoff rate are sigmoidal. Given the modulation format, the amount of information that a channel can pass should follow the sigmoidal curves instead of the unbounded AWGN channel capacity. There may not exist an exact information measure for practical channel codes; nevertheless, the information measure should be bounded by the modulation format

and the given bandwidth. It is predictable that, as the SNR gets higher, a convex function will overestimate the information that can be delivered. Particularly, logarithmic ESM also underestimates the information at low SNR. It is expected that practical channel codes with a given modulation format will be better modeled by sigmoidal curves. Especially, for channel code with performance close to channel capacity under a fixed modulation format, the mutual information would better describe the information delivered by the given channel symbol SNR. Therefore, the key to effective-SNR mapping should lie in the sigmoidal property of the information measure.

So, the aim of the ESM technique is to predict the data link layer performance (e.g. PER) of a coded transmission through a single (scalar) SNR value γ_{eff} related to an "equivalent" coded system operating over an AWGN channel. The quantity γ_{eff} compresses the multicarrier channel state, or in other words, the set of the instantaneous received SNR levels experienced by the active subchannels $\boldsymbol{\gamma} \triangleq \left[\gamma^{(\mathbf{c}_0)}, \gamma^{(\mathbf{c}_1)}, \cdots, \gamma^{(\mathbf{c}_{|\Psi|-1})}\right]^T$, with $\gamma^{(\mathbf{c})} \triangleq \frac{\left|A^{(\mathbf{c})}\right|^2}{{\sigma_w^{(\mathbf{c})}}^2}$, $\mathbf{c} \in \Psi$ representing the index pair indicating the position of the subcarrier within the OFDM spectrum and the MIMO stream of the selected subcarrier, respectively, so that the equality condition

$$\mathrm{PER}_{\mathrm{AWGN}}(\gamma_{\mathrm{eff}}) = \mathrm{PER}(\boldsymbol{\gamma})$$

refer to the AWGN equivalent system and that to be modelled, respectively. Hence, according to the specific rule adopted to map the array

$\boldsymbol{\gamma}$ into the scalar γ_{eq}, a number of ESM-based abstraction methods may come up with different level of performance capability

3.3 EESM

The effective SNR γ_{EESM} of the EESM is derived applying the Union-Chernoff bound [30], [31], [44] with the binary system restriction.

The union bound of symbol error probability P_s is given by

$$P_s \leq \sum_{d=d_{\min}}^{\infty} \alpha_d PEP(d, \gamma)$$

where γ is signal-to-noise ratio (SNR) per symbol, $d_{\min}$ is the minimum distance of the binary code, α_d is the number of codewords with Hamming weight d and $PEP(d, SNR)$ is the pair wise error probability for a given Hamming distance d and SNR. For BPSK transmission under an AWGN channel, PEP is equal to

$$PEP_{BPSK}(d, \gamma) = Q\left(\sqrt{2d\gamma}\right)$$

The Chernoff bound of this is given by

$$Q\left(\sqrt{2d\gamma}\right) \leq \exp(-d\gamma)$$

And continuing

$$PEP_{BPSK}(d, S\gamma) \leq Q\left(\sqrt{2d \cdot \gamma}\right)$$

For QPSK, similarly, PEP is given by:

$$PEP_{QPSK}(d, \gamma) = Q\left(\sqrt{d \cdot \gamma}\right) \leq \exp\left(-\frac{d \cdot \gamma}{2}\right)$$

For 16QAM and 64QAM, the closed form solution is given by a sum of Q functions(cit). However, if Gray mapping is employed, then the PEP approximation for 16QAM and 64QAM can be given by a single Q function which can be generalized as,

$$PEP_M(d,\gamma) \approx Q\left(\sqrt{\frac{d\cdot\gamma}{b}}\right) \leq a\exp\left(-\frac{d\cdot\gamma}{b}\right)$$

where a and b are generic constant which depend on the M-ary modulation and the approximation is accurate for high SNR. Without loss of generality, the SISO-OFDM system model is considered for the derivation of γ_{eff}. Since the output is considered as the output of an equivalent Gaussian channel, the probability of at least one pairwise error for N Gaussian channels is

$$\begin{aligned} PEP_M\left(d,\left(\begin{array}{cccc}\gamma^{(0)} & .... & \gamma^{(N-1)}\end{array}\right)\right) &= 1-\prod_{k=0}^{N-1}\left(1-PEP\left(d,\gamma^{(k)}\right)\right) \\ &\leq 1-\prod_{k=0}^{N-1}\left(1-a\exp\left(-\frac{d\cdot\gamma^{(k)}}{b}\right)\right) \\ &\leq 1-\left[1-\sum_{k=0}^{N-1}a\exp\left(-\frac{d\cdot\gamma^{(k)}}{b}\right)\right] \\ &= \sum_{k=0}^{N-1}a\exp\left(-\frac{d\cdot\gamma^{(k)}}{b}\right) \end{aligned} \tag{3.1}$$

Now, the aim is to and a scalar LQM γ_{eff}, such that it fulfills the condition provided before. So, taking mean of last equation such that the

single scalar γ_{eff} can map the set of N SNRs as given below

$$PEP_M\left(d, \gamma_{eff}\right) \approx \left(\frac{1}{N}\right) PEP_M\left(d, \left(\begin{array}{cccc} \gamma^{(0)} & .... & \gamma^{(N-1)} \end{array}\right)\right)$$

$$PEP_M\left(d, \gamma_{eff}\right) \approx \left(\frac{1}{N}\right) \sum_{k=0}^{N-1} a \exp\left(-\frac{d \cdot \gamma^{(k)}}{b}\right)$$

$$a \exp\left(-\frac{d \cdot \gamma^{(k)}}{b}\right) = \left(\frac{1}{N}\right) \sum_{k=0}^{N-1} a \exp\left(-\frac{d \cdot \gamma^{(k)}}{b}\right)$$

$$\left(\frac{-d}{b}\right) \gamma_{eff} = \log\left(\left(\frac{1}{N}\right) \sum_{k=0}^{N-1} \exp\left(-\frac{d \cdot \gamma^{(k)}}{b}\right)\right)$$

$$\gamma_{eff} = \left(\frac{-b}{d}\right) \log\left(\left(\frac{1}{N}\right) \sum_{k=0}^{N-1} \exp\left(-\frac{d \cdot \gamma^{(k)}}{b}\right)\right)$$

$$\gamma_{eff} = -\beta og\left(\left(\frac{1}{N}\right) \sum_{k=0}^{N-1} \exp\left(-\frac{\gamma^{(k)}}{\beta}\right)\right)$$

where β has to be numerically optimized. The reason is that the derivation of γ_{eff} starts with Chernoff upper bound which is not a tight bound for low SNR regime[cit] and other approximations are also used. So, a suitable β is not found to be equal to b/d after optimizing numerically. Thus, β is a correction factor which minimizes the mismatch between the actual PER and the estimated PER. Various optimization criteria are conceivable to compute β.

3.3.1 Simulation results

In this section are presented the graphics of simulation results for EESM physical abstraction, and values of tuning factor β_{opt}. The signal experiences either the afore mentioned 6-tap channel in SISO and MIMO

with $N_r = N_t = 2$ antennas, with each path modeled as an independent Rayleigh channel. The values of the adjusting factor β, tabulated in Table 3.1 and Table 3.2, has been calculated through a least-squares fit [35] :

$$\beta_{opt} = \arg\min_{\beta} \left(\sum_{c=1}^{N_c} |10 \log_{10} \gamma_{\text{eff}} (\beta, PER_i) - 10 \log_{10} \gamma_{\text{AWGN}} (\text{PER}_{AWGN})|^2 \right) \tag{3.2}$$

The variable N_h denotes the number of different channel realization taken into account in optimization process, $\overline{PER_i}$ is the measured packet error rate derived from a link level simulation with a fixed channel realization i, and PER_{AWGN} is the target packet error rate,which is acquired from a link level simulation in AWGN channel and is used to create the look-up table. Generally, not all collected data from link level simulation are relevant or sufficiently reliable. Since the number of transmitted packets for each realization channel is 100000, it is sensible to limit the set of $\gamma_{_{eff},i}(\beta, \overline{PER_i})$ so as PER interval is

$$\overline{PER_i} \in [0.01 : 0.95]$$

The points of PER used for calibration in following graphics (3.3,3.4 3.5,3.6) are variable around 600 for each modulation and coding scheme. EESM abstraction is related to M-QAM AWGN curves with $M = (4, 16, 64)$ For high modulation order, like MCS 5,6,7,8, it is evident the different slope of AWGN reference curves and cloud of PER values vs Effective SNR, which denote not much accuracy in prediction for PER in multipath channel.

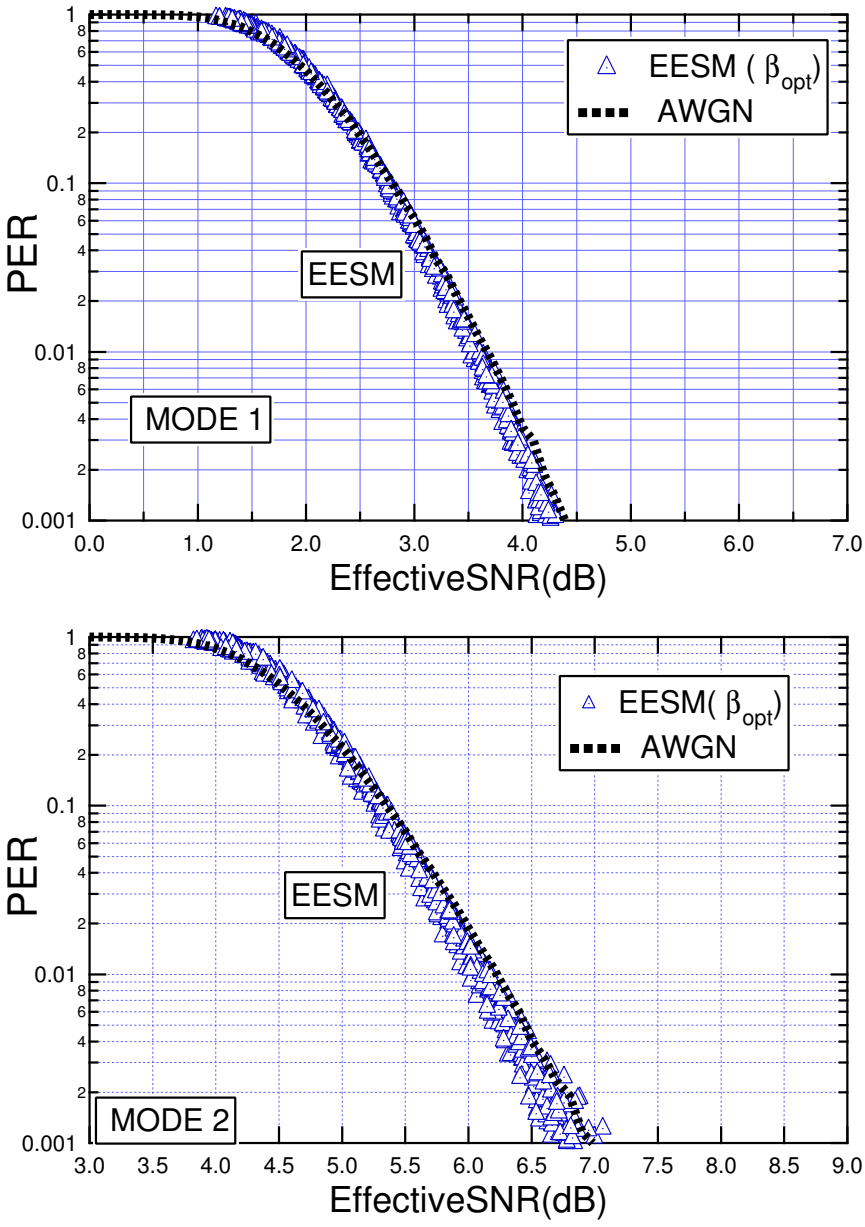

Figure 3.3. PER vs EESM abstraction 4QAM

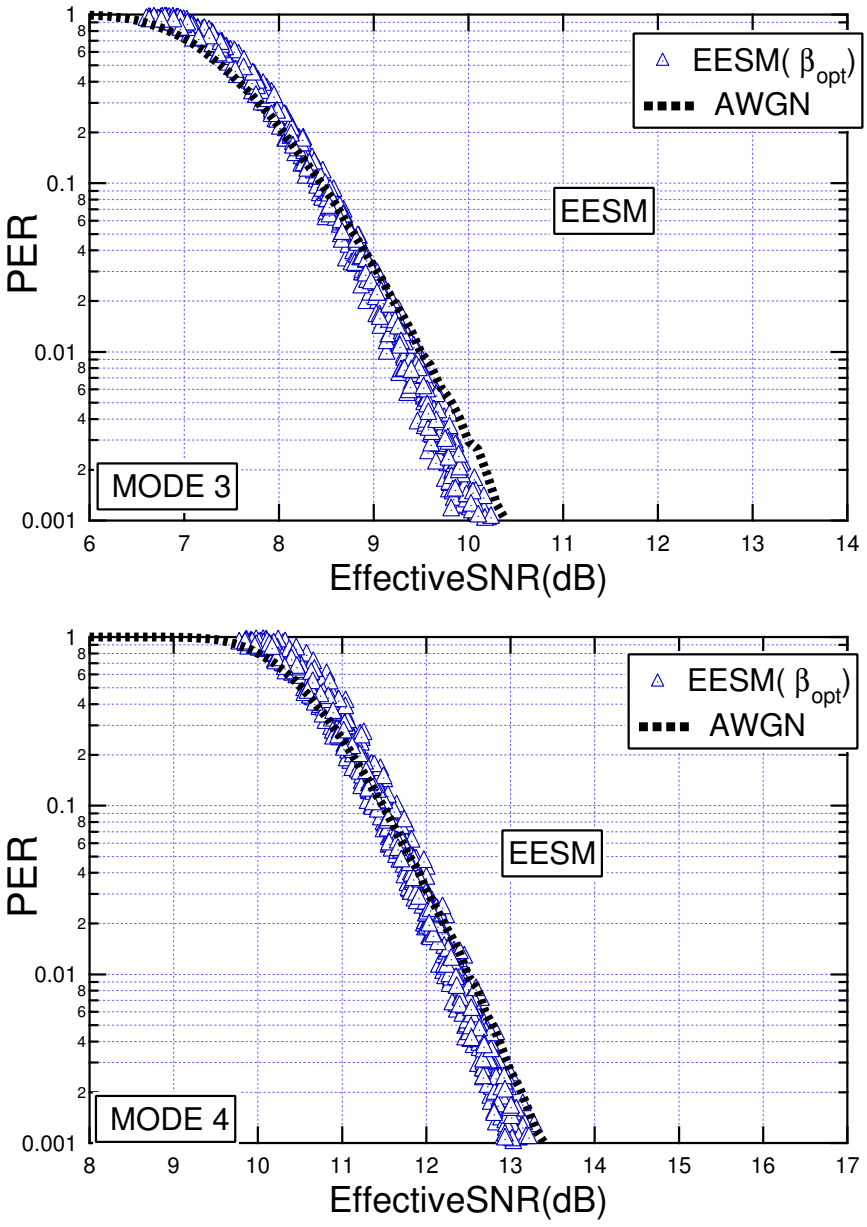

Figure 3.4. PER vs EESM abstraction 16QAM

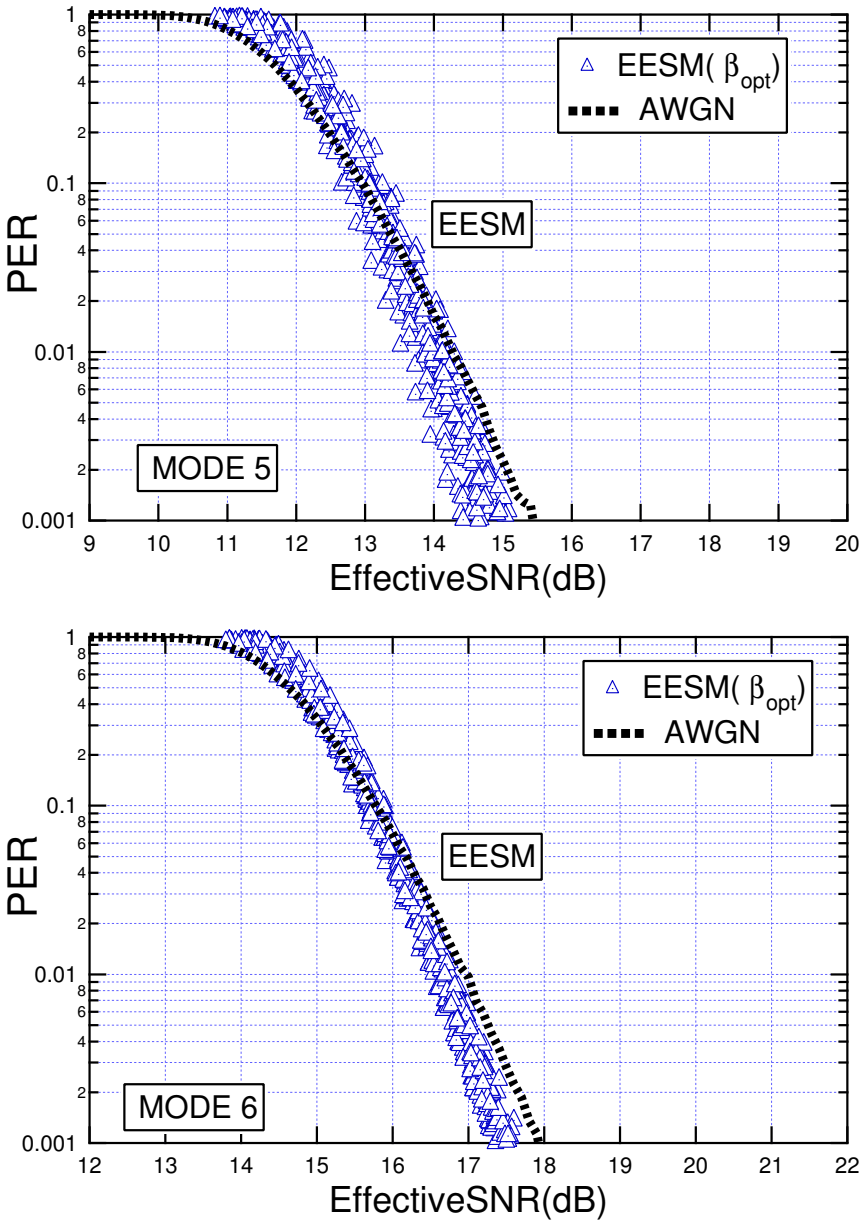

Figure 3.5. PER vs EESM abstraction 64QAM

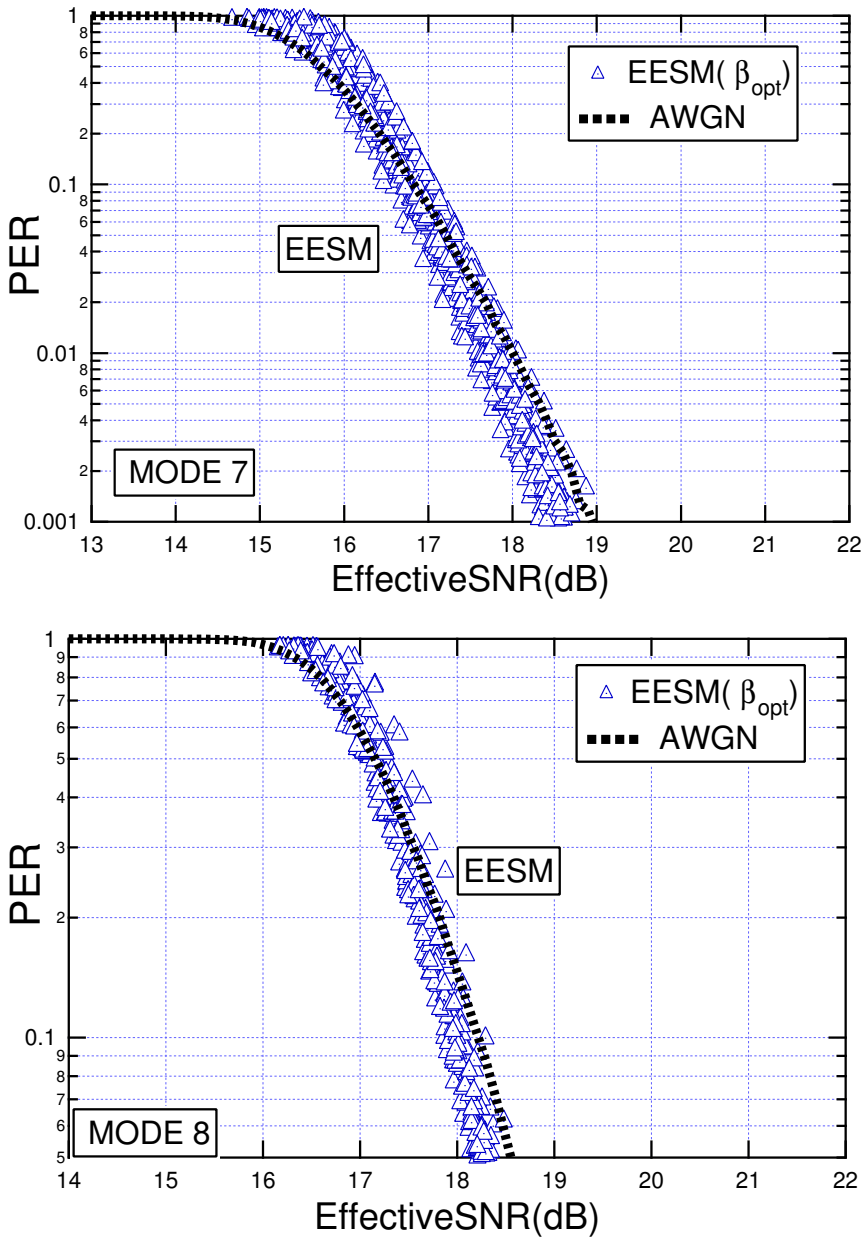

Figure 3.6. PER vs EESM abstraction 64QAM

Mode	β_{opt}
1	1.77
2	1.83
3	6.65
4	7.96
5	19.74
6	28.08
7	29.09
8	32.5

Table 3.1. Optimum tuning factor β table for SISO case

Mode	β_{opt}
1 SM	1.79
3 SM	6.65
5 SM	20.21
5 STBC	18.71

Table 3.2. Optimum tuning factor β table for MIMO case

3.4 MIESM

The accuracy of a mutual information-based metric depends on the equivalent channel over which this metric is defined. Capacity is the mutual information based on a Gaussian channel with Gaussian inputs. Modulation constrained capacity is the mutual information of a "symbol channel" (i.e. constrained by the input symbols from a complex set).

The mutual information (MI) of the coded bit is dependent on the actual constellation mapping. The MI of each bit-channel is obtained and averaged across the bits in a QAM symbol. After encoding (e.g. Turbo or CTC), a binary coded bit stream is generated before QAM mapping. The QAM

modulation can be represented as a labeling map , where is the set of -tuples, to represent QPSK, 16 and 64-QAM, of binary bits and is the constellation. Given the observation corresponding to the QAM symbol in a codeword, the demodulator computes the log-likelihood ratio (LLR) of the bit comprising the symbol via the following expression (where the symbol index is dropped for convenience)

$$\mathcal{L}_k(b_k) = \log\left(\frac{P(z_{l_k}^{(n_k)}|b_k = 1)}{P(z_{l_k}^{(n_k)}|b_k = 0)}\right)$$

When the coded block sizes are very large in a bit-interleaved coded modulation system, the bit interleaver effectively breaks up the memory of the modulator, and the system can be represented as a set of parallel independent bit-channels ?[39]. Due to the asymmetry of the modulation map, each bit location in the modulated symbol experiences a different 'equivalent' bit-channel. In the above model, each coded bit is randomly mapped (with probability) to one of the bit-channels. The mutual information of the equivalent channel can be expressed as: $I(b, \mathcal{L}) = \frac{1}{m}\sum_{i=1}^{m} I(b_i, \mathcal{L}(b_i))$ where $I(b_i, \mathcal{L}(b_i))$ is the mutual information between input bit and output $\mathcal{L}$ for bit in the modulation map of a $M^{(n)}$ QAM.

More generally, however, the mean mutual information - computed by considering the observations over symbols (or channel uses) - over the codeword may be computed as

$$M_I = \frac{1}{mN}\sum_{n=1}^{N}\sum_{i=1}^{m} I\left(b_i^{(n)}, \mathcal{L}\left(b_i^{(n)}\right)\right)$$

The mutual information function is, of course, a function of the QAM symbol SINR, and so the mean mutual information (MMIB) may be alternatively

written as

$$M_I = \frac{1}{N}\sum_{n=1}^{N} I_m\left(\gamma_n\right)$$

The mean mutual information is dependent on the SNR on each modulation symbol and the code bit (or i-th bit channel), and varies with the constellation order . Accordingly, the relationship is required for each modulation type and component bit index in order to construct$I_m\left(\gamma_n\right)$ For BPSK/QPSK, a closed form expression is given in [39]-[40], which is a non-linear function that can be approximated in polynomial form. For the particular case of BPSK/QPSK, the function would be the same as that obtained by defining the mutual information of a symbol channel (symbol channel is just a bit channel for BPSK).

For BPSK, conditional LLR PDF is Gaussian and the MIB can be expressed as

$$J(x) \approx \begin{cases} a_1x^3 + b_1x^2 + c_1x, & \text{if} x \leq 1.6363 \\ 1 - \exp(\mathrm{a_2x^3} + b_2x^2 + c_2x + d_2) & \text{if} 1.6363 \leq x \leq \infty \end{cases}$$

where$a_1 = -0.04210661, b_1 = 0.209252$ and

$$c_1 = -0.00640081$$

for the first approximation, and where

$$a_2 = 0.00181492, b_2 = -0.142675, c_2 = -0.0822054$$

$$d_2 = 0.0549608$$

for the second approximation.

The inverse function needed for the effective SINR computation is given by

$$J^{-1}(y) \approx \begin{cases} a_3 y^2 + b_3 y + c_3\sqrt{y}, & \text{if} 0 \leq y \leq 0.3646 \\ a_4 \log_e\left[b_4\left(y-1\right)\right] + c_4 y & \text{if} 0.3646 < y \leq 1 \end{cases}$$

where $a_3 = 1.09542$ $b_3 = 0.214217$ $c_3 = 2.33727$ $a_4 = -0.706692$, $b_4 = -0.386013$ $c_4 = 1.75017$ It can be shown that the LLR PDFs for any other modulation can be approximated as a mixture of Gaussian distributions that are non-overlapping at high SINR. It then follows that the corresponding MIB can be expressed as a sum of functions, i.e

$I_m\left(x\right) = \sum_{k=1}^{K} a_k J\left(c_k x\right)$ and $\sum_{k=1}^{K} a_k = 1$

We will use this parameterized function for expressing all non-linear MIB functions. The corresponding parameters themselves would be a function of the modulation

The optimized functions for QPSK, 16-QAM and 64-QAM are given in

$I_2(\gamma)$(QPSK))	$J(2\sqrt{\gamma})$(Exact)
$I_4(\gamma)$	$\frac{1}{2}J\left(0.8\sqrt{\gamma}\right) + \frac{1}{4}J\left(2.17\sqrt{\gamma}\right) + \frac{1}{4}J\left(0.965\sqrt{\gamma}\right)$
$I_6(\gamma)$	$\frac{1}{3}J\left(1.47\sqrt{\gamma}\right) + \frac{1}{3}J\left(0.529\sqrt{\gamma}\right) + \frac{1}{3}J\left(0.366\sqrt{\gamma}\right)$

Table 3.3. MIESM

Lookup tables for the AWGN reference curves for different MCS levels can be used in order to map the MMIB to PER

Differently from the EESM, the MIESM quality model (shown in figure 3.7), presents two independent models for coding and modulation mapping [34], [33], where the model specific function can be expressed as [12]:

$$I(\gamma^{(\mathbf{c})}, m^{(\mathbf{c})}) = m^{(\mathbf{c})} -$$
$$-\frac{1}{2^{m^{(\mathbf{c})}}} \sum_{x \in \chi^{(\mathbf{c})}} E_U \left\{ \log_2 \left(1 + \sum_{\tilde{x} \in \chi^{(\mathbf{c})}, \tilde{x} \neq x} \exp \left[-\frac{|\tilde{x} - x + U|^2 - |U|^2}{1/\gamma^{(\mathbf{c})}} \right] \right) \right\} \tag{3.3}$$

being $\chi^{(\mathbf{c})}$ the M-QAM symbols constellation on the subchannel $\mathbf{c}$ and U a zero mean complex gaussian variable with variance $1/(2\gamma^{(\mathbf{c})})$.

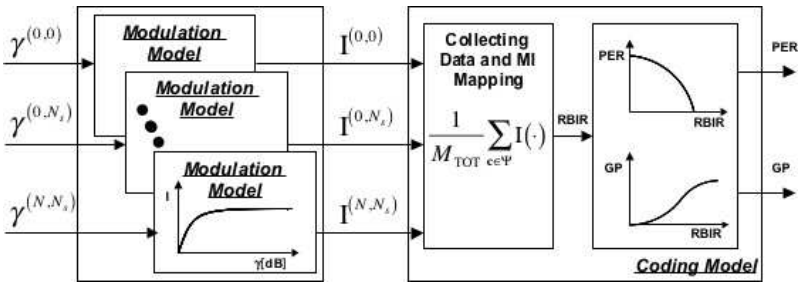

Figure 3.7. MIESM quality model structure

Unfortunately, since a simple closed form is not available, polynomial approximations for QPSK, 16QAM and 64QAM have been proposed (see [12]).

The modulation model, simply maps the post processing SNR into the corresponding amount of mutual information. On the other hand, the coding model firstly collects the total mutual information within one coding block. Assuming the codec to have uniform protection for all the coded bit within a coding block, the coding model normalizes the accumulated mutual information of the coded bits of the block, denoted as RBIR (received Bit Mutual Information Rate) [33], expressed as

$$\text{RBIR} \triangleq \frac{1}{\sum_{\mathbf{u} \in \Psi} m^{(\mathbf{u})}} \sum_{\mathbf{c} \in \Psi} \text{I}(\gamma^{(\mathbf{c})}/\beta, m^{(\mathbf{c})}), , \tag{3.4}$$

β being a scaling factor depending on the adopted coding scheme. This final association is independent of the modulation scheme and make possible computing the link quality model for cases where the OFDM symbol comprises of mixed modulation symbols. As final step, the RBIR is mapped into the PER quality metric so that the effective SNR γ_{MIESM} can be provided as

$$\gamma_{MIESM} \triangleq \beta \mathrm{I}^{-1}(\mathrm{RBIR}, \overline{m}), \tag{3.5}$$

where $\overline{m}$ is the chosen modulation size value for the AWGN performance curve used as the reference. This mapping function is non-linear, so it is computed a table wich shown SNR to RBIR mapping, for our case scenario.

Table can be found in Appendix A, and refers to

$$\gamma^{(\mathbf{c})} \in \{-10 : 0.1 : 30\}$$

where $\gamma^{(\mathbf{c})}$ is expressed in dB for a 401 points table for each modulation order.

In order to derive the mapping between RBIR and BLER, the following steps may be considered:

1) Calculate the effective SNR (γ_{MIESM}) based on RBIR and Table

2) Reference the AWGN link performance curves to obtain the mapping between SNR and PER

3)Use the γ_{eff} obtained in Step 1 and the mapping obtained in Step 2 to derive the mapping between γ_{MIESM} and BLER

It is worth remarking that the mapping related to the coding model is independent of the modulation scheme and allows the MIESM link quality prediction to be defined also for systems wherein the coded block may include symbols

with mixed modulation order. Although an adjusting factor β is included in the analysis of MIESM for the coding model, it has been demonstrated in [33] that the model provides accurate PER estimate even if this factor is omitted. However β is calibrated, so a β_{opt} is computed with same criterion as in EESM section.

3.4.1 Numerical Results

The MIESM abstraction methods is consistently better than EESM abstraction. Various simple motivations allow to explain that. The results shown in 3.8, 3.9, 3.10, 3.11 speak for themselves. Good accuracy for error prediction and good performances make MIESM a reliable candidate for link error prediction in 802.16m Standardization . Calibration results for tuning factor β tabled in Table 3.4 Table 3.5 are similar to what found in literature like paper published by Blankenship et al.

Mode	β_{opt}
1	1.15
2	1.08
3	1.14
4	1.05
5	1.03
6	1.07
7	0.98
8	1.03

Table 3.4. Optimum tuning factor β table for SISO case

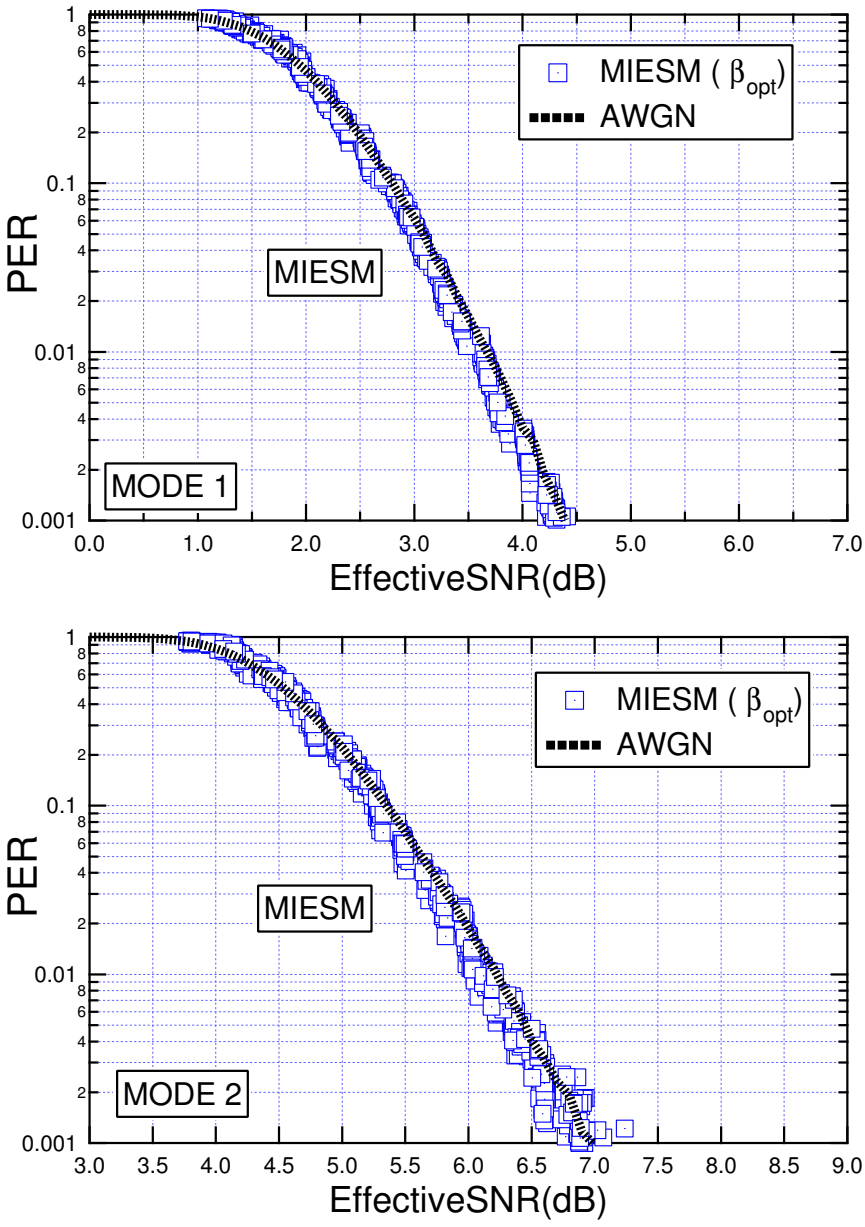

Figure 3.8. PER vs MIESM abstraction 4QAM

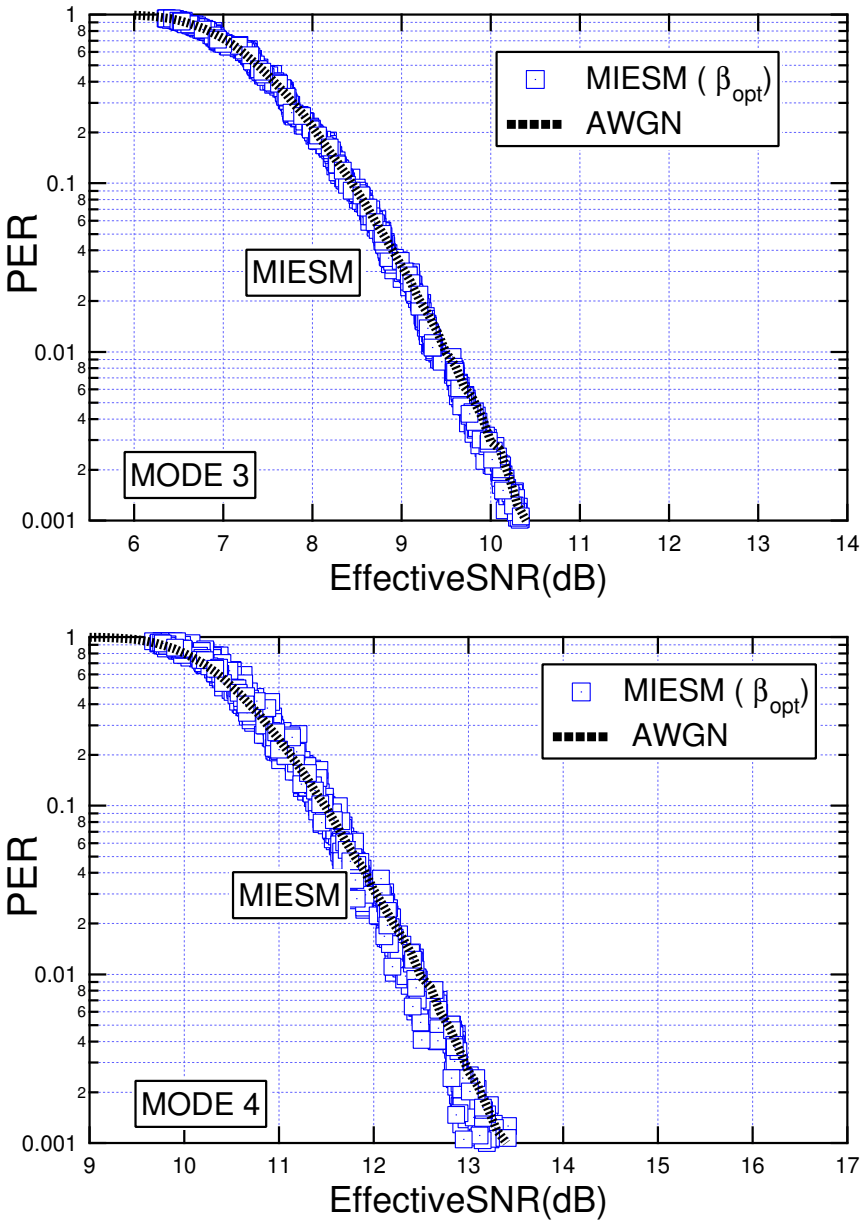

Figure 3.9. PER vs MIESM abstraction 16QAM

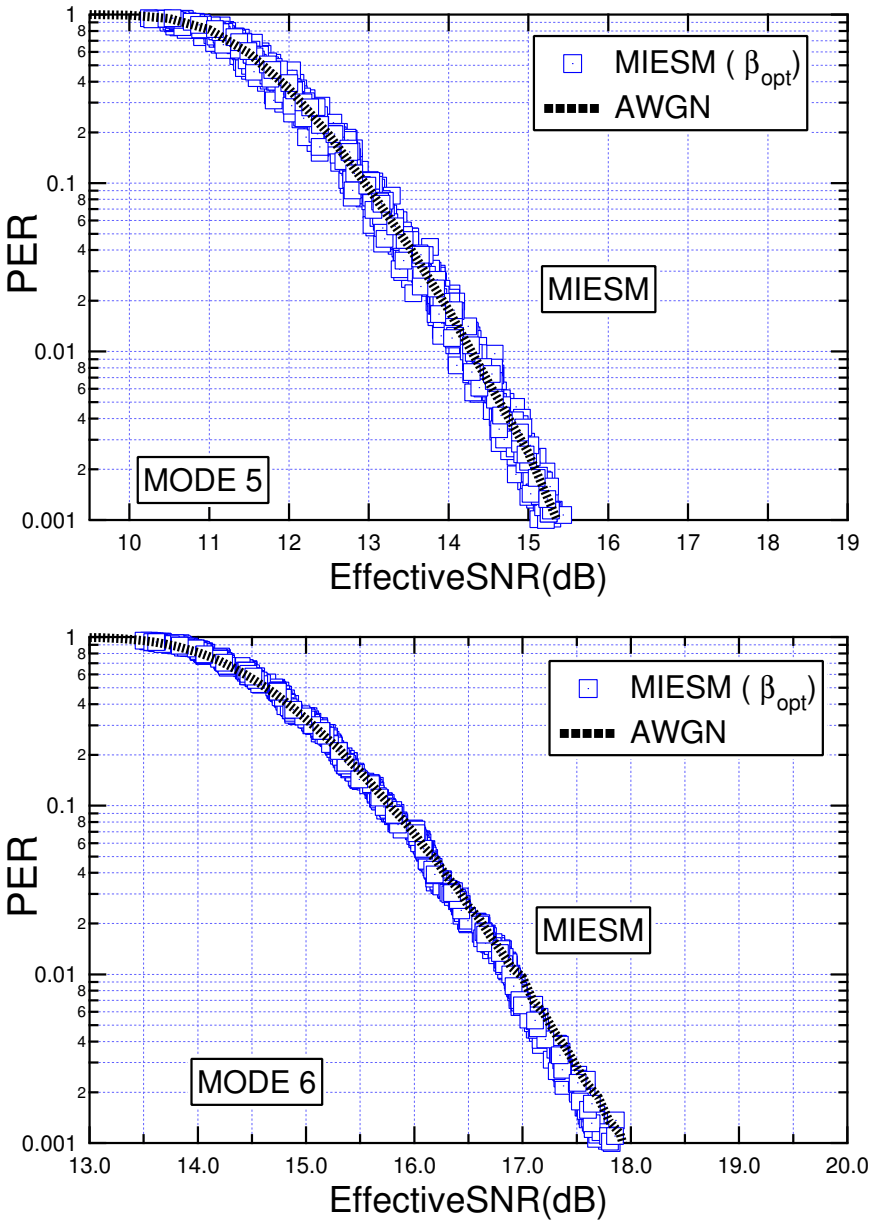

Figure 3.10. PER vs MIESM abstraction 64QAM

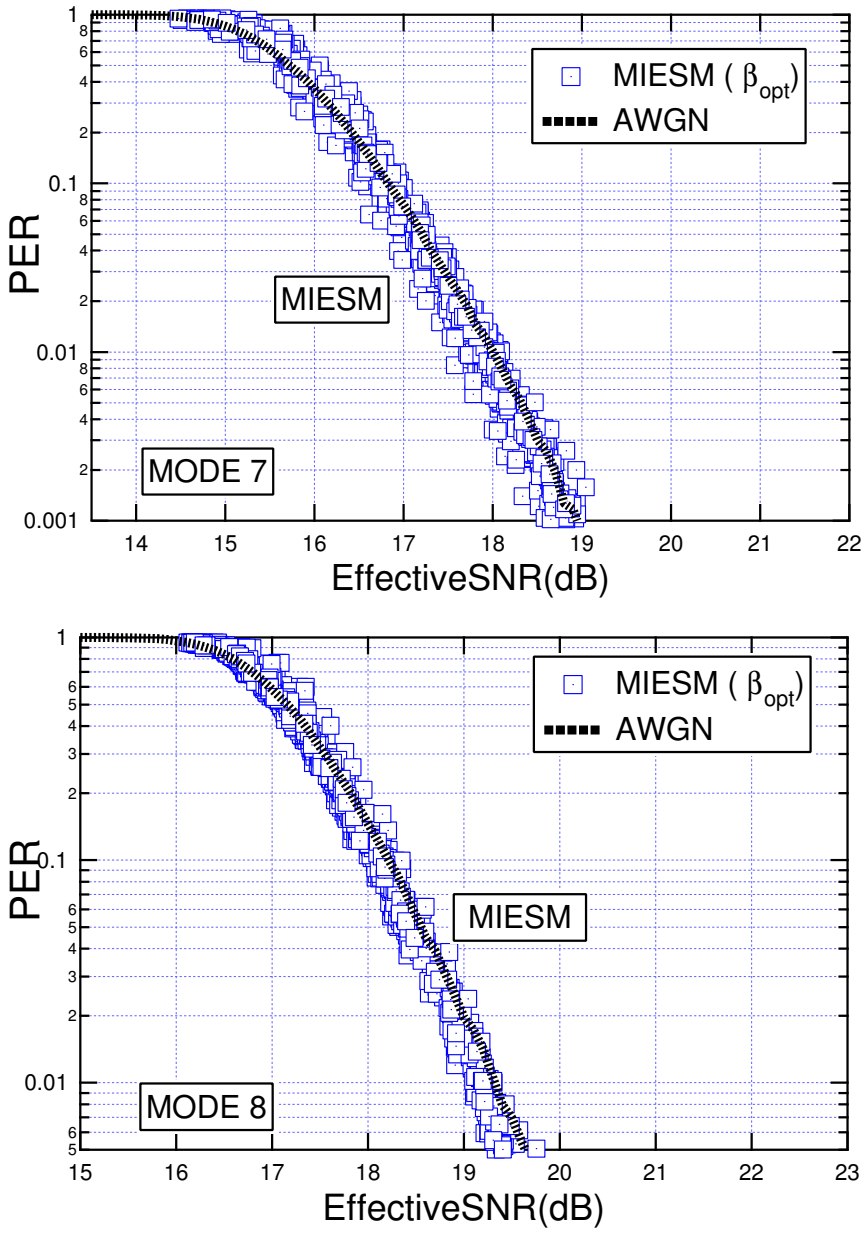

Figure 3.11. PER vs MIESM abstraction 64QAM

Mode	β_{opt}
1 SM	1.15
3 SM	1.09
5 SM	1.08
5 STBC	0.90

Table 3.5. Optimum tuning factor β table for MIMO case

Chapter 4

Novel Packet Error Rate prediction method: kESM

4.1 Intro to κESM

In this section, the focus is to explain a novel PER prediction scheme for BIC-OFDM transmission links over frequency-selective channels based on the novel concept of κESM (cit). Differently from the conventional ESM methods, the κESM relies on an accurate evaluation of the PEP figure through the statistical description of the BIC log-likelihood metrics, thus offering an efficient accuracy versus manageability tradeoff.

4.2 PEP Analysis

Let first consider two distinct codewords, i.e., two sequences of coded binary symbols which originate from the same state of the code and merge after d trellis steps, and let denote them as two d-dimensional arrays $\underline{\mathbf{b}}$ and $\underline{\mathbf{b}}'$, whose kth elements are b_k and b'_k, respectively.

$\hat{\underline{\mathbf{b}}}$ denote a codeword at the decoder output. Recalling the system model description outlined in the previous chapter, the discrete-time signal relevant to the subchannel (n, q) in the lth OFDM block can be equivalently expressed as

$$z_l^{(n,q)} = \sqrt{\gamma^{(n,q)}} x_l^{(n,q)} + n_l^{(n,q)}, \tag{4.1}$$

where $\gamma^{(n,q)}$ is the post-processing SNR experienced on the subchannel (n, q) and $n_l^{(n,q)}$ is a Gaussian RV with variance $\sigma_n^2 = 1$ representing the equivalent noise contribution. Resorting to a vectorial notation, the I/O relationship relevant to the nth subcarrier of the lth MIMO-OFDM block can be expressed as

$$\mathbf{z}_l^{(n)} = \Upsilon^{(n)^{1/2}} \mathbf{x}_l^{(n)} + \mathbf{n}_l^{(n)} \tag{4.2}$$

where $\Upsilon^{(n)}$ is a diagonal matrix defined as $\Upsilon^{(n)} \triangleq \mathbf{D}(\gamma^{n,1}, \cdots, \gamma^{n,N_s})$, while the noise vector is $\mathbf{n}_l^n \triangleq [n_l^{(n,1)}, \cdots, n_l^{(n,N_s)}]^T$.

The aim of this sub-section is to evaluate the Pairwise Error Probability (PEP), defined as

$$PEP \triangleq \Pr\left\{\hat{\underline{\mathbf{b}}} = \underline{\mathbf{b}}' | \underline{\mathbf{b}}, \Upsilon\right\}, \tag{4.3}$$

where Υ is a block diagonal matrix defined as $\Upsilon \triangleq \mathbf{D}(\Upsilon^{(1)}, \cdots, \Upsilon^{(N)})$. In case of ideal CSI, i.e., assuming that the actual value of the post processing SNR

matrix Υ is known, the BICM log-likelihood metric for the kth coded binary symbol at the decoder input can expressed as

$$\mathcal{L}_k = \log \frac{\sum_{\tilde{x} \in \chi_{b'_k}^{(i_k,n_k,q_k)}} p\left(z_{l_k}^{(n_k,q_k)} | x_{l_k}^{(n_k,q_k)} = \tilde{x}, \Upsilon\right)}{\sum_{\tilde{x} \in \chi_{b_k}^{(i_k,n_k,q_k)}} p\left(z_{l_k}^{(n_k,q_k)} | x_{l_k}^{(n_k,q_k)} = \tilde{x}, \Upsilon\right)} \tag{4.4}$$

where

$$p\left(z_{l_k}^{(n_k,q_k)} | x_{l_k}^{(n_k,q_k)} = \tilde{x}, \Upsilon\right) \propto \exp\left(-\frac{\left|z_{l_k}^{(n_k,q_k)} - \sqrt{\gamma^{(n_k,q_k)}}\tilde{x}\right|^2}{\sigma_n^2}\right) \tag{4.5}$$

is the Gaussian-shaped Probability Density Function (p.d.f.) of the received sample value, conditioned on the transmitted symbol $\tilde{x}$ and on the post-processing SNRs Υ, while $\chi_a^{(i,n,q)}$ represents the subset of all the M-QAM symbols belonging to $\chi^{(n,q)}$ whose ith label bit is equal to a. By replacing (4.5) into (4.4) (and recalling that $\sigma_n^2 = 1$), the log-likelihood metric $\mathcal{L}_k$ can be rewritten as

$$\mathcal{L}_k = \log \frac{\sum_{\tilde{x} \in \chi_{b'_k}^{(i_k,n_k,q_k)}} \exp\left(-\left|z_{l_k}^{(n_k,q_k)} - \sqrt{\gamma^{(n_k,q_k)}}\tilde{x}\right|^2\right)}{\sum_{\tilde{x} \in \chi_{b_k}^{(i_k,n_k,q_k)}} \exp\left(-\left|z_{l_k}^{(n_k,q_k)} - \sqrt{\gamma^{(n_k,q_k)}}\tilde{x}\right|^2\right)}. \tag{4.6}$$

Under the assumption of ideal interleaving, the BICM subcarriers behave as a memoryless BIOS channels and the PEP can be computed as the tail probability [25]

$$PEP = \Pr\left\{\sum_{k=1}^{d} \mathcal{L}_k > 0\right\} = \Pr\left\{\Theta > 0\right\}, \tag{4.7}$$

where is defined $\Theta \triangleq \sum_{k=1}^{d} \mathcal{L}_k$. Unfortunately, the computation of (4.7) by the p.d.f. of Θ reveals too involved. It is resorted then to the Moment Generating Function (m.g.f.) of the RV Θ, which is given by

$$M_\Theta(s) \triangleq \mathrm{E}_\Theta\left\{\exp(s\Theta)\right\} = \left[M_\mathcal{L}(s)\right]^d, \tag{4.8}$$

where $M_{\mathcal{L}}(s) \triangleq \mathrm{E}_{\mathcal{L}_k}\{\exp(s\mathcal{L}_k)\}$ is the m.g.f. of the RV $\mathcal{L}_k$, and it is exploited the fact that the LLRs $\mathcal{L}_k$ are Independent and Identically-Distributed (i.i.d.) RVs. By this way, the PEP can be evaluated by using the following integral[1] [41]

$$PEP = \frac{1}{2\pi\jmath}\int_{\sigma-\jmath\infty}^{\sigma+\jmath\infty} M_{\Theta}(s)\frac{\mathrm{d}s}{s} = \frac{1}{2\pi\jmath}\int_{\sigma-\jmath\infty}^{\sigma+\jmath\infty} [M_{\mathcal{L}}(s)]^d \frac{\mathrm{d}s}{s}. \tag{4.9}$$

From (4.6), the m.g.f. to be used in (4.9), turns out

$$M_{\mathcal{L}}(s) = \mathrm{E}_k\left\{\left[\frac{\sum_{\tilde{x}\in\chi_{b'_k}^{(i_k,n_k,q_k)}}\exp\left(-\left|z_{l_k}^{(n_k,q_k)}-\sqrt{\gamma^{(n_k,q_k)}}\tilde{x}\right|^2\right)}{\sum_{\tilde{x}\in\chi_{b_k}^{(i_k,n_k,q_k)}}\exp\left(-\left|z_{l_k}^{(n_k,q_k)}-\sqrt{\gamma^{(n_k,q_k)}}\tilde{x}\right|^2\right)}\right]^s\right\}, \tag{4.10}$$

where the statistical expectation is to be taken with respect to all those parameters that depend on the index k.

Substituting the expression of the subcarrier output (4.1), and under the assumption of ideal CSI

$$M_{\mathcal{L}}(s) =$$

$$\mathrm{E}_k\left\{\left[\frac{\sum_{\tilde{x}\in\chi_{b'_k}^{(i_k,n_k,q_k)}}\exp\left(-\left|\sqrt{\gamma^{(n_k,q_k)}}\left(x_{l_k}^{(n_k,q_k)}-\tilde{x}\right)+n_{l_k}^{(n_k,q_k)}\right|^2\right)}{\sum_{\tilde{x}\in\chi_{b_k}^{(i_k,n_k,q_k)}}\exp\left(-\left|\sqrt{\gamma^{(n_k,q_k)}}\left(x_{l_k}^{(n_k,q_k)}-\tilde{x}\right)+n_{l_k}^{(n_k,q_k)}\right|^2\right)}\right]^s\right\}$$

Similarly to the approach suggested in [25], the m.g.f. can be upper-bounded and, it is also demonstrated that, at high SNRs, the bound is dominated by the term relevant to the nearest neighbor (in the sense of Euclidean distance) of

[1] In (4.9), σ is any real number which ensures that the contour path lies in the region of convergence.

$x_{l_k}^{(n_k,q_k)}$ in the complementary subset $\chi_{b'_k}^{(i_k,n_k,q_k)}$. As a consequence, it's applied the Dominated Convergence Theorem (DCT) [25], [28] obtaining

$$M_{\mathcal{L}}(s) \simeq \mathrm{E}_k \left\{ \exp\left(-\gamma^{(n_k,q_k)} d^2\left(x_{l_k}^{(n_k,q_k)}, \overline{x} \right) \left(s - s^2 \right) \right) \right\}, \tag{4.11}$$

where $\overline{x}$ is the nearest neighbor of $x_{l_k}^{(n_k,q_k)}$ in the complementary subset $\chi_{b'_k}^{(i_k,n_k,q_k)}$, and $d(y,w)$ is the Euclidean distance between the complex-valued symbols y and w. Let us note that, for Gray mapping rule, the distance $d^2(x_{l_k}^{(n_k,q_k)}, \overline{x})$ can be expressed as

$$d^2\left(x_{l_k}^{(n_k,q_k)}, \overline{x} \right) \triangleq \left(\Delta^{(n_k,q_k)} d_{min}^{(n_k,q_k)} \right)^2, \tag{4.12}$$

where $d_{min}^{(n_k,q_k)}$ is the minimum Euclidean distance between the symbols in the complete QAM set $\chi^{(n_k,q_k)}$ associated with the n_kth subcarrier, and $\Delta^{(n_k,q_k)}$ is a positive integer coefficient. The statistical expectation in (4.11) shall be evaluated with respect to the possible values of the transmitted symbol $x_{l_k}^{(n_k,q_k)}$ and to the possible position of the coded binary symbol b_k into the label of the QAM symbols of the complementary subset. Now, let us note that, for each subchannel $\mathbf{c} \triangleq (n,q)$, there are $m^{(\mathbf{c})}$ label bits, and each label bit has $2^{m^{(\mathbf{c})}}/2$ symbols on its complementary subset, so that the number of terms to be averaged results $m^{(\mathbf{c})} \cdot 2^{m^{(\mathbf{c})}-1}$. However, it can be easily verified that there are only $m^{(\mathbf{c})}/2$ distinct values. For example, assuming for the sake of simplicity a 16QAM modulation, we have 32 terms, of which 24 are at distance $d_{min}^{(\mathbf{c})^2}$, and 8 are at distance $2d_{min}^{(\mathbf{c})^2}$. Thus, by averaging with respect to the binary coded symbol index k, the it's ended up with

$$M_{\mathcal{L}}(s) \simeq \sum_{\mathbf{c}\in\Psi} \frac{\Pr(\mathbf{c})}{m^{(\mathbf{c})} 2^{m^{(\mathbf{c})}-1}} \sum_{\Delta=1}^{K} \psi^{(\mathbf{c})}(\Delta) \cdot \mathrm{e}^{-\gamma^{(\mathbf{c})}\left(\Delta \cdot d_{min}^{(\mathbf{c})}\right)^2 \left(s - s^2\right)}, \tag{4.13}$$

where Ψ is the subspace containing all the possible values of the pair $\mathbf{c} = (n, q)$, with $1 \leq n \leq N$, $1 \leq q \leq N_s$,

$$\Pr(\mathbf{c}) \triangleq \frac{m^{(\mathbf{c})}}{M_{TOT}} \tag{4.14}$$

is the probability that a codeword bit is sent through the subchannel $\mathbf{c}$ in the case of ideal random interleaving, $M_{TOT} \triangleq \sum_{\mathbf{u}\in\Psi} m^{(\mathbf{u})}$ is the total number of bits transmitted during an OFDM symbol period and $\psi^{(\mathbf{c})}(\Delta)$ is the number of symbols at distance $\Delta \cdot d_{min}^{(\mathbf{c})}$ in the complementary subset.

4.2.1 Gaussian Approximation

A simple way to estimate the PEP integral (4.9) is the so called *Gaussian approximation*, expressed by [25]

$$PEP \simeq \mathrm{Q}\left(\sqrt{-2d\,\kappa_{\mathcal{L}}(\hat{s})}\right), \tag{4.15}$$

where $\kappa_{\mathcal{L}}(\cdot)$ is the Cumulant Generating Function (c.g.f.) defined as

$$\kappa_{\mathcal{L}}(s) \triangleq \log M_{\mathcal{L}}(s), \tag{4.16}$$

and $\hat{s}$ is the so-called "saddlepoint", which is defined as that value for which $\kappa'(\hat{s}) = 0$ [42]. In the case of BIOS channels, we have $\hat{s} = 1/2$ [43], so that

$$\kappa_{\mathcal{L}}(\hat{s}) \simeq \log\left(\sum_{\mathbf{c}\in\Psi} \frac{1}{M_{TOT}2^{m^{(\mathbf{c})}-1}} \sum_{\Delta=1}^{K} \psi^{(\mathbf{c})}(\Delta) \cdot \mathrm{e}^{-\frac{\gamma^{(\mathbf{c})}\left(\Delta\cdot d_{min}^{(\mathbf{c})}\right)^2}{4}}\right). \tag{4.17}$$

Let us notice that approximation (4.15) is actually the *zero*-th order of the Lugannani-Rice asymptotic series [38], and corresponds to the PEP of an equivalent system with binary modulation (labelled as Equivalent Binary Modulation, EBM) that experiences a simple AWGN channel with SNR

$$SNR_{EBM} \triangleq -\kappa_{\mathcal{L}}(\hat{s}). \tag{4.18}$$

According to the results above, the Gaussian approximation can be rewritten as

$$\begin{aligned} PEP &\simeq \mathrm{Q}\left(\sqrt{2d\, SNR_{EBM}}\right) \\ &= \mathrm{Q}\left(\sqrt{-2d\, \log \sum_{\mathbf{c}\in\Psi} \sum_{\Delta=1}^{K} \frac{\psi^{(\mathbf{c})}(\Delta) \mathrm{e}^{-\frac{\gamma^{(\mathbf{c})}\left(\Delta \cdot d_{min}^{(\mathbf{c})}\right)^2}{4}}}{M_{TOT} 2^{m^{(\mathbf{c})}-1}}}\right) \end{aligned} \tag{4.19}$$

4.2.2 κESM definition

Recalling that eqn. (**??**) corresponds to the PEP of an equivalent system with binary modulation that experiences a simple AWGN channel. For maximum-likelihood decoding, the packet error probability (PER) of linear binary codes over BIOS channels can be estimated by using the union-bound. Thus, explicitly indicating the dependence of the PEP on the distance d and on the post processing SNR matrix Υ, PER can be upper-bounded as

$$PER\left(\Upsilon\right) \leq \sum_{d=d_{free}}^{N_c} \omega\left(d\right) PEP\left(d, \Upsilon\right) \tag{4.20}$$

where $\omega\left(d\right)$ is the weight of all error events at Hamming distance d, and d_{free} is the minimum distance between two codewords. Thus, the PER performance can estimated by computing the PEP. These considerations suggest then the choice of a LQM based on the c.g.f. for the BIC-OFDM system considered. Figure 4.1 depicts the proposed link quality model structure carried out from the previous consideration, showing two separate models for modulation and coding. The modulation model gives the m.g.f. evaluated at the saddlepoint

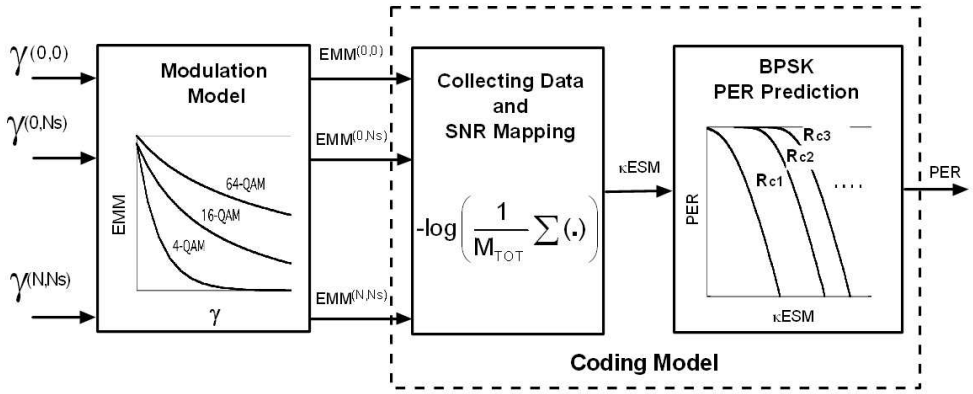

Figure 4.1. κESM quality model structure.

relevant to a certain modulation scheme over an AWGN channel with SNR γ. The m.g.f. is estimated by a weighted sum of exponential functions. For this reason, in the sequel, the modulation model is tagged as "exponential modulation model" (EMM), which can be expressed as

$$EMM^{(\mathbf{c})} \triangleq \sum_{\Delta=1}^{K} \frac{\psi^{(\mathbf{c})}(\Delta)}{2^{m^{(\mathbf{c})}-1}} \cdot \mathrm{e}^{-\frac{\gamma^{(\mathbf{c})}\left(\Delta \cdot d_{min}^{(\mathbf{c})}\right)^2}{4\,\beta_{cod}}}, \tag{4.21}$$

where β_{cod} is an optimization factor which depends only on the particular coding scheme/rate. The coding model is obtained by firstly collecting and normalizing the moment generating functions and, eventually, taking the natural logarithm. The resulting equivalent SNR value, given by

$$\gamma\kappa ESM \triangleq -\beta_{cod}\ \log\left(\frac{1}{M_{TOT}}\sum_{\mathbf{c}\in\Psi} EMM^{(\mathbf{c})}\right), \tag{4.22}$$

is then mapped into a PER number. Let us remark that, being separated the modulation and coding scheme, the κESM allows an accurate PER prediction also in the case of mixed modulation.

As suggested in [25], let us determine the asymptotic value of the quantity

$\kappa_{\mathcal{L}}(\hat{s})/S$ as

$$\lim_{S\to\infty} \frac{\kappa_{\Lambda}(\hat{s})}{S}$$

$$= \lim_{S\to\infty} -\frac{\log\left(\sum_{\mathbf{c}\in\Psi} \frac{\Pr(\mathbf{c})}{m^{(\mathbf{c})}2^{m^{(\mathbf{c})}-1}} \sum_{\Delta=1}^{K} \psi^{(\mathbf{c})}(\Delta)\cdot \mathrm{e}^{-\frac{\gamma^{(\mathbf{c})}\left(\Delta\cdot d_{min}^{(\mathbf{c})}\right)^2}{4}}\right)}{S}. \quad (4.23)$$

If we define

$$x_n \triangleq \log\Pr(n) - p^{(n)}/\gamma^{(n)} = \log\Pr(n) - \frac{p^{(n)}S|H^{(n)}|^2 {d_{min}^{(n)}}^2}{4}, \quad (4.24)$$

the asymptotic value (4.23) can be rewritten as

$$d_{\infty}^2 = \lim_{S\to\infty} -\frac{\log\left(\sum_{n=1}^{N}\exp(x_n)\right)}{S}. \quad (4.25)$$

Notice that for $S\to\infty$, we have

$$x_n \to \frac{-p^{(n)}S|H^{(n)}|^2 {d_{min}^{(n)}}^2}{4}. \quad (4.26)$$

Now, the expression of the Jacobian logarithm is derived at the numerator of (4.25). We start by recalling that the Jacobian logarithm for a two-variable case is

$$\log\left(\mathrm{e}^{x_1}+\mathrm{e}^{x_2}\right) = \max\{x_1,x_2\} + \log\left(1+\mathrm{e}^{-|x_1-x_2|}\right). \quad (4.27)$$

Without loss of generality, let assume that the N-variable sequence $\{x_n\}_{n=1}^{N}$ is sorted in a decreasing order (i.e., $x_1 > x_2 > \ldots > x_N$), and let

$$y_1 \triangleq x_1 = \max\{x_n\}, \quad (4.28)$$

and

$$y_n \triangleq x_n - x_{n-1} \ , \ 1 < n \leq N. \quad (4.29)$$

Notice that, due to the decreasing order sorting, $y_n < 0$, for $1 < n \leq N$. For $S \to \infty$, we have

$$y_n \to \frac{p^{(n-1)}|H^{(n-1)}|^2 {d_{min}^{(n-1)}}^2 - p^{(n)}|H^{(n)}|^2 {d_{min}^{(n)}}^2}{4} \tag{4.30}$$

$$\triangleq -|K| \cdot S \tag{4.31}$$

with K an opportune coefficient, $1 < n \leq N$. The Jacobian logarithm for the N-variable case can be cast into the following recursive form

$$\log\left(\sum_{n=1}^{N} \exp\left(x_n\right)\right) = y_1 + \epsilon\left(y_2 + \epsilon\left(y_3 + \cdots + \epsilon\left(y_{N-1} + \epsilon\left(y_N\right)\right)\right)\right), \tag{4.32}$$

where it's defined

$$\epsilon\left(\alpha\right) \triangleq \log\left(1 + \mathrm{e}^{\alpha}\right). \tag{4.33}$$

Recalling the following property

$$\lim_{\alpha \to -\infty} \epsilon\left(\alpha\right) = 0, \tag{4.34}$$

for $S \to \infty$, then

$$\log\left(\sum_{n=1}^{N} \exp\left(x_n\right)\right) \to y_1 = x_1 = \max\left\{x_n\right\}. \tag{4.35}$$

The asymptotic value (4.25) becomes then

$$\begin{aligned} d_{\infty}^2 &= \lim_{S \to \infty} -\frac{\max\left(x_n\right)}{S} = \lim_{S \to \infty} -\frac{\max\left(\log \Pr\left(n\right) - p^{(n)}/\gamma^{(n)}\right)}{S} \\ &= \lim_{S \to \infty} \frac{\min\left(p^{(n)}/\gamma^{(n)} - \log \Pr\left(n\right)\right)}{S}. \end{aligned} \tag{4.36}$$

Recalling (**??**)

we get

$$d_{\infty}^{2} = \lim_{S\to\infty} \frac{\min\left(p^{(n)} S|H^{(n)}|^{2} {d_{min}^{(n)}}^{2}/4 - \log \Pr(n)\right)}{S}$$
$$= \frac{\min\left(p^{(n)}|H^{(n)}|^{2} {d_{min}^{(n)}}^{2}\right)}{4}. \quad (4.37)$$

Such a result shows that, at the limit for large SNR, the error probability decays exponentially with SNR and the BIC-OFDM system behaves as a binary modulation, as conjectured in the previously.So, the decay of the instantaneous PER for increasing signal-to-noise ratio has exponential nature. Moreover the estimated PER obtained through the κESM methodology preserves the asymptotic slope properties of the actual instantaneous PER.

4.3 Numerical Results

The approach for simulation of link performance, system parameters and methodology are the exact the same as MIESM and EESM section made by a c++ scripts. The only difference are the AWGN reference curves, which are BPSK at different rate. Now, in order to compare κESM with the others methods, when the β value used into the model is been achieved, the accuracy of the link performance prediction model is quantified by evaluating the complementary cumulative density function (CCDF) of the effective SNR error defined as :

$$\epsilon_{\gamma} = \gamma_{\mathit{eff},i}(\beta, \overline{PER}_i)|_{dB} - \gamma_{AWGN}(PER_{AWGN})|_{dB} \quad (4.38)$$

Complementary density function is generally defined as

$$F_c(\varepsilon_\gamma) = 1 - F(\varepsilon_\gamma)$$

where

$$F(\varepsilon_\gamma) = \int_{-\infty}^{\varepsilon_\gamma} f_\varepsilon(\tau) d\tau$$

4.3.1 SISO case

The comparison between the three abstraction methods for a single transmitting and receiving antenna case is shown from figure 4.2 to 4.5. For mode 1 (e.g. 4-QAM modulation and coding rate $R = 1/2$) the performances are almost the same for each abstraction. Error prediction does not strictly depend on choosing a specific method. Corresponding CCDF graph relevant to mode 1 in figure 4.2 shows that only 5% of absolute errors are more than 0.16 in the worst case (EESM) and around 0.11 in the best case (MI-ESM and κESM). Remarkable differences can be found for mode 3 (e.g. 16-QAM $R_c = 1/2$). Especially EESM abstraction does not follow the slope of the AWGN reference curve for decreasing PER values, so an evident cross point occurs. Therefore, it is worth noting that in CCDF figure the 95% of errors are lower than 0.40, unlike MI-ESM or κESM, which yield a corresponding value around 0.11. Generally, for higher modulation orders, EESM exhibit worse accuracy than κESM and MIESM, whose performances are comparable. In some cases, κESM is even slightly superior than MIESM. Considering mode 5 for a CCDF level of 0.05, the κESM yields an absolute error of 0.20, whereas for the MIESM an error around 0.23 is obtained. Exponential mapping is not worth mentioning. Examining CCDF graphics of MCS 7 and MCS 8 we could notice

better results by the novel abstraction method, with gaps of 0.07 dB and 0.03 dB respectively, despite 64-QAM is been employed as modulation format. Due to statements mentioned above, we could not get these considerations straight by observing figure 4.4 and 4.5 (mode 5 and mode 7) except for EESM case. MIESM and κESM abstractions do not seem to differentiate clearly. Focusing on the case in which these two models are not optimized through tuning factor, e.g. 64-QAM with different code rate, noting that κESM is almost unsensitive to tuning factor in mode 5 case, and comparable to MIESM in case of higher coding rate. However, adjusting factor for κESM depends only on coding rate, unlike MIESM, which needs an optimization factor for different modulation orders.

4.3.2 Testcase B: MIMO case

Figure **??** and figure 4.10 show results concerning MIMO transmission system, SM with MMSE receiver and STBC with MRC receiver, employing κESM , MIESM and EESM abstraction methodology. SM technique produces a large frequency selectivity with respect to the STBC technique, making an accurate PER prediction more troublesome. For mode 5 with SM (STBC) there is considerable improvement of κESM compared to MIESM. The gap is around 0.10 dB, κESM yields an error lower than 0.20 dB (0.05 dB) for the 95% of all cases. The good quality of κESM error prediction is also recognizable in PER vs Effective SNR, figure 4.7.

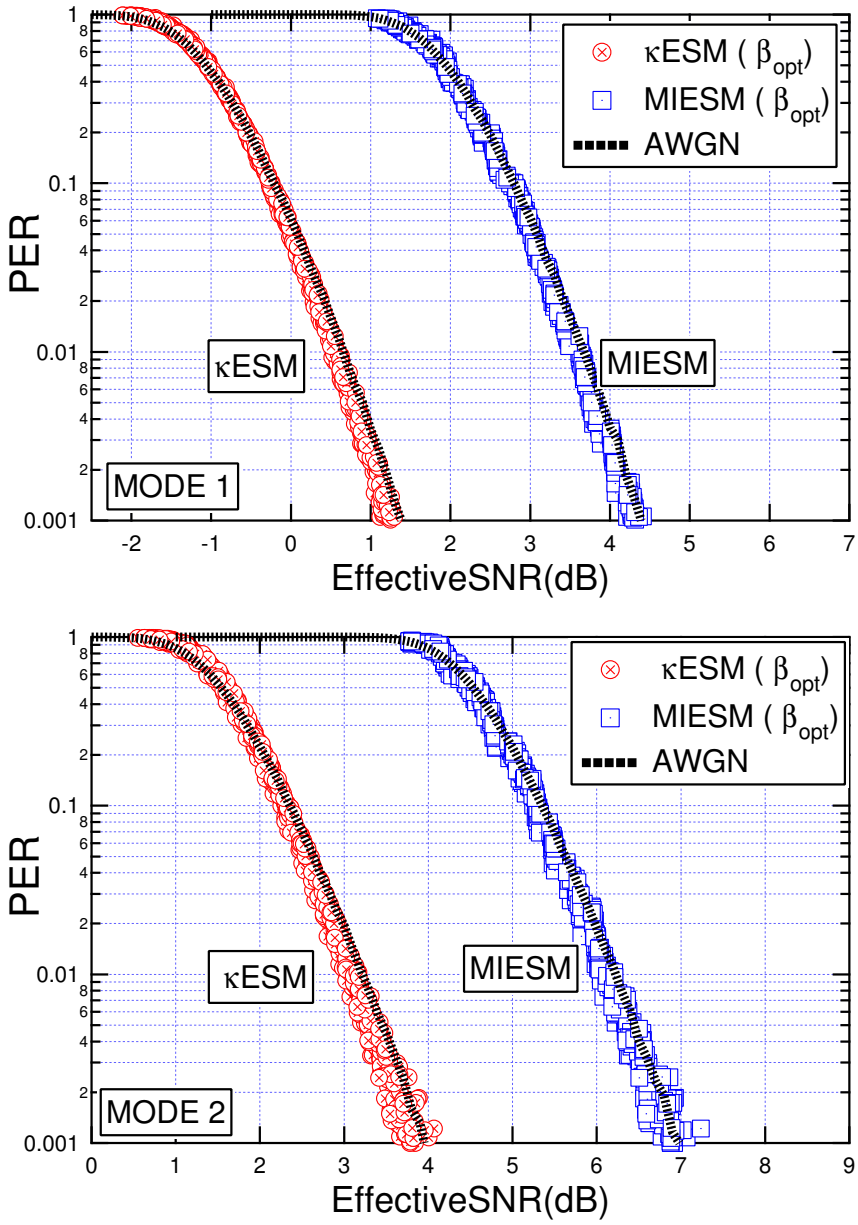

Figure 4.2. PER prediction comparison: κESM vs MIESM

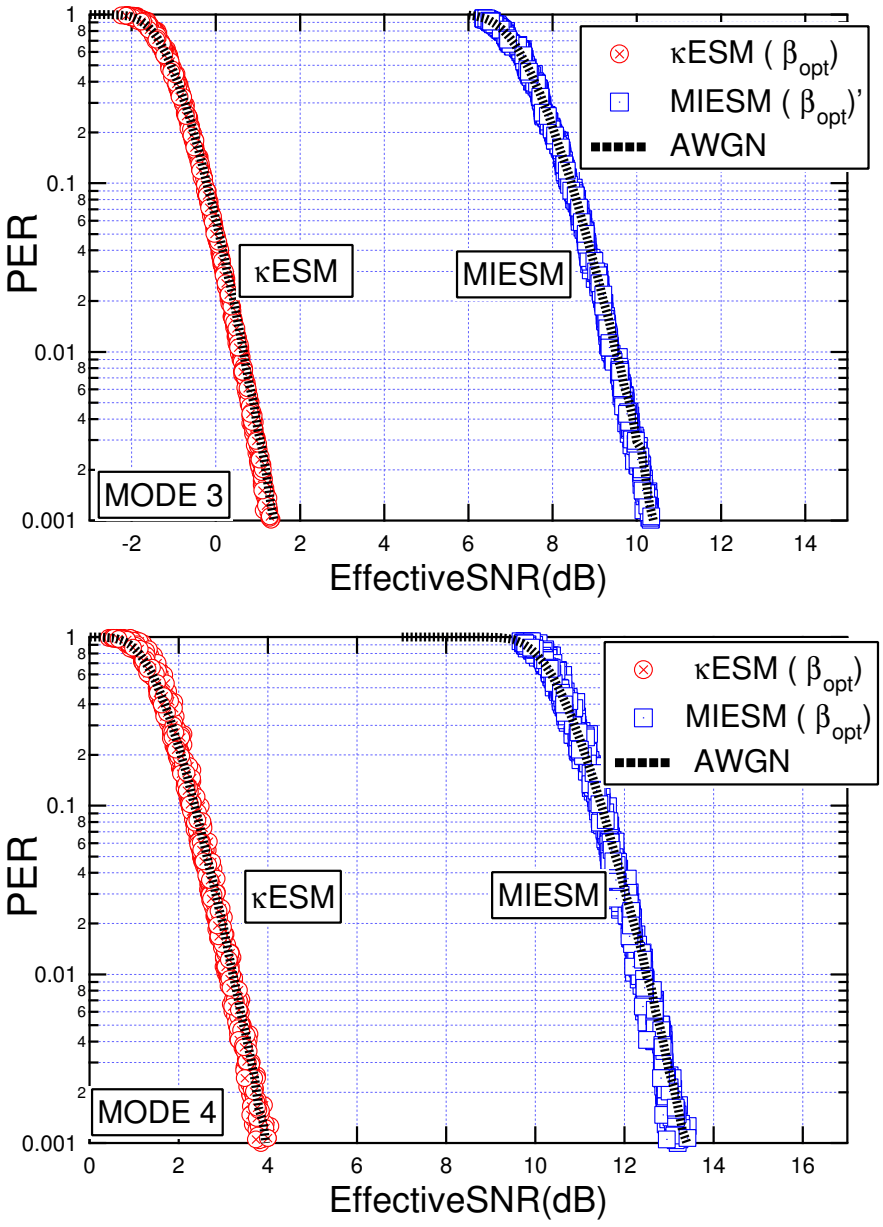

Figure 4.3. PER prediction comparison: κESM vs MIESM

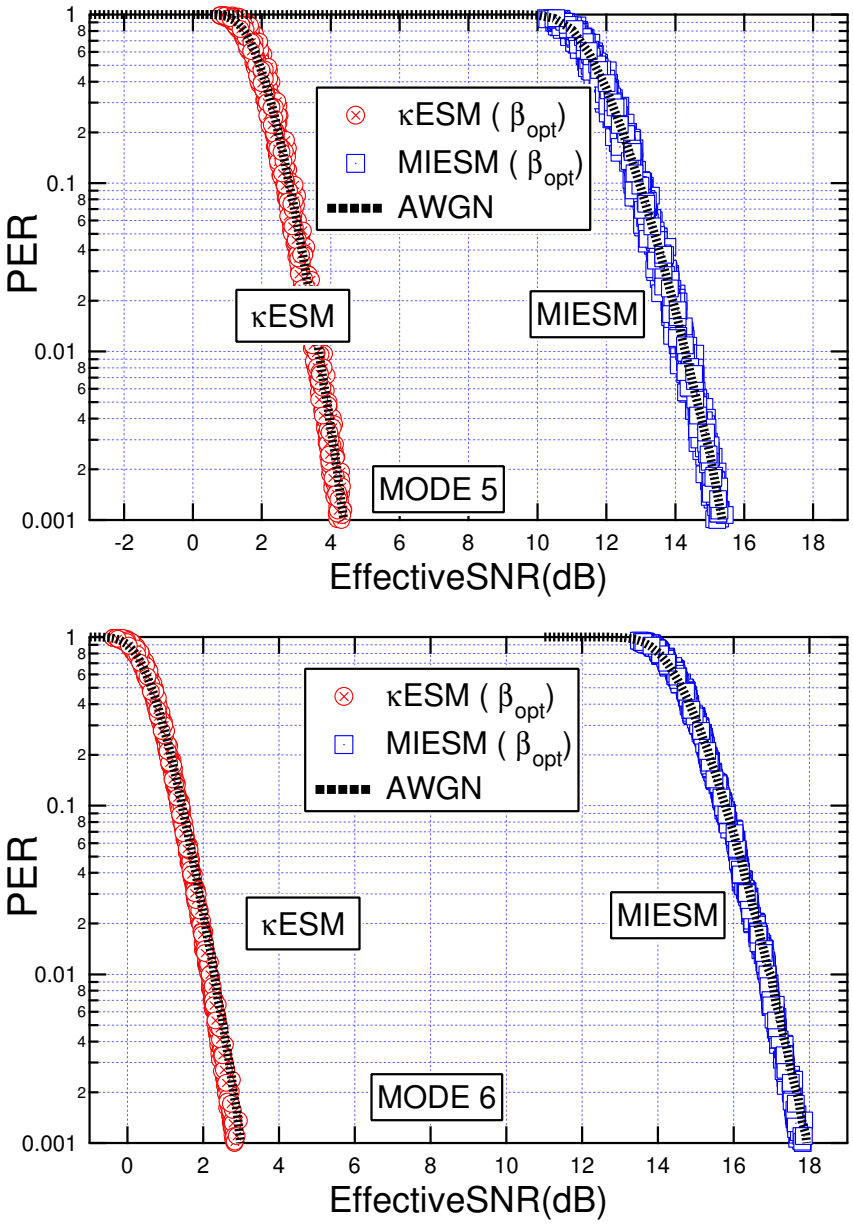

Figure 4.4. PER prediction comparison: κESM vs MIESM

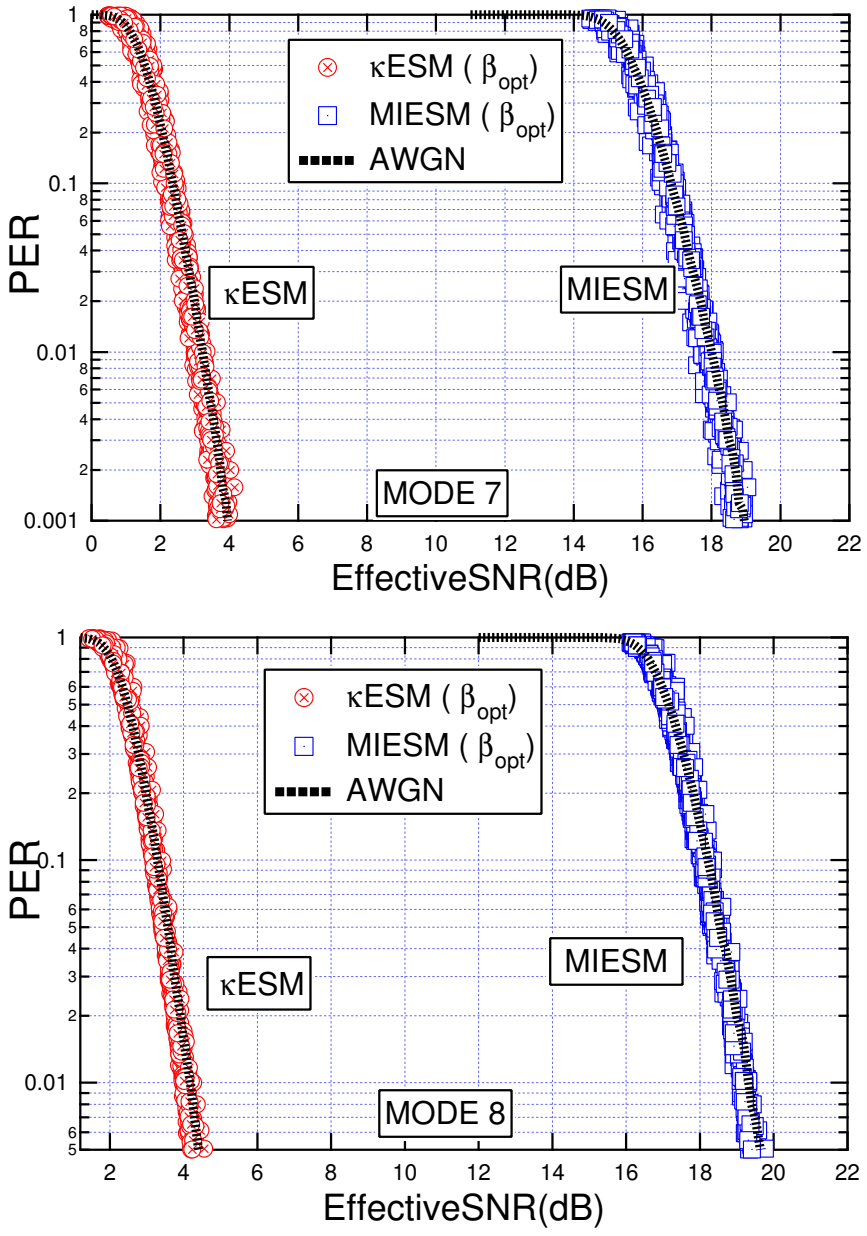

Figure 4.5. PER prediction comparison: κESM vs MIESM

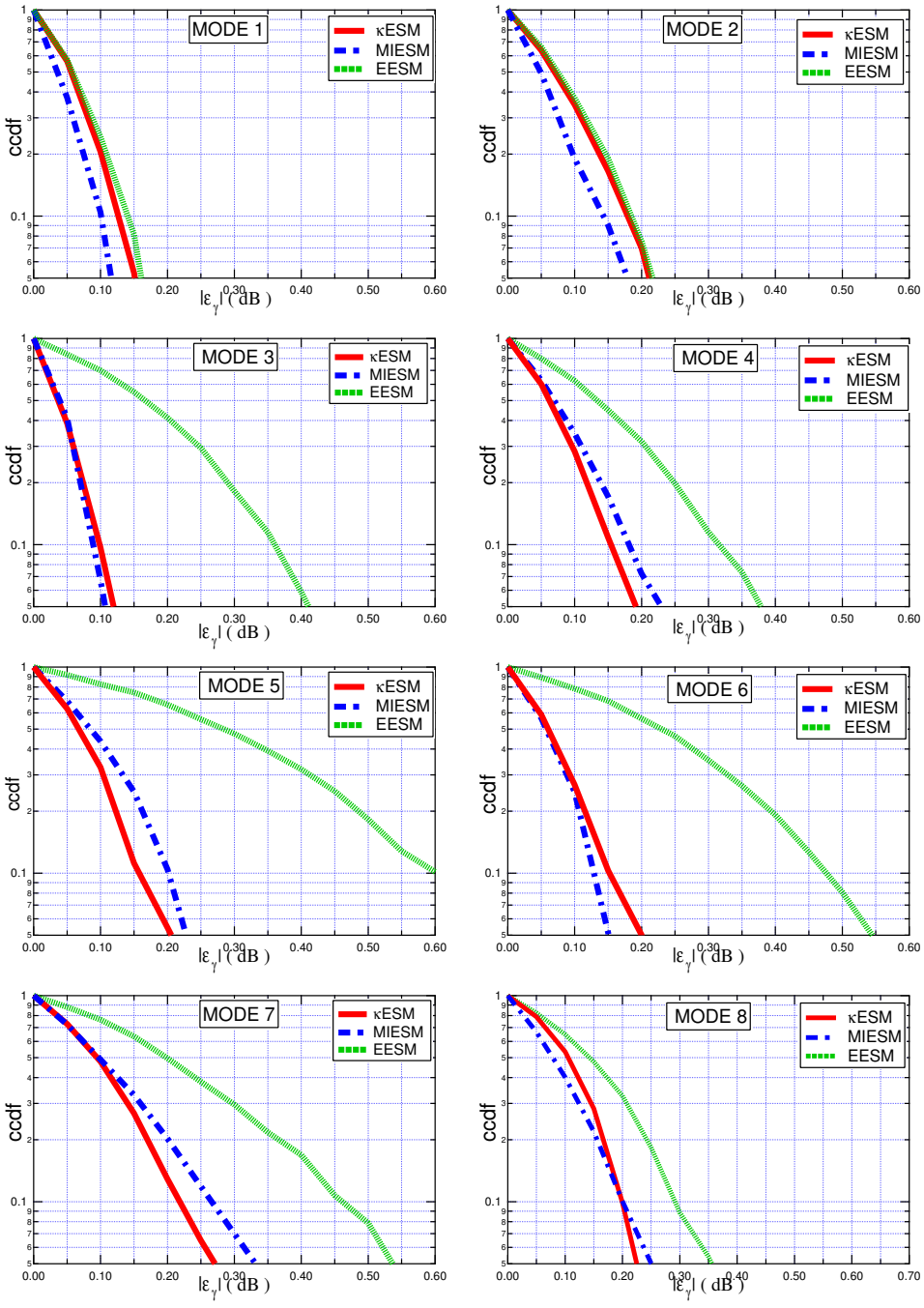

Figure 4.6. Link Performance Metric Accuracy. Complementary Cumulant Density Functions.

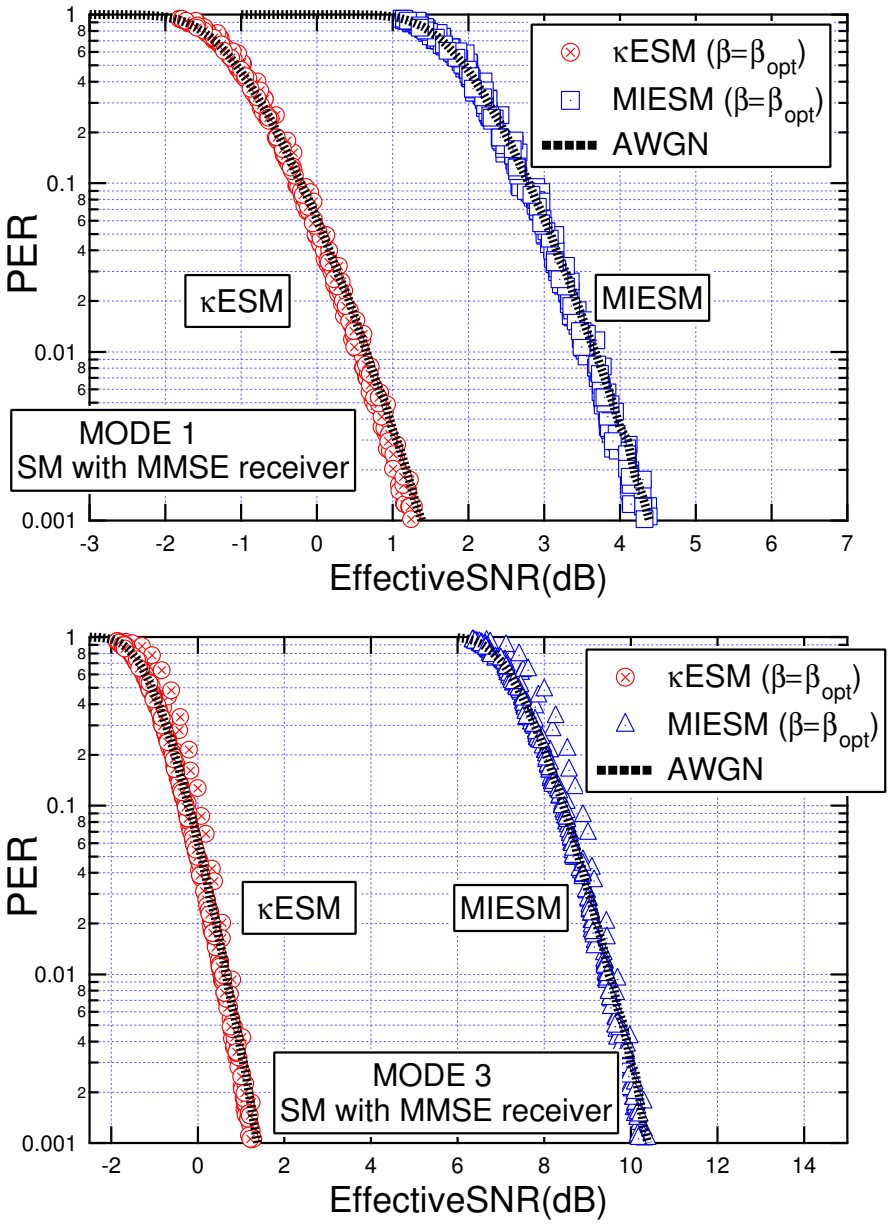

Figure 4.7. PER prediction comparison MIMO case: κESM vs MIESM

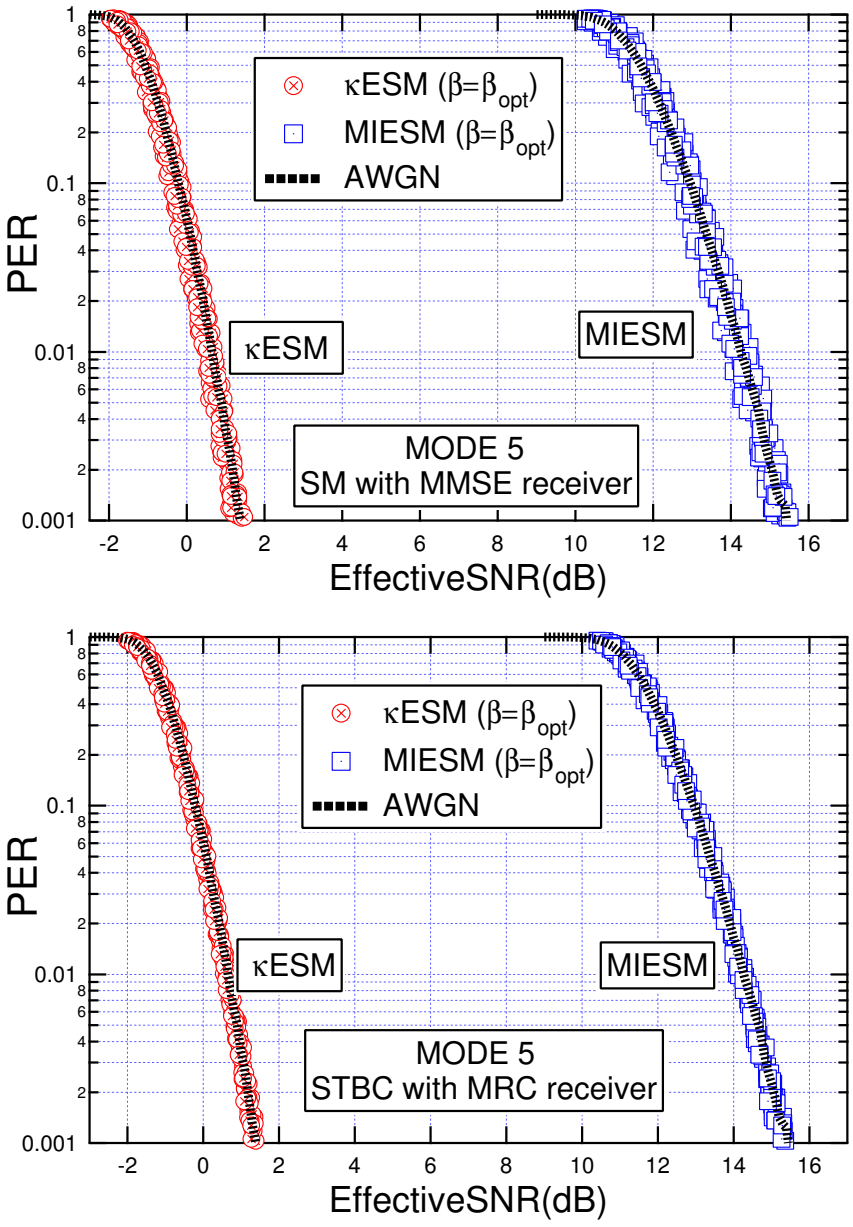

Figure 4.8. PER prediction comparison MIMO case: κESM vs MIESM

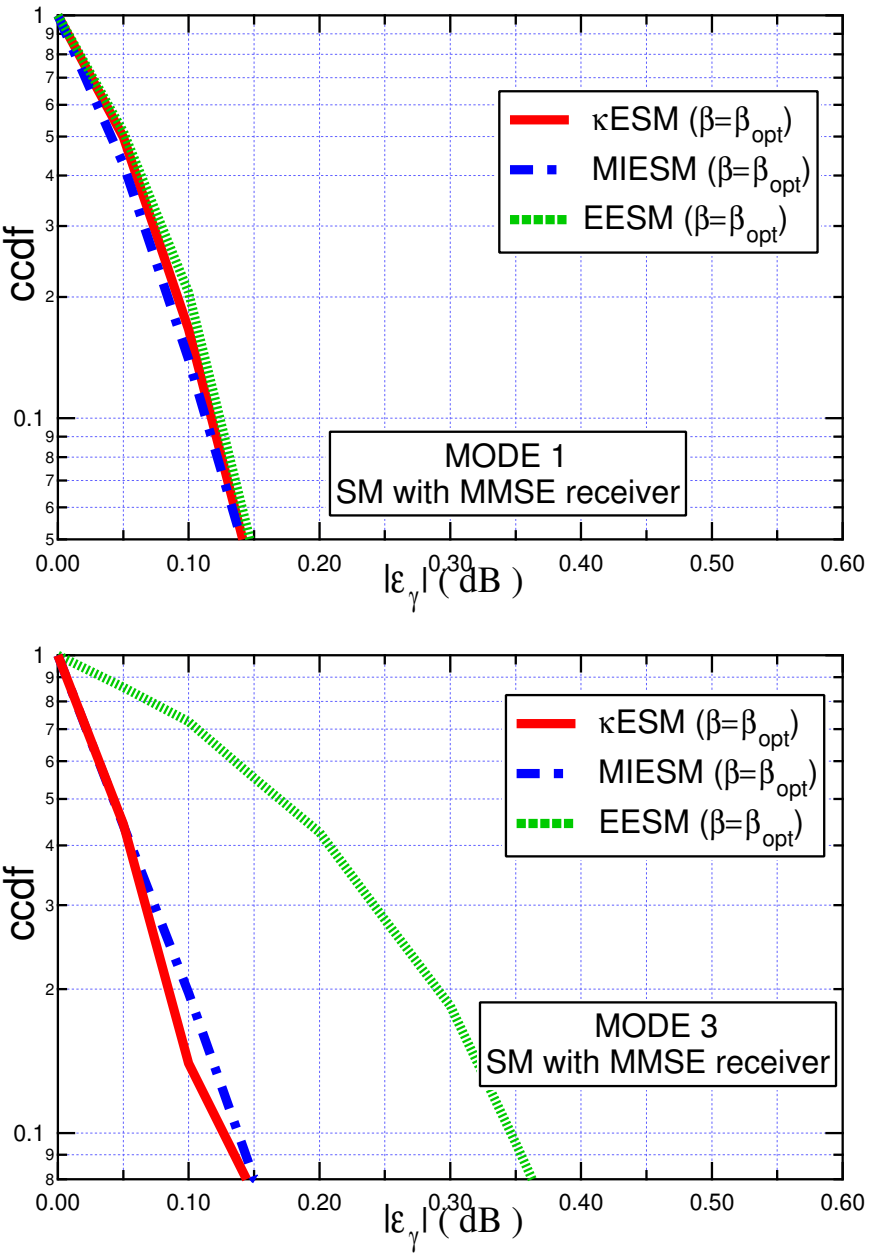

Figure 4.9. Performance Metric Accuracy. Complementary Cumulant Density Functions.

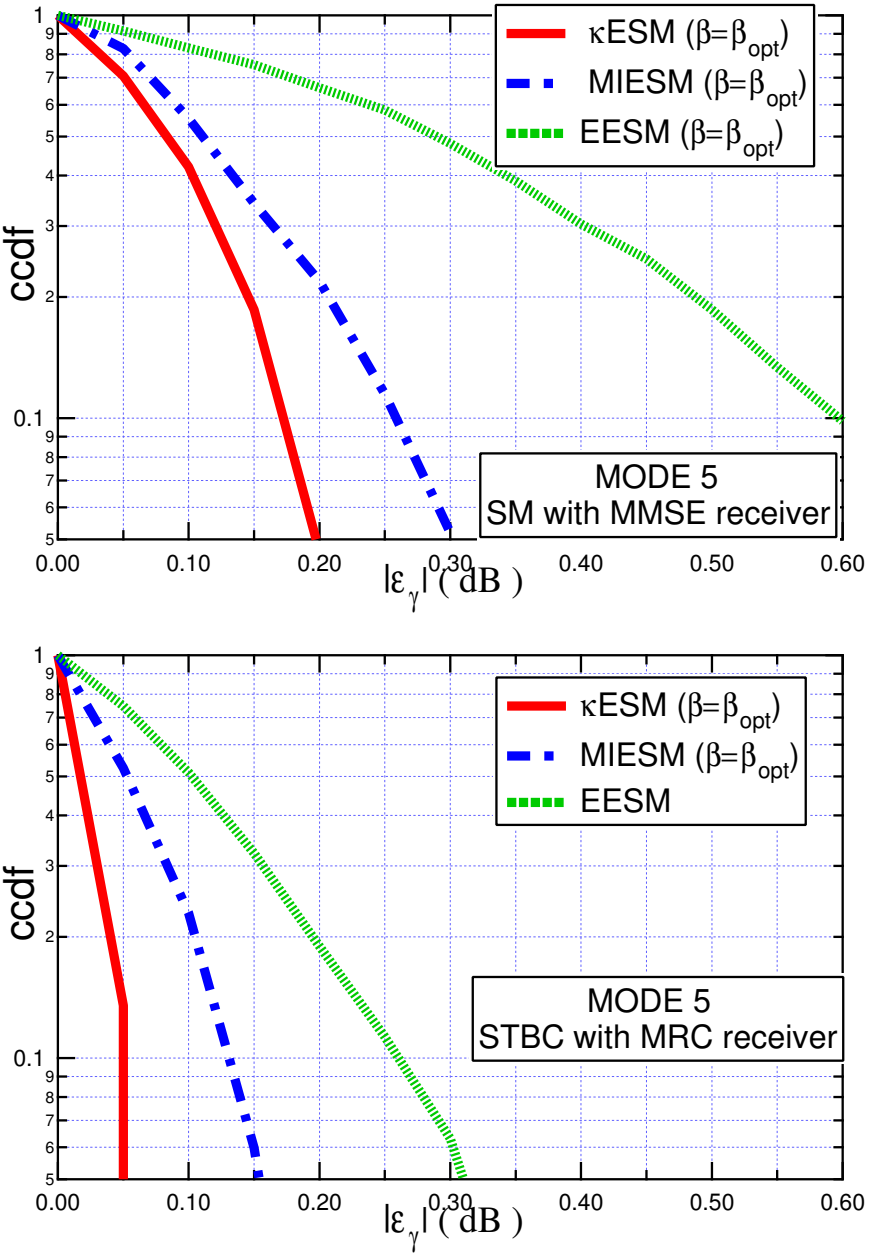

Figure 4.10. Performance Metric Accuracy. Complementary Cumulant Density Functions.

Chapter 5

Goodput based Adaptive Modulation and Coding

5.1 Introduction

When a system does not adapt the transmission parameters to the actual channel conditions, the designer must consider a fixed link margin to maintain acceptable performance also in the worst case channel condition. As apparent, this strategy leads to a very inefficient utilization of the bandwidth. Link resources adaptation (LRA) has therefore received a considerable attention as an effective tool for improving the spectrum efficiency of next-generation high-speed wireless links over fading channels. According to the LRA paradigm, some link parameters including data rate, transmit power and code rate or scheme, are adaptively modified according to the channel fading dynamics, so

as to make an as high as possible efficient usage of the available resources. The idea of adapting transmission parameters according to the channel variations was first proposed in the late sixties and early seventies [8], [9]. However, mainly due to hardware constraints and lack of reliable channel estimation techniques, the interest on these techniques has grown only in recent years when these issues became less constraining (see [10] and reference therein) As a result, many current and upcoming wireless systems such as IEEE 802.16e/m, IEEE 802.11n and 3GPP-LTE, as well as research activities such as WINNER and WINNER/II projects are using or planning to use adaptive transmission techniques ([11] – [13], [49], [48]). A promising approach to provide spectrally efficient and flexible data rate access is called adaptive modulation technique which adapts the modulation parameters and the transmission power according to the instantaneous channel conditions, [14], [15]. A further degree of freedom can be obtained by using different channel code rates (i.e. by using rate-compatible punctured convolutional (RCPC) codes) to provide different amounts of coding gain to the transmitted bits, [16], [17]. For example a stronger error correction code may be used for harsh propagation conditions, while a weaker code may be used for favorable channel conditions. The joint use of adaptive modulation and adaptive coding techniques, commonly referred to adaptive modulation and coding (AMC), has gained attention as an enticing technique to increase spectral efficiency for 3rd generation wireless systems. In practical systems, a pragmatic AMC technique involves the selection of the "best suited" modulation and coding scheme (MCS) pair for the current channel status.

5.2 Adaptive Modulation Technique

In variable-rate modulation the data rate is varied relative to the channel gain. This can be done by fixing the symbol rate of the modulation and using multiple modulation schemes or constellation sizes, or by fixing the modulation (e.g. BPSK) and changing the symbol rate. Symbol rate variation is difficult to implement in practice since a varying signal bandwidth is impractical and complicates bandwidth sharing. In contrast, changing the constellation size or modulation type with a fixed symbol rate is fairly easy, and these techniques are used in current systems. In this work we consider variable rate QAM transmission, where the number of QAM levels is varied according to the channel status and the quality criteria adopted [14].

5.3 Adaptive Coding Techniques

In adaptive coding different channel codes are used to provide different amounts of coding gain to the transmitted bits. For example a stronger error correction code may be used for harsh propagation conditions, while a weaker code may be used for favorable channel conditions. A possible implementation for adaptive coding can be obtained by multiplexing together codes with different error correction capabilities. However, this approach requires that the channel remain roughly constant over the block length or constraint length of the code [17]. On such slowly-varying channels adaptive coding is particularly useful when the modulation must remain fixed, as may be the case due to complexity or peak-to-average power ratio constraints. An alterna-

tive technique to code multiplexing is rate-compatible punctured convolutional (RCPC) codes [19]. RCPC codes consist of a family of convolutional codes at different code rates R. The basic premise of RCPC codes is to have a single encoder and decoder whose error correction capability can be modified by not transmitting certain coded bits (e.g. puncturing the code). Moreover, RCPC codes have a rate-compatibility constraint so that the coded bits associated with a high-rate (weaker) code are also used by all lower-rate (stronger) codes. Thus, to increase the error correction capability of the code, the coded bits of the weakest code are transmitted along with additional coded bits to achieve the desired level of error correction. The rate compatibility makes it very easy to adapt the error protection of the code, since the same encoder and decoder are used for all codes in the RCPC family, with puncturing at the transmitter to achieve the desired error correction. Decoding is performed by a Viterbi algorithm operating on the trellis associated with the lowest rate code, with the puncturing incorporated into the branch metrics. Adaptive coding through either multiplexing or puncturing can be done for fixed modulation or combined with adaptive modulation as a hybrid technique.

5.4 Adaptive BICM paradigm

The considered system supports a variety of modulation and coding schemes which can be selected at each packet transmission depending on channel condition. The supported modes of operation are summarized in table 2.3

Each MCS is selected by using the adaptive BICM paradigm originally pro-

posed in [**?**]. With reference to figure 5.1, the FEC block is concatenated with a mapper through a bit level interleaver. M-QAM modulation with Gray mapping is used in order to minimize the number of bit errors in every channel symbol error event. The considered system operates with a feedforward punctured 64-state convolutional encoder with mother code rate $R = 1/2$ and $d_{free} = 10$ where the polynomial generators are:

$$g_1 = 133_8 = 1011011$$
$$g_2 = 171_8 = 1111001 \tag{5.1}$$

The higher coding rates have been obtained from the mother convolutional code using the puncturing patterns show in table 2.2

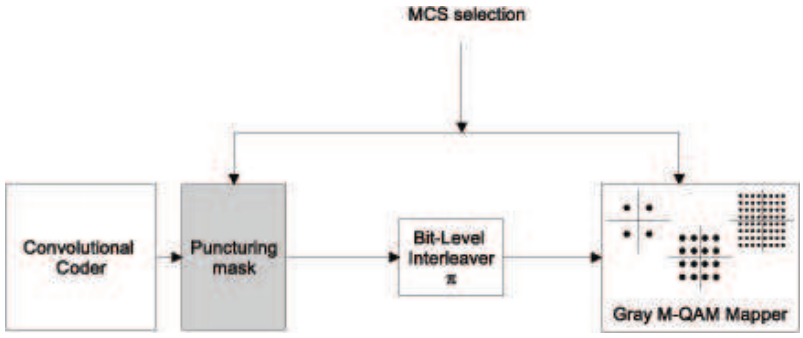

Figure 5.1. Adaptive BICM paradigm.

For the termination of convolutional code, there are three possibilities:

- Truncation: encoding is terminated with the last bit of the message and the encoder terminates in a state which is not known at the receiver side.
- Zero-termination: after encoding of the message, some tails bits are appended which drive the encoder state to zero.

- Tail-biting: the initial state is chosen such that it coincides with the final state.

The first possibility provides a bad protection of the last bits of the message, which leads to an error floor, and should therefore be avoided. Zero-termination offers the same protection for all the bits of the message, but requires some extra bits to drive the encoder states to zero. The third method combines the advantages of the previous ones and results in equal protection for all bits while maintaining the code rate, and therefore is the chosen solution.

5.5 The Goodput Criterion

In heterogeneous systems, different service classes are supported, so as the first step to design an efficient LRA algorithm consists in identifying a significative figure of merit (e.g., objective function) according to the particular requirements of each class. Only error-free RLC-PDUs are kept by the receiver, while for the others a retransmission is required. This specific feature clearly acts upon the structure of LRA, thus leading to two different classes of strategies: *i* aimed at avoiding frequent retransmission by keeping the packet error rate (PER) below a given threshold, called as delay oriented (DO) algorithms, *ii* aimed at maximizing the amount of received error-free data per unit of time, or *goodput* (GP) for short, irrespective of the rate of retransmissions, called as GP oriented (GO) algorithms. Each of these strategy is suitable for particular service classes. The most common applications can be divided in four service

classes characterized by different quality of service (QoS) requirements [46], as listed below.

- *Unsolicited Grant Service* (UGS) supports constant bit rate of fixed throughput connections such as voice over IP (VoIP). This service provides guarantees on throughput and latency.
- *Real-time Polling Service* (rtPS) provides guarantees on throughput and latency, but with greater tolerance on latency relative to UGS. This class supports services such as MPEG video conferencing and video streaming.
- *Nonreal-time Polling Service* (nrtPS) provides guarantees in terms of throughput only and is therefore suitable applications like File Transfer Protocol.
- *Best Effort* (BE) service provides no guarantees on delay or throughput and is used for Hypertext Transport Protocol (HTTP) and electronic mail (e-mail).

Let note that the last two classes do not require strict delay constraint. For these applications, the users are only interested in one quantity: the number of data bits delivered in error-free packets per unit of time (i.e., the offered layer 3 data rate) which is exactly what the goodput criterion expresses. In this work, we propose a LRA algorithm which exploits the *expected goodput* metric as originally proposed in [39] and [40]. Loosely speaking, when a wireless station is ready to transmit a data packet, its expected goodput is defined as the ratio between the data payload to be delivered and the expected transmission

time assuming that the signal will experience the current channel conditions known at the transmitter. Clearly, depending on the data payload length and the wireless channel conditions, the expected goodput varies with different transmission strategies. The more robust the transmission strategy, the more likely the frame will be delivered successfully within the frame retry limit, however with less spectral efficiency. So, there is a tradeoff and the key idea of the link adaptation is to select the most appropriate transmission strategy such that the frame can be successfully delivered in the shortest possible transmission time.

5.6 Goodput-Oriented AMC algorithm

A pragmatic algorithm to effectively select the MCS which maximizes the expected goodput is necessary for AMC technique. As shown in chapter 1, each RLC-PDU consists of the following components: N_h bits of *RLC header* including the ARQ-PR identifier, N_p bits of *payload* and the *CRC*. Thus, the total RLC-PDU length is given by

$$N_{\text{PDU}} = N_h + N_p + N_{\text{CRC}}. \tag{5.2}$$

Being $m_i^{(\mathbf{c})}$ and R_i the number of binary coded symbol transmitted on the subchannel $\mathbf{c}$ and the coding rate associated with the ith protocol round, respectively, the number of RLC-PDU bits transmitted during an OFDM symbol period is given by

$$\mathcal{V}\left(\hat{\phi}_i\right) \triangleq R_i \sum_{\mathbf{c}\in\Psi_i} m_i^{(\mathbf{c})}, \tag{5.3}$$

where $\hat{\phi}_i$ is the selected transmission mode and Ψ_i is the subspace containing the indexes of all the active subchannels. Based on this, the duration of an RLC-PDU transmission is

$$T_{\text{PDU}}\left(\hat{\phi}_i\right) \triangleq \frac{N_{\text{PDU}}}{\mathcal{V}\left(\hat{\phi}_i\right)} T_{\text{OFDM}}. \tag{5.4}$$

When the RLC-PDU is transmitted using the transmission mode $\hat{\phi}_i$ over the wireless channel condition summarized by the effective SNR value $\gamma_{\kappa ESM}\left(\hat{\phi}_i\right)$, the probability of a successful frame transmission can be calculated as

$$P_{\text{succ}}\left(\hat{\phi}_i\right) \triangleq 1 - PER\left(\gamma_{\kappa ESM}\left(\hat{\phi}_i\right), \hat{\phi}_i\right) \tag{5.5}$$

.

Assuming perfect knowledge of channel state information at transmitter side, the only adjustable parameters are the coding rate and the number of transmitted bits. Imposing the condition $m_i^{(\mathbf{c})} = \overline{m}_i \quad \forall \quad \mathbf{c} \in \Psi_i$, the corresponding transmission mode can be simply represented by the pair $\hat{\phi}_i = \left(\hat{m}_i, \hat{R}_i\right)$.

So, we should base the selection of the transmission mode under the assumption that the channel will remain the same and then $\hat{\phi}_i = \overline{\phi}, \forall i$. Recalling that the average goodput is defined as ratio of expected delivered data payload to average transmission time, the expression is :

$$GP\left(\overline{\phi}\right) = \frac{N_p}{\frac{N_{\text{PDU}}}{\mathcal{V}\left(\overline{\phi}\right)} T_{\text{OFDM}}} \left[1 - PER\left(\gamma_{\kappa ESM}\left(\overline{\phi}\right), \overline{\phi}\right)\right] \tag{5.6}$$

Let define objective function of the optimization task, the normalized GP metric:

$$\widetilde{GP}\left(\hat{\phi}\right) \triangleq \frac{GP\left(\hat{\phi}\right)}{T_{\mathrm{OFDM}} N} \tag{5.7}$$

where N represents the number of active subcarriers

Substituting (5.6) into (5.7) we obtain

$$\widetilde{GP}\left(\overline{\phi}\right) = \frac{N_p}{N_{\mathrm{PDU}}\, N}\, \overline{m}\, \overline{R}|\Psi|\, \left[1 - PER\left(\gamma_{\kappa ESM}\left(\overline{\phi}\right), \overline{\phi}\right)\right] = \overline{m}\, \widetilde{GP}_{\mathrm{eff}} \tag{5.8}$$

with

$$\widetilde{GP}_{\mathrm{eff}}\left(\overline{\phi}\right) \triangleq \frac{N_p}{N_{\mathrm{PDU}}\, N}\, \overline{R}|\Psi|\, \left[1 - PER\left(\gamma_{\kappa ESM}\left(\overline{\phi}\right), \overline{\phi}\right)\right] \tag{5.9}$$

representing the value of normalized goodput for a binary transmission over an AWGN channel with SNR equal to $\gamma_{\kappa ESM}\left(\overline{\phi}\right)$, or *effective expected goodput*. The effective expected goodput can be evaluated off-line as function of the coding rate through numerical simulations. Then, the optimum coding rate can be simply computed by using a look-up table whose entries are selected by the effective SNR value. Bearing in mind these considerations, the optimization problem

$$\begin{aligned} &\underset{\phi}{\text{maximize}} && \widetilde{GP}\left(\phi\right) \\ &\text{subject to} && \overline{m} \in \{0, 2, \cdots, m_{max}\}\,. \\ &\text{subject to} && \overline{R} \in \{R_1, R_2, \cdots, R_{max}\}\,. \end{aligned}$$

has been solved through the low-complexity algorithm outlined hereafter.

AMC Algorithm

1) Initialize the modulation size, $\overline{m} = \max(m), \quad m \in \mathcal{M}$

2) Compute the effective SNR value, $\overline{\gamma}_{\text{eff}} = \gamma_{\kappa\text{ESM}}(\overline{m})$

3) Initialize the code rate, $\overline{R} = R(\overline{\gamma}_{\text{eff}})$

4) Initialize the maximum goodput value, $GP_{\max} = GP(\overline{\gamma}_{\text{eff}})$

5) Set the variable m, $m = \overline{m} - 2$

6) Compute the effective SNR, $\gamma_{\text{eff}} = \kappa\text{ESM}(m)$

7) while $GP_{\max} \leq GP(\gamma_{\text{eff}})$

Set the number of bits allocated per subchannel,$\overline{m} = m$

Repeat points from 2) to 6)

end while,

end.

5.6.1 Numerical Results

Simulation results are obtained using c++ scripts and it++ libraries. Figure 5.3 shows the effectiveness of the GO AMC algorithm when compared with the non adaptive case. The average goodput performance obtained by adaptively selecting the "best suited" MCS (solid line) is always better than the performance obtained for static transmission (dotted lines). The GO algorithm has been compared with a DO algorithm with $PER = 10^{-2}$ constraint. The DO algorithm simply chooses the pair of coding and modulation size with

the highest bit rate respecting the given PER constraint. As apparent from figures 5.4 and 5.5, the GO algorithm guarantees better GP performance at the price of an increased delay especially for low SNR values.

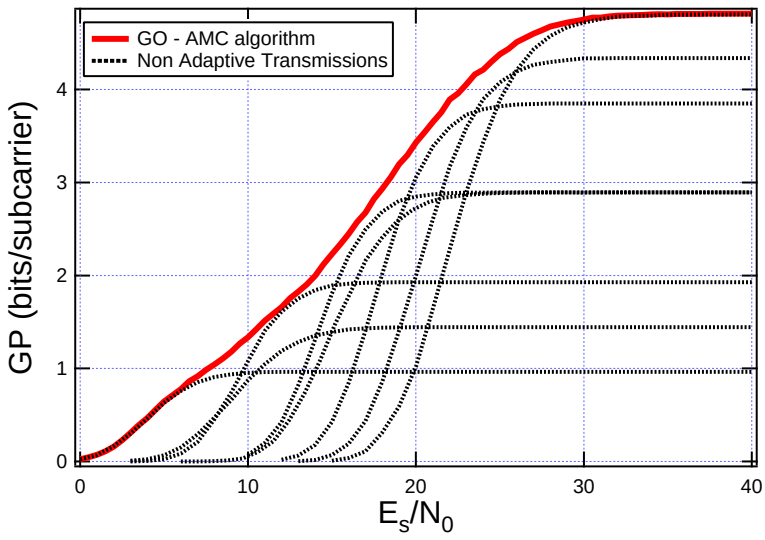

Figure 5.2. Comparison between GO-AMC and Non-adaptive transmission. Goodput performance

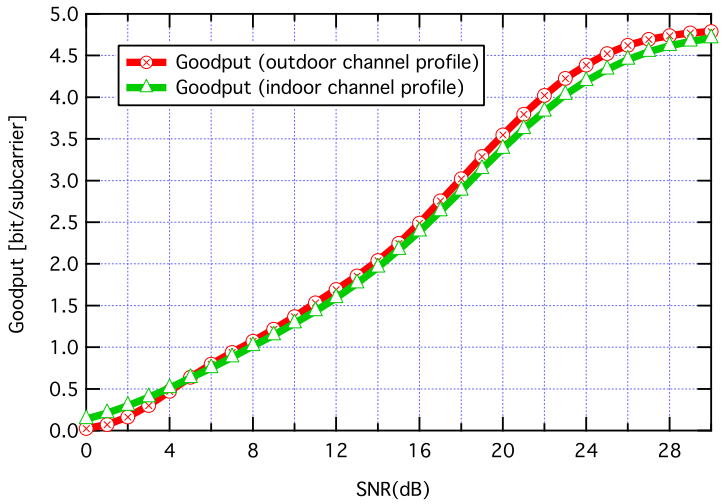

Figure 5.3. Comparison between GO-AMC and Non-adaptive transmission. Goodput performance

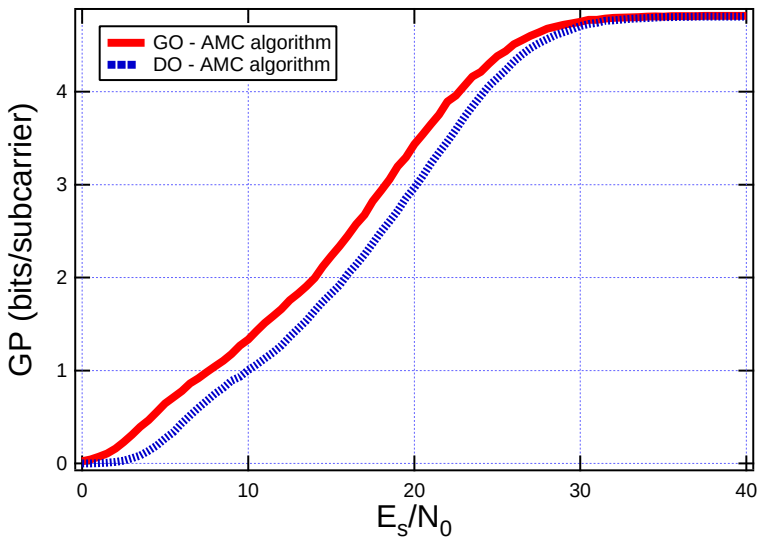

Figure 5.4. Comparison between GO-AMC and DO-AMC. Goodput performance

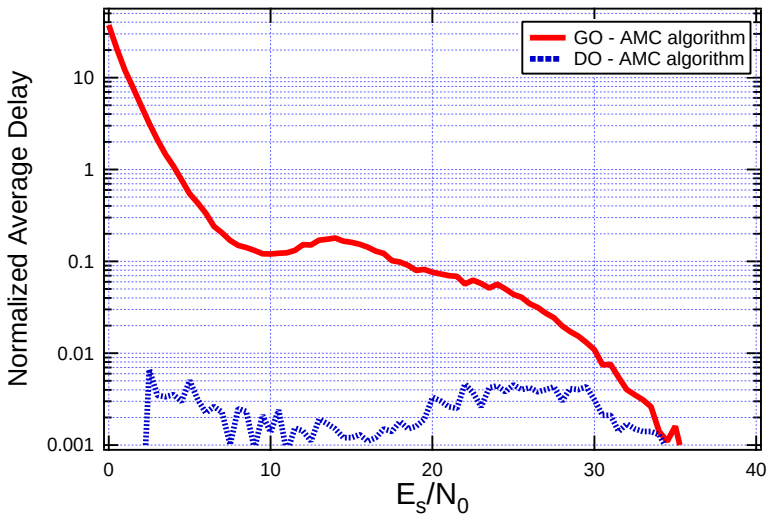

Figure 5.5. Comparison between GO-AMC and DO-AMC. Average Delay.

Chapter 6

Conclusion

This work addresses the design of a novel GO-based LRA strategy, specifically intended for MIMO BIC-OFDM transmissions. Compared with previous works, several features differentiate the proposed approach and define the core concepts our contribution relies on.

1. According to the PEP analysis proposed in [25]– [28], a novel link level performance evaluation methodology, which offers improved accuracy and low complexity together.

2. Once the link level performance estimate is given, a simple model for the evaluation of the expected goodput figure of merit is derived. Based on this, a low complexity GO-based LRA strategy is proposed. Then, the GO algorithm proposed is compared with a DO-based strategy in terms of average goodput and transmission delay.

3. When CSI is assumed to be perfectly known at the transmitter, the

adaptation algorithm utilizes the frequency selectivity of the channel to properly allocate the power among the subchannels through a novel power allocation strategy based on the maximization of the goodput figure of merit.

The main points (each corresponding to distinct consecutive sections) this work is structured on can be summarized as follows.

- *Multiple Antenna BIC-OFDM System.* The description of the MIMO BIC-OFDM system model is provided up to the expression of the receiver DFT output samples. The system parameters are defined with special emphasis on modulation and coding schemes .

- *Link Level Performance Modeling for Multiple Antenna BIC-OFDM Systems.* Capitalizing on a simple approximation of the Pairwise Error Probability (PEP), a novel strategy to evaluate the link level performance (e.g. packet error rate, goodput) is provided. The proposed method is then fairly compared with the literature.

- *Goodput Oriented AMC algorithms for Coded OFDM systems.* Efficient GO strategies to allocate the available resources are formalized.

References

[1] IEEE Standard for Local and Metropolitan Area Networks Part 16: Air Interface for Fixed Broadband Wireless Access Systems, IEEE Std. 802.16-2004, October 2004.

[2] IEEE Standard for Local and Metropolitan Area Networks Part 16: Air Interface for Fixed Broadband Wireless Access Systems, IEEE Std. 802.16e-2005, February 2006.

[3] ITU, The World Radiocommunication Conference 2007 (WRC-07), Geneva, november 2007.

[4] ITU-Radiocommunication, List of ITU Member countries by regions. http://life.itu.int/radioclub/rr/itureg.htm. Accessed 27th May 2008

[5] M. Luise, "Introduzione all' OFDM", file pdf consultabile sul sito dell'autore:

`http://www2.ing.unipi.it/~d7384/HTML/TeachFrm_ita.html`

[6] S. Plass, S. Sand, M. Sternad, and A. Svensson"High spectral efficient and flexible next generation mobile communications",*Journal on Wireless Personal Communications*, pp. 11, Oct. 2007

[7] D. Haccoun, G. Bgin, "High-rate punctured convolutional codes for Viterbi and sequential decoding", Transactions on Communications, vol. 37, N 11, November 1989

[8] J.F. Hayes,"Adaptive Feedback Communications", *IEEE Transactions on Communication Technology*, Vol. 16, pp. 29–34, Feb. 1968.

[9] J.K. Cavers,"Variable-Rate Transmission for Rayleigh Fading Channels", *IEEE Transactions on Communications*, Vol. 20, pp. 15–22, Feb. 1972.

[10] G. Klang et Al.,"Identification of Radio-Link Technologies", *IST-2003-507581*, WINNER,D2.1 Public Deliverable.

[11] IEEE 802.16e-2005,"802.16 IEEE Standard for Local and Metropolitan Area Networks, Part 16: Air Interface for Fixed and Mobile Broadband Wireless Access Systems", 2005.

[12] IEEE 802.16m-08/004r5,"Project 802.16m Evaluation Methodology Document (EMD)", January 2009.

[13] IST-4-027756 WINNER II "D2.2.3 Modulation and Coding Schemes for the WINNER II System", November 2007.

[14] W.T. Webb and R. Steele"Variable Rate QAM for Mobile Radio", *IEEE Transactions on Communications*, pp. 2223–2230, July 1995.

[15] S.T. Chung, A.J.Goldsmith,"Degrees of Freedom in Adaptive Modulation: a Unified View", *IEEE Transactions on Communications*, Vol. 49, pp. 1561–1571, Sep. 2001.

[16] B. Vucetic,"An Adaptive Coding Scheme for Time-Varying Channels", *IEEE Transactions on Communications*, Vol. 39, pp. 653–663, May 1991.

[17] M. Rice and S.B. Wicker,"Adaptive Error Control for Slowly Varying Channel", *IEEE Transactions on Communications*, Vol. 42, pp. 917–926, Feb.-Apr. 1994.

[18] G. J. Foschini, M. Gans, "On limits of wireless communications in a fading environment when using multiple antennas," Wireless Pers. Commun., vol. 6, pp. 311-355, March 1998

[19] J. Hagenauer, Rate-compatible punctured convolutional codes (RCPC codes) and their applications, IEEETrans. Commun., Vol. 36, No. 4, pp. 389400, April 1988.

[20] G.J. Foschini, "Layered Space-Time Architecture for Wireless Communications in Fading Environment When Using Multi-Element Antennas" *Bell Lab. Tech. J.*, Vol. 1, no. 2, pp. 41–59, 1996.

[21] I.E. Telatar, "Capacity of Multi-Antenna Gaussian Channels" *Eur. Trans. Commun.*, Vol. 10, no. 6, pp. 585–595, Nov./Dec. 1999.

[22] S.M. Alamouti, "A Simple Transmit Diversity Technique for Wireless Communication" *IEEE J. Select. Areas Commun.*, Vol. 16, pp. 1451–1458, Oct. 1998.

[23] E. Zehavi,"8-PSK Trellis Codes for a Rayleigh Channel", *IEEE Transactions on Communications*, Vol. 40, pp. 873–884, May 1992.

[24] G. Caire, G. Taricco, E. Biglieri,"Bit-Interleaved Coded Modulation", *IEEE Transactions of Information Theory*, Vol. 44, pp. 927–946, May 1998.

[25] A. Martinez, A.G. Fabregas, G. Caire,"Error Probability Analysis of Bit-Interleaved Coded Modulation", *IEEE Transactions of Information Theory*, Vol. 52, pp. 262–271, Jan. 2006.

[26] I. Stupia, F. Giannetti, V. Lottici, L. Vandendorpe, "A Novel Link Performance Prediction Method for Coded MIMO-OFDM Systems", *WCNC 2009*, Budapest, Hungary, April 2009

[27] I. Stupia, F. Giannetti, V. Lottici, L. Vandendorpe, "A Novel Exponential Link Error Prediction Method for MIMO Systems", *MCSS 2009*, , Germany, March 2009

[28] R. McKay, I.B. Collings , A. Forenza, R.W. Heath Jr.,"A Throughput-Based Adaptive MIMO-BICM Approach for Spatially-Correlated Channels", *ICC 2006*, June 2006.

[29] R. W. Heath Jr. and D. J. Love, "Multi-mode Antenna Selection for Spatial Multiplexing with Linear Receivers", *IEEE Trans. on Signal Processing*, 2005.

[30] Y. Blankenship, P. Sartori, B. Classom, V. Deasy, K.L. Baum, "Link Error Prediction Methods for Multicarrier Systems", *VTC 2004-Fall*, Vol.6 , pp. 4175–4179, September 2004.

[31] Nortel, "OFDM Exponential Effective SIR Mapping Validation, EESM Simulation Results for System-Level Performance Evaluations", *3GPP TSG-RAN1 Ad Hoc, R1-04-0089*, January, 2004.

[32] S. Tsai,"Effective-SNR Mapping for Modeling Frame Error Rates in Multiple-State Channels", 3GPP2-C30-20030429-010, Apr 2003.

[33] L. Wan, S. Tsai,and M. Almergn, A fading-Insensitive Performance Metric for a Unified Link Quality Model, *IEEE WCNC*, Vol.4, pp. 2110-2114, Apr 2006.

[34] Xiang Chen, Lei Wan, Zhenyuan Gao, Zesong Fei, Jingming Kuang, "The Applicationof the MI-Based Link Quality Model for Link Adaptation of Rate Compatible LDPC Codes", *VTC-2007 Fall*, pp. 1288-1292, Oct. 2007

[35] K. Brueninghaus, D. Astely, Th. Slzer, S. Visuri, A. Alexiu, St. Karger, G. A. Seraji, Link Performance Models for System Level Simulations of Broadband Radio Access Systems, *PIMRC*, Berlin 2005

[36] E. Tuomaala, H. Wang, "Effective SINR approach of link to system mapping in OFDM/multi-carrier mobile network", *Proc. of the 2nd International Conference on Mobile Technology, Applications and Systems*, 5 pp., 1517 Nov. 2005.

[37] S. Simoens, S. Rouquette-Lveil, P. Sartori, Y. Blankenship, B. Classon,"Error prediction for adaptive modulation and coding in multiple-antenna OFDM systems", *Signal Processing*, Vol. 86, Issue 8, pp. 1911 - 1919, Aug. 2006

[38] R. Lugannani, S. Rice,"Saddle-Point Approximation for the Distribution of the Sum of Independent Random Variables", *Advances in Applied Probability*, Vol. 12, n. 2, pp. 475–490, June 1980.

[39] D. Qiao, S. Choi, K.Shin,"Goodput Analysis and Link Adaptation for IEEE 802.11a Wireless LANs", *IEEE Tr. on Mobile Computing*, Vol. 1, pp. 278–292, Dec. 2002.

[40] M. Realp, A. Perez-Neira, C. Mecklenbrauker,"A Cross-Layer Approach to Multi-User Diversity in Heterogeneous Wireless Systems", *ICC 2005*.

.

[41] E. Biglieri, G. Caire, G. Taricco,"Computing Error Probabilities over Fading

Channel: a Unified Approach", *European Transactions on Telecommunications*, Vol. 9, pp. 15–25, Jan.-Feb. 1998.

[42] J.I. Jensen,*Saddlepoint Approximations*, Oxford U.K., Clarendon 1995.

[43] R.G. Gallager,*Information Theory and Reliable Communications*, New York, Wiley 1968.

[44] Ericsson, "System Level Evaluation of OFDM - Further Considerations", *TSG-RAN WG1 35, R1-03-1303*, Nov. 2003.

[45] Nortel, "Effective SIR Computation for OFDM System-Level Simulations", *TSG-RAN WG1 35, R03-1370*, Nov. 2003.

[46] Q. Liu, X. Wang, G.B. Giannakis "A Cross Layer Scheduling Algorithm With QoS Support in Wireless Network", *IEEE Transactions on Vehicular Technology*, Vol. 55, pp. 839–847, May 2006.

[47] J.-F. Cheng,"Coding Performance of Hybrid ARQ Scheme", *IEEE Transactions on Communications*, Vol. 54, Issue 6, pp. 1017–1029, Jun. 2006.

[48] C.K. Sung, S. Chung, J. Heo, I. Lee, "Adaptive Bit-Interleaved Coded OFDM With Reduced Feedback Information", *IEEE Transactions on Communications*, Vol. 55, pp. 1649–1655, Sep. 2007.

[49] 216715 NEWCOM++ DR3.1 - First report: Review of State-of the art and research on AMC for concatenated coded multi-carrier systems

Appendix A

RBIR to SNR mapping table

4QAM	16QAM	64QAM
0.1299, 0.1333, 0.1366, 0.1389, 0.1418,	0.0649, 0.0667, 0.0687, 0.0700, 0.0714,	0.0433, 0.0445, 0.0458, 0.0467, 0.0476,
0.1477, 0.1480, 0.1516, 0.1531, 0.1585,	0.0724, 0.0743, 0.0771, 0.0766, 0.0792,	0.0483, 0.0495, 0.0514, 0.0511, 0.0528,
0.1593, 0.1678, 0.1688, 0.1745, 0.1775,	0.0813, 0.0822, 0.0835, 0.0856, 0.0876,	0.0542, 0.0548, 0.0557, 0.0571, 0.0584,
0.1770, 0.1842, 0.1875, 0.1906, 0.1935,	0.0898, 0.0904, 0.0921, 0.0944, 0.0983,	0.0599, 0.0603, 0.0614, 0.0630, 0.0655,
0.2000, 0.1994, 0.2049, 0.2108, 0.2147,	0.1000, 0.1015, 0.1008, 0.1049, 0.1072,	0.0667, 0.0677, 0.0672, 0.0699, 0.0715,
0.2174, 0.2183, 0.2250, 0.2313, 0.2390,	0.1117, 0.1118, 0.1149, 0.1149, 0.1177,	0.0745, 0.0746, 0.0766, 0.0766, 0.0785,
0.2379, 0.2437, 0.2502, 0.2565, 0.2599,	0.1222, 0.1246, 0.1244, 0.1275, 0.1315,	0.0815, 0.0831, 0.0829, 0.0850, 0.0877,
0.2630, 0.2703, 0.2742, 0.2816, 0.2843,	0.1348, 0.1380, 0.1393, 0.1392, 0.1443,	0.0899, 0.0921, 0.0929, 0.0928, 0.0963,
0.2913, 0.2973, 0.3054, 0.3076, 0.3140,	0.1454, 0.1484, 0.1506, 0.1544, 0.1592,	0.0970, 0.0990, 0.1004, 0.1030, 0.1062,
0.3245, 0.3273, 0.3341, 0.3311, 0.3423,	0.1595, 0.1630, 0.1648, 0.1704, 0.1741,	0.1064, 0.1087, 0.1100, 0.1137, 0.1162,
0.3477, 0.3566, 0.3586, 0.3648, 0.3810,	0.1780, 0.1778, 0.1823, 0.1822, 0.1929,	0.1188, 0.1186, 0.1216, 0.1216, 0.1287,
0.3814, 0.3849, 0.3922, 0.3987, 0.4041,	0.1938, 0.1964, 0.1984, 0.2049, 0.2067,	0.1293, 0.1311, 0.1324, 0.1367, 0.1380,
0.4161, 0.4177, 0.4244, 0.4332, 0.4379,	0.2079, 0.2116, 0.2195, 0.2200, 0.2226,	0.1388, 0.1412, 0.1465, 0.1469, 0.1486,
0.4554, 0.4540, 0.4590, 0.4688, 0.4779,	0.2278, 0.2314, 0.2333, 0.2399, 0.2441,	0.1521, 0.1545, 0.1558, 0.1603, 0.1631,
0.4913, 0.4952, 0.4990, 0.5134, 0.5166,	0.2489, 0.2554, 0.2571, 0.2584, 0.2618,	0.1663, 0.1707, 0.1718, 0.1727, 0.1750,
0.5243, 0.5309, 0.5398, 0.5492, 0.5559,	0.2712, 0.2730, 0.2760, 0.2819, 0.2854,	0.1812, 0.1825, 0.1845, 0.1884, 0.1908,
0.5633, 0.5679, 0.5760, 0.5813, 0.5979,	0.2904, 0.2950, 0.3038, 0.3057, 0.3072,	0.1942, 0.1973, 0.2032, 0.2045, 0.2055,
0.6000, 0.6116, 0.6182, 0.6291, 0.6289,	0.3104, 0.3182, 0.3223, 0.3232, 0.3304,	0.2076, 0.2129, 0.2157, 0.2163, 0.2212,
0.6454, 0.6489, 0.6516, 0.6635, 0.6704,	0.3361, 0.3395, 0.3427, 0.3547, 0.3524,	0.2250, 0.2273, 0.2295, 0.2376, 0.2361,
0.6828, 0.6878, 0.6994, 0.7042, 0.7180,	0.3602, 0.3635, 0.3711, 0.3710, 0.3844,	0.2413, 0.2436, 0.2487, 0.2487, 0.2577,
0.7153, 0.7285, 0.7402, 0.7447, 0.7448,	0.3861, 0.3934, 0.4003, 0.3989, 0.4071,	0.2589, 0.2639, 0.2685, 0.2676, 0.2732,
0.7666, 0.7620, 0.7706, 0.7765, 0.7931,	0.4126, 0.4180, 0.4214, 0.4279, 0.4340,	0.2770, 0.2806, 0.2829, 0.2874, 0.2915,
0.7959, 0.8021, 0.8085, 0.8153, 0.8222,	0.4351, 0.4453, 0.4503, 0.4527, 0.4548,	0.2923, 0.2992, 0.3027, 0.3043, 0.3057,
0.8358, 0.8336, 0.8394, 0.8460, 0.8501,	0.4613, 0.4693, 0.4805, 0.4789, 0.4871,	0.3102, 0.3156, 0.3233, 0.3222, 0.3278,
0.8627, 0.8624, 0.8745, 0.8747, 0.8792,	0.4926, 0.4983, 0.5042, 0.5100, 0.5146,	0.3316, 0.3355, 0.3396, 0.3436, 0.3468,
0.8866, 0.8867, 0.8982, 0.9022, 0.9066,	0.5228, 0.5272, 0.5323, 0.5411, 0.5450,	0.3524, 0.3554, 0.3589, 0.3650, 0.3677,
0.9103, 0.9165, 0.9181, 0.9285, 0.9274,	0.5538, 0.5577, 0.5644, 0.5698, 0.5799,	0.3739, 0.3765, 0.3811, 0.3849, 0.3919,
0.9299, 0.9376, 0.9408, 0.9436, 0.9432,	0.5829, 0.5830, 0.5881, 0.5992, 0.6054,	0.3940, 0.3940, 0.3976, 0.4053, 0.4096,
0.9520, 0.9552, 0.9581, 0.9571, 0.9617,	0.6091, 0.6132, 0.6270, 0.6297, 0.6335,	0.4122, 0.4151, 0.4248, 0.4267, 0.4294,
0.9642, 0.9670, 0.9682, 0.9708, 0.9728,	0.6402, 0.6432, 0.6515, 0.6591, 0.6624,	0.4341, 0.4362, 0.4420, 0.4474, 0.4496,
0.9773, 0.9802, 0.9771, 0.9816, 0.9817,	0.6679, 0.6749, 0.6798, 0.6919, 0.6942,	0.4536, 0.4587, 0.4622, 0.4709, 0.4726,
0.9849, 0.9862, 0.9864, 0.9892, 0.9899,	0.6968, 0.7048, 0.7135, 0.7255, 0.7287,	0.4746, 0.4801, 0.4861, 0.4948, 0.4978,
0.9892, 0.9917, 0.9913, 0.9910, 0.9940,	0.7283, 0.7400, 0.7451, 0.7514, 0.7560,	0.4971, 0.5059, 0.5098, 0.5142, 0.5177,
0.9956, 0.9937, 0.9959, 0.9964, 0.9950,	0.7602, 0.7689, 0.7730, 0.7820, 0.7833,	0.5208, 0.5275, 0.5311, 0.5376, 0.5389,
0.9967, 0.9976, 0.9974, 0.9977, 0.9986,	0.7886, 0.7938, 0.8035, 0.8072, 0.8141,	0.5428, 0.5470, 0.5548, 0.5570, 0.5628,
0.9983, 0.9988, 0.9985, 0.9990, 0.9989,	0.8217, 0.8252, 0.8292, 0.8375, 0.8382,	0.5690, 0.5727, 0.5763, 0.5832, 0.5835,
0.9989, 0.9994, 0.9992, 0.9995, 0.9995,	0.8433, 0.8502, 0.8542, 0.8620, 0.8655,	0.5879, 0.5937, 0.5976, 0.6045, 0.6094,
0.9995, 0.9997, 0.9999, 0.9996, 0.9998,	0.8714, 0.8774, 0.8846, 0.8845, 0.8868,	0.6133, 0.6192, 0.6257, 0.6272, 0.6308,
0.9996, 0.9999, 1.0000, 1.0000, 1.0000,	0.8970, 0.8992, 0.9029, 0.9101, 0.9098,	0.6398, 0.6442, 0.6458, 0.6548, 0.6538,
1.0000, 1.0000, 1.0000, 1.0000, 1.0000,	0.9150, 0.9148, 0.9256, 0.9289, 0.9303,	0.6611, 0.6624, 0.6750, 0.6784, 0.6805,
1.0000, 1.0000, 1.0000, 1.0000, 1.0000,	0.9347, 0.9385, 0.9405, 0.9444, 0.9495,	0.6861, 0.6917, 0.6951, 0.7011, 0.7057,
1.0000, 1.0000, 1.0000, 1.0000, 1.0000,	0.9491, 0.9527, 0.9540, 0.9608, 0.9583,	0.7074, 0.7127, 0.7152, 0.7267, 0.7253,
1.0000, 1.0000, 1.0000, 1.0000, 1.0000,	0.9658, 0.9637, 0.9667, 0.9703, 0.9700,	0.7360, 0.7343, 0.7416, 0.7467, 0.7478,
1.0000, 1.0000, 1.0000, 1.0000, 1.0000,	0.9721, 0.9766, 0.9765, 0.9784, 0.9806,	0.7562, 0.7632, 0.7645, 0.7703, 0.7738,
1.0000, 1.0000, 1.0000, 1.0000, 1.0000,	0.9808, 0.9847, 0.9850, 0.9844, 0.9874,	0.7804, 0.7865, 0.7916, 0.7925, 0.7993,
1.0000, 1.0000, 1.0000, 1.0000, 1.0000,	0.9887, 0.9893, 0.9891, 0.9911, 0.9929,	0.8036, 0.8086, 0.8087, 0.8159, 0.8241,
1.0000, 1.0000, 1.0000, 1.0000, 1.0000,	0.9937, 0.9920, 0.9939, 0.9944, 0.9942,	0.8274, 0.8306, 0.8372, 0.8386, 0.8431,
1.0000, 1.0000, 1.0000, 1.0000, 1.0000,	0.9957, 0.9957, 0.9962, 0.9968, 0.9976,	0.8461, 0.8514, 0.8608, 0.8617, 0.8680,
1.0000, 1.0000, 1.0000, 1.0000, 1.0000,	0.9973, 0.9976, 0.9980, 0.9984, 0.9985,	0.8693, 0.8774, 0.8773, 0.8842, 0.8882,
1.0000, 1.0000, 1.0000, 1.0000, 1.0000,	0.9985, 0.9989, 0.9989, 0.9989, 0.9995,	0.8901, 0.8952, 0.8998, 0.9041, 0.9064,
1.0000, 1.0000, 1.0000, 1.0000, 1.0000,	0.9995, 0.9992, 0.9996, 0.9998, 0.9995,	0.9090, 0.9127, 0.9168, 0.9228, 0.9235,
1.0000, 1.0000, 1.0000, 1.0000, 1.0000,	0.9996, 0.9999, 0.9995, 0.9998, 0.9998,	0.9269, 0.9295, 0.9316, 0.9382, 0.9385,
1.0000, 1.0000, 1.0000, 1.0000, 1.0000,	0.9999, 0.9999, 1.0000, 1.0000, 1.0000,	0.9419, 0.9458, 0.9497, 0.9522, 0.9536,
1.0000, 1.0000, 1.0000, 1.0000, 1.0000,	1.0000, 1.0000, 1.0000, 1.0000, 1.0000,	0.9571, 0.9579, 0.9588, 0.9614, 0.9659,
1.0000, 1.0000, 1.0000, 1.0000, 1.0000,	1.0000, 1.0000, 1.0000, 1.0000, 1.0000,	0.9664, 0.9695, 0.9706, 0.9722, 0.9729,
1.0000, 1.0000, 1.0000, 1.0000, 1.0000,	1.0000, 1.0000, 1.0000, 1.0000, 1.0000,	0.9770, 0.9778, 0.9797, 0.9799, 0.9820,
1.0000, 1.0000, 1.0000, 1.0000, 1.0000,	1.0000, 1.0000, 1.0000, 1.0000, 1.0000,	0.9832, 0.9841, 0.9858, 0.9877, 0.9878,
1.0000, 1.0000, 1.0000, 1.0000, 1.0000,	1.0000, 1.0000, 1.0000, 1.0000, 1.0000,	0.9898, 0.9901, 0.9902, 0.9910, 0.9921,
1.0000, 1.0000, 1.0000, 1.0000, 1.0000,	1.0000, 1.0000, 1.0000, 1.0000, 1.0000,	0.9926, 0.9935, 0.9942, 0.9945, 0.9953,
1.0000, 1.0000, 1.0000, 1.0000, 1.0000,	1.0000, 1.0000, 1.0000, 1.0000, 1.0000,	0.9958, 0.9963, 0.9966, 0.9971, 0.9972,
1.0000, 1.0000, 1.0000, 1.0000, 1.0000,	1.0000, 1.0000, 1.0000, 1.0000, 1.0000,	0.9975, 0.9980, 0.9982, 0.9983, 0.9984,
1.0000, 1.0000, 1.0000, 1.0000, 1.0000,	1.0000, 1.0000, 1.0000, 1.0000, 1.0000,	0.9989, 0.9986, 0.9989, 0.9990, 0.9993,
1.0000, 1.0000, 1.0000, 1.0000, 1.0000,	1.0000, 1.0000, 1.0000, 1.0000, 1.0000,	0.9994, 0.9995, 0.9996, 0.9997, 0.9998,
1.0000, 1.0000, 1.0000, 1.0000, 1.0000.	1.0000, 1.0000, 1.0000, 1.0000, 1.0000.	0.9999, 1.0000, 1.0000, 1.0000, 1.0000.